Report 3700

of the L-1011
onal Flight
System

ffler

NASA Contractor Report 3700

Development of the L-1011 Four-Dimensional Flight Management System

H. P. Lee and M. F. Leffler
Lockheed-California Company
Burbank, California

Prepared for
Langley Research Center
under Contract NAS1-16199

National Aeronautics
and Space Administration

**Scientific and Technical
Information Office**

1984

TABLE OF CONTENTS

TABLE OF CONTENTS (Continued)

TABLE OF CONTENTS (Continued)

LIST OF ILLUSTRATIONS

LIST OF ILLUSTRATIONS (Continued)

LIST OF ILLUSTRATIONS (Continued)

LIST OF ILLUSTRATIONS (Continued)

LIST OF TABLES

ACKNOWLEDGMENTS

The authors would like to express appreciation to R. L. Heimbold of the Lockheed-California Company for his assistance, guidance and support throughout the course of this study. Also to A. Palmieri who headed up Lockheed's software development efforts on the 4-D FMS, to the Air Traffic Service personnel at Dallas/Fort Worth ARTCC and TRACON, and to L. V. Clark, NASA's Technical Monitor for the NASA/Lockheed ATOPS Program. Acknowledgement is also made of the support given by ARMA/Hamilton Standard in providing modified Flight Management System hardware for this program effort.

DEVELOPMENT OF THE L-1011 FOUR-DIMENSIONAL FLIGHT MANAGEMENT SYSTEM

H. P. Lee and M. F. Leffler
Lockheed-California Company

SUMMARY

This report describes in detail the development of the 4-D guidance algorithms for the Lockheed L-1011 Flight Management system (FMS). 4-D Flight Management is a concept by which an aircraft's flight is optimized along the most fuel conservative 3-D path through climb, cruise and descent within the constraints of today's ATC environment, while its arrival time is controlled to fit into the air traffic flow without incurring or causing delays. The 4-D strategy followed in this study is not a rigid strategic method; rather it is one that provides a measure of flexibility to accommodate limited path and arrival time changes to fit into real-world terminal airspace. The methods developed herein have been designed to be compatible with the time-based en-route metering techniques that have been recently developed by the Dallas/ Fort Worth and Denver Air Route Traffic Control Centers (ARTCC). These techniques assign arrival times to approaching aircraft for locations called metering-fixes; the air traffic controllers then manually control arriving aircraft to meet these assigned times. The 4-D concept fits in well with this system because it uses the metering fix time as its arrival time requirement.

The 4-D Flight Management System also provides a measure of automated navigation capabilities which offer a potential for substantially reducing pilot and controller workloads, enhancing terminal safety and increasing fuel savings.

The development activities in this study included the evaluation of the L-1011 aircraft's capabilities of achieving time and flight path flexibility within typical ATC airspace. Also included were the development of accurate wind models for use in descent, the synthesis of 4-D guidance algorithms, synthesis of the automatic 4-D descent and cruise control laws, and the development of the operational procedures for the 4-D FMS.

Throughout the course of this effort, several meetings were held with the Dallas/Fort-Worth air traffic controllers and system analysts to discuss various approaches of integrating the 4-D system with the metering program. It was concluded that the 4D-equipped airplane must be capable of flexible operation to be able to fit in with today's ATC environment. That is, it must be able to accept changes to its existing flight plan and arrival time requirement by offering a measure of flight path flexibility and arrival time flexibility. Also, a measure of time flexibility must be available to compensate for various error sources such as wind prediction errors, differences between ATC and FMS descent trajectory models and integral minute ATC arrival time assignments.

As a result of these meetings, it became apparent that the flexibility of the L-1011 must be determined. Various path flexibility techniques (e.g., leveling-off in descent and vectoring), as well as methods of providing time flexibility were evaluated and incorporated into the guidance algorithms. To minimize arrival time errors, a segmented wind model was developed for use in descent. A cruise wind model was also developed. Both models consider the age of the wind forecast and the persistence of winds and blend these data on a continuous basis into the real-time winds encountered by the aircraft in flight. Methods of improving descent trajectory modeling were also evaluated and incorporated.

Four-dimensional guidance algorithms were then developed. These algorithms provide the computation of an accurate time-referenced flight path for guiding the aircraft to a metering fix using the ATC-specified ground track, altitude profile, assigned metering-fix time, and end-of-descent airspeed restriction as constraints. These 4-D flight algorithms must: (1) predict winds along the descent profile and at each waypoint at cruise altitude; (2) generate a ground track trajectory which consists of straight-line and circular-arc segments; (3) compute correct cruise and descent speed schedules to meet the required time assignment at the metering fix, and (4) generate and store the nominal 4-D descent trajectory (a table of time, altitude and range) for guiding the aircraft to the metering-fix.

Control laws were then synthesized to automatically track the output commands of the guidance algorithms. In the cruise portion of flight, the objective is to arrive at the beginning-of-descent point (B*D) at a computed required-time-of-arrival (RTA). An airspeed requirement is continually computed using the latest wind update and the distance and time remaining to B*D calculated; the existing L-1011 FMS cruise control laws are then used to hold the computed airspeed command. In the descent region, engine thrust and spoilers are utilized to track the required spatial profile; speed changes effected through the pitch channel of the autopilot are used to achieve arrival time control.

A prediction of the total time in flight would be useful for flight planning purposes; given the metering fix RTA, a takeoff time requirement could then be readily calculated. It was therefore necessary to develop a climb model for computing time-in-climb and the distance to top-of-climb. Guidance algorithms were not developed to control the aircraft's arrival to the top-of-climb ETA since adequate time flexibility is available in cruise and descent to null out any time errors which might exist.

After much discussion with ATC personnel at the Fort Worth ARTCC and DFW TRACON facilities, operational procedures were then developed for the new 4-D FMS. Various Control and Display Unit (CDU) pages were specified for inserting the metering-fix arrival time requirement and inputting wind profile data into the FMS, and for the displaying of 4-D data/status to the flight crew.

The guidance algorithms and control laws were developed and evaluated using various computer aids for the required performance analysis. These

included the L-1011 Mission Analysis Program, various non-linear aircraft simulations using the IBM Continuous System Modeling Program (CSMP), numerous Fortran programs and classical analyses using the Advanced System Analysis Program (ASAP).

INTRODUCTION

Fuel prices have increased sharply since the 1970s, from about 10 cents per gallon in 1970 to $1.30 per gallon in 1981. As depicted in figure 1, the percentage of an airline's direct operating cost (DOC) attributable to fuel has risen from about 25 percent in 1970 to about 68 percent in 1981. Fuel cost thus has became the dominant factor in aircraft operation. This has resulted in industry requirements for more efficient operation of aircraft and led to the development of numerous airborne systems to minimize fuel consumption. Lockheed developed the first Flight Management System (FMS) and introduced it into air line service in 1977 for this purpose (1,2). Using flight path optimization techniques, the FMS is capable of offering cost savings of up to 6 percent of DOC.

Over the same time period, air traffic delays and associated airport congestion have continued to grow. During peak traffic hours, aircraft sometimes encounter delays of 30 minutes or more per flight segment. This trend is expected to worsen in the future. The Federal Aviation Administration (FAA) forecasts air traffic demands will more than double in the next two decades while airport capacity will be increased less than 30 percent. This will result in even more crowded skies and delays, and further aggravate airspace safety and the nation's fuel supply problems.

Recognizing this problem early, the FAA has been actively pursuing more efficient techniques for controlling air traffic in the terminal areas (3, 4, 5, 6). In November, 1976, the FAA issued Local Flow Traffic Management National Order 7110.72 to establish high profile descent procedures for traffic transitioning into airport terminal airspace. The objectives were to increase airport capacity, provide fuel savings, enhance airspace safety and reduce low altitude noise. In addition, a program was established to develop an automated time-based en route metering system to provide automation aids to the ATC controllers. These include delay absorption techniques and fuel-optimal descent profiles for transitioning en route aircraft. The primary objective of the new time-based system was to organize the traffic at higher altitudes so that congestion and delays (and attendant fuel inefficient maneuvers) in the terminal area can be kept to a minimum.

The time-based metering system works as shown in figure 2. In operation, the Air Route Traffic Control Center (ARTCC) regulates the flow of air traffic to an airport through geographical points called metering fixes. These metering fixes are usually located 40-60 flying miles from the airport and roughly describe the jurisdictional boundary between ARTCC and TRACON (Terminal Radar Approach Control). The metering computer program in the ARTCC predicts the arrival time at the airport runway threshold for each approaching aircraft and

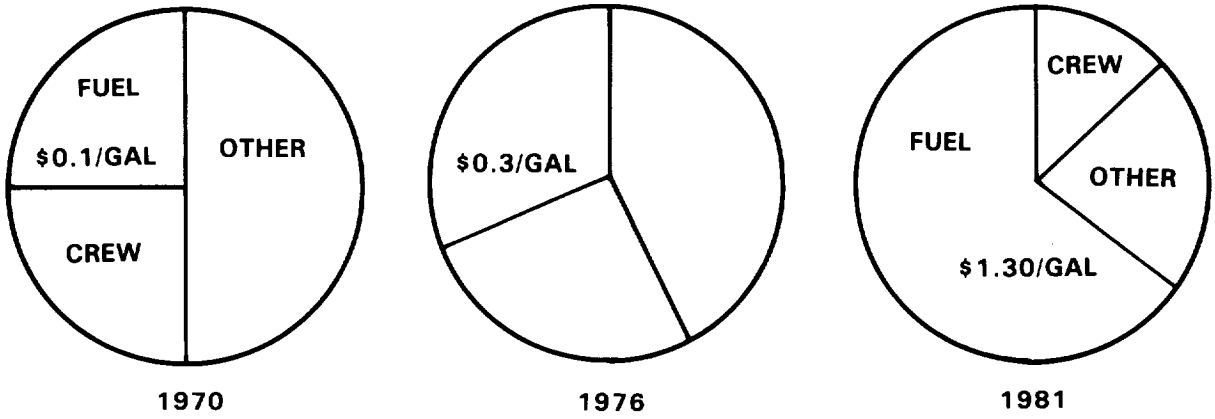

Figure 1. - Fuel costs.

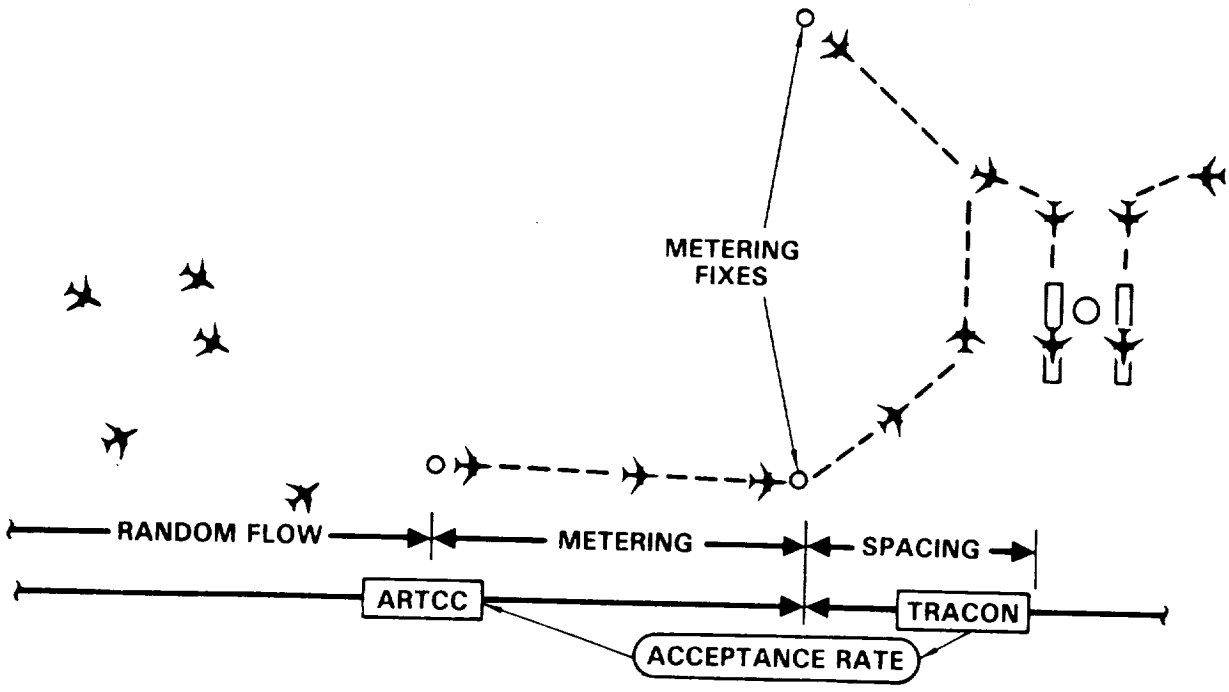

Figure 2. - Metering and spacing.

continuously checks to see if the acceptance rate of the airport will be exceeded. If so, action is taken by the ATC controllers to delay the metering fix arrival times as required. Individual sector controllers are given the required metering fix crossing time for each arriving aircraft and they then utilize speed changes, vectoring or a combination of both to control the approaching aircraft to make good these assigned times. In this way, the acceptance rate of the airport is not exceeded and flow peaks do not result in low altitude holding maneuvers. Delay maneuvers, when required, are executed at higher altitudes to minimize fuel consumption. The en route metering program is now operational at Dallas/Fort Worth and Denver and as part of the National Airspace System Plan, will be installed at all of the nation's ARTCCs by mid-1983 (7).

The Advanced Transport Operating System (ATOPS) Program, formerly called the Terminal Configured Vehicle (TCV) program, managed by the NASA-Langley Research Center, was established to research, develop, and demonstrate new concepts that will be needed for efficient aircraft operation in future high density terminal areas. The program's principal interest is to develop flight crew management tools that will complement the FAA's development of improved ground systems. One element of the ATOPS program was to develop a four-dimensional flight management concept (the three spatial dimensions plus the time dimension). The 4-D FMS has the capability of delivering an airplane to a specific waypoint at a specific time. When integrated with the time-based metering system, it will allow the pilot to plan his fuel-optimal flight path, fit it in with the ATC environment and meet the ATC-specified metering fix arrival time. The 4-D system therefore has the potential of reducing the crew and controller workloads substantially.

The 4-D system can also do a better job of time control; controllers can bring aircraft to the metering fix within one to two minutes of the assigned time whereas the 4-D equipped aircraft can get there within seconds. Additionally, 4-D can be used to maximize fuel savings by calculating and flying a precise time-referenced fuel-optimal flight path based on the specific aircraft performance, rather then flying a series of speed and heading changes as specified by the controller. The 4-D FMS thus provides significant advantages to the airline operator.

The 4-D flight management concept fits in quite well with the existing Lockheed L-1011 FMS. Certified in 1977, the L-1011 FMS already had an automatic 3-D guidance capability. Only relatively simple software changes were required to add the 4-D capability into the system. In 1979, Lockheed was given a TCV program contract (NAS1-15546) to incorporate a prototype 4-D descent capability. Evaluation flight tests were conducted in the California coastal areas and at the Dallas/Fort-Worth airport and demonstrated a highly accurate time control capability. A two-sigma arrival time error of 19 seconds was observed for nine of the eleven descents flown (9).

However, the prototype did not resolve the tough problem of integrating the system with ATC's metering program. The prototype system had only one descent speed schedule and did not have the capability to accept a time

assignment from ATC. Also, the 4-D descent flight tests suggested further improvements in various techniques could be made to reduce crew workload, improve performance and make the system more flexible in its use within the ATC environment.

In this present study, under NASA Contract NAS1-16199, various techniques to improve the performance of the following areas were investigated:

- Wind modeling
- Time and flight path flexibility
- Descent trajectory modeling

This report discusses the ensuing development of the 4-D guidance algorithms, the necessary control laws and operational procedures. Results of a simulation evaluation of the guidance algorithms and control laws are also presented, along with a description of the software development procedures utilized.

LIST OF SYMBOLS AND ABBREVIATIONS

A	ratio of windspeed to airspeed
ACC	accessory
ACLT	Actual Computed Landing Time
ADI	attitude direction indicator
AERA	Automated En Route ATC
AFCS	automatic flight control system
ALT	altitude
ARTCC	Air Route Traffic Control Center
ASAP	Advanced System Analysis Program
ATC	air traffic control
ATOPS	Advanced Transport Operating System
ATS	auto throttle system
Bmax	maximum bank angle, deg
B*D	beginning-of-descent point
C	speed of sound, ft/sec
CADC	central air data computer
CAS	calibrated airspeed
CDU	control and display unit

CRT	cathode ray tube
CSMP	Continuous System Modeling Program
D	straight-line ground distance between two waypoints, n.mi.
d	distance error
DA	drift angle
d_c	incremental distance command
Dcap	distance from waypoint at which turn begins, n.mi.
DCAS	Direct Computing Access System
DELDIS	incremental distance
DFW	Dallas/Fort Worth
DLC	direct lift control
DME	distance measuring equipment
DOC	direct operating cost
DPS	degrees per second
$\frac{dVw}{dh}$	change of windspeed with respect to altitude, kt/ft
ECS	environmental control system
E*D	end-of-descent point
EPR	engine pressure ratio
ETA	estimated time-of-arrival
FAA	Federal Aviation Administration
FD	Flight Director
FMC	Flight Management Computer
FMS	Flight Management System
f( )	functional notation
g	gravitational acceleration constant, 32.2 ft/sec^2
GMT	Greenwich Mean Time
H	altitude, ft
Hc	cruise altitude, ft
h_c	incremental altitude command
h	altitude error, ft
HSI	Horizontal Situation Indicator
IAS	indicated airspeed

IASD	Selected Descent IAS Schedule
INS	Inertial System
K	Conversion factor from knots to ft/sec, 1.688 ft/sec/knot
K_D	distance error to airspeed feedback gain, knot/n.mi.
$K_H^{\bullet}$	altitude rate feedback gain
K_H	altitude error feedback to DLC gain, deg/ft
K_θ	pitch feedback gain, deg/deg
K_Q	pitch rate feedback gain, deg/deg/sec
kts	knots
Kws	wind decay correction coefficient for ΔR, ft/kt
LAT	latitude
LFTM	local flow traffic management
LONG	longitude
M*F	metering fix point
N	number of cruise segments from aircraft position to B*D
n.mi.	nautical miles
NWS	National Weather Service
r	lag correlation coefficient of forecast wind
R	turn radius, n.mi.
R_c	cruise range, n.mi.
R_D	descent range, n.mi.
RGCMD	range command
RNAV	area navigation
RSS	root sum square
RTA	required time-of-arrival
S	Laplace Operator
SAT	static air temperature, deg. C
STAR	standard terminal arrival route
SY	predicted heading during the turn
SYD	heading rate
SYG	ground heading
SYW	wind heading at straight line portion
SYWP	predicted wind heading at the waypoint

t	time to fly straight-line portion of a cruise segment, sec
t'	time to fly circular-arc portion of a cruise segment, sec
T	age of forecast wind, hours
TAS	true airspeed
Tbias	descent time bias, sec
Tc	required cruise time, sec
TCV	Terminal Configured Vehicle
Td	descent time to metering fix using descent speed schedule of Vd, sec
TE	trailing edge
TKE	track error, n.mi.
Tmax	maximum flight time to metering fix, sec
Tmf	required flight time to metering fix, sec
Tmin	minimum flight time to metering fix, sec
TRACON	Terminal Radar Approach Control
U	aircraft inertial speed, knots
U_a	airspeed error, knots
Vc	cruise airspeed, knots
Vcmax	maximum cruise airspeed, knots
Vcmin	minimum cruise airspeed, knots
Vd	descent speed schedule, Mach/CAS/CAS
Vg	ground speed, knots
VGCA	predicted ground speed during the turn
VGREQ	required ground speed, knots
VGS	ground speed, knots
VHF NAV	very high frequency navigation (radio)
V_{MIN}	minimum speed, kts
VNAV	vertical navigation
V_0	initial aircraft true airspeed, knots
VOR	VHF omnidirectional range
VORTAC	colocated VOR and TACAN
VT	true airspeed, knots
VTAS	true airspeed, knots

Vu	true airspeed, knots
VUREQ	required cruise airspeed, knots
VW	averaged wind speed at straight-line portion of a cruise segment, knots
$\hat{V}w$	predicted descent windspeed, knots
VWc	predicted windspeed at B*D for descent wind model computation, knots
VWF	forecast windspeed at a waypoint, knots
VWL	descent windspeed predicted by the linear model, knots
VWM	measured windspeed at current aircraft position, knots
VWP	predicted windspeed at a waypoint, knots
W	weight, lb
WPT	waypoint
W/δ	weight per atmospheric pressure ratio, lb
Z	ground heading wind direction, $\psi_g - \psi_w$, deg
ρ	interlevel wind velocity correlation coefficient
σ_d	standard deviation of wind velocity separated by observing distance ΔD, knots
σ_t	standard deviation of forecast wind during time interval T, knots
σ_W	climatological standard deviation of windspeed, knots
σ_{WF}	standard deviation of forecast wind knowing lag correlation r and climatological standard deviation σ_W, knots
σ_{WL}	standard deviation of descent windspeed predicted by the linear model, knots
δ_{DLC}	incremental DLC, deg
α	angle of attack, deg
γ	flight path angle, deg
γ_o	initial aircraft flight path angle, deg
γ_e	earth referenced flight path angle, deg
γ_i	wind referenced flight path angle, deg
Δalt	incremental altitude
ΔALT	incremental altitude above E*D altitude where deceleration begins, ft.
Δh	incremental altitude, ft
Δr	incremental range, n.mi.

ΔD	direct distance between aircraft position and a given waypoint, n.mi.
ΔR	descent trajectory incremental distance, n.mi.
ΔRo	ΔR before corrections of wind and wind decay effects, n.mi.
$\Delta range$	range error, n.mi.
Δt	incremental time
$\Delta\psi$	off-course angle, deg
$\Delta\psi g$	track angle change at waypoint, deg
ψg	ground track heading, deg
ψw	wind heading at straight-line portion of a cruise segment, deg
ψWF	forecasted wind heading at a waypoint, deg
ψWM	measured wind heading at current aircraft position, deg
ψWP	predicted wind heading at a waypoint, deg
$\Sigma\Delta t$	time in descent, sec
ΔT	time flexibility from a given aircraft altitude to a metering fix, sec
ΔT_{ac}	time flexibility from aircraft altitude to 10,000 feet, sec
ΔT_{m*f}	time flexibility from metering fix altitude to 10,000 feet, sec
θ	pitch angle, deg
δ_H	horizontal stabilizer deflection, deg

Subscript:

i	denotes i-th altitude, or i-th waypoint
j	denotes j-th altitude
x	denotes east-west component
y	denotes north-south component

Superscript:

k	denotes k-th iteration solution

1. TIME-BASED EN ROUTE METERING SYSTEM

The Fort Worth Air Route Traffic Control Center (ARTCC) is one of the pioneers in the development and in-field evaluation of the en route metering system. Throughout the development of the 4-D FMS, meetings were held with controllers and system analysts from the Dallas/Fort Worth area to gain a better understanding of the program. Several workshops were held to discuss and evaluate the arrival time assignment algorithm and the Standard Terminal Arrival Routes (STARs) in use for the Dallas/Fort Worth (DFW) airport area. This information was then compared with FMS-derived data. Results of these comparisons are presented in this section.

1.1 Background

Escalating fuel costs and increasing air traffic growth have resulted in the FAA's development of more efficient methods of air traffic control. In 1976 a system named local flow traffic management (LFTM) was introduced (6). Through its procedures, fuel savings are achieved by utilizing fuel-conservative profile descents (figure 3) and by reducing low altitude flying times.

The LFTM was initially a manual system based on controllers permitting aircraft to descend in a fuel efficient manner at the pilot's discretion. To ensure the long-term success of LFTM, air traffic must be efficiently metered into airport terminal airspace at an optimum acceptance rate. To enhance the controllers' ability to accomplish this, an automated function called en route arrival metering was developed. Under this system, each airplane has a computer calculated time to cross a metering fix based on the airport's acceptance rate. The assigned metering fix times are displayed to the controllers so they can manage delays in the high altitude en route airspace where aircraft operate more efficiently. In this way, airplanes approaching a terminal area will not exceed the airport's acceptance rate and costly low altitude delay maneuvers will therefore be kept to a minimum.

The FAA is now in the process of installing the en route arrival metering program at all of the U.S.'s domestic ARTCCs. Other research and development programs which use time as the basis for control are en route arrival metering II which is planned for 1984, and a more sophisticated system called automated en route ATC (AERA) which is projected for operation in the early 1990's.

1.2 DFW Time-Based ATC Description

The DFW terminal area uses four metering fixes as handoff points from ARTCC controllers to the terminal radar approach control (TRACON) controllers. From the metering fixes to the airport, a path and speed profile is used to provide a fuel-efficient, uninterrupted descent into the runways. Figure 4

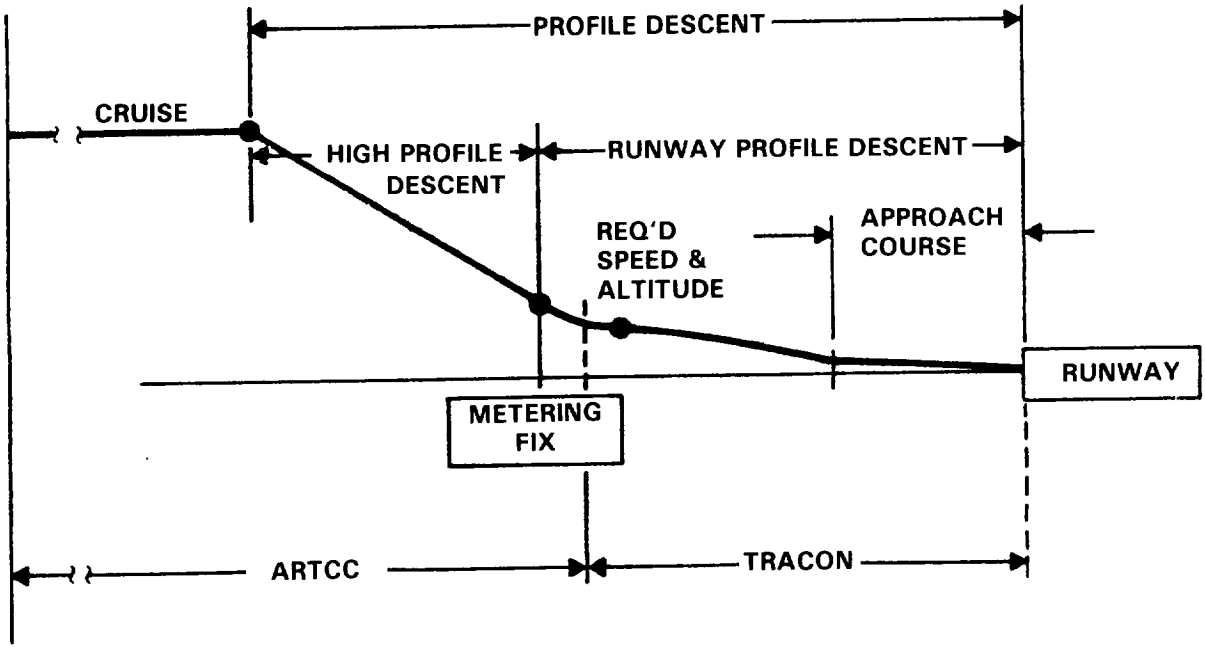

Figure 3. - Decent profile.

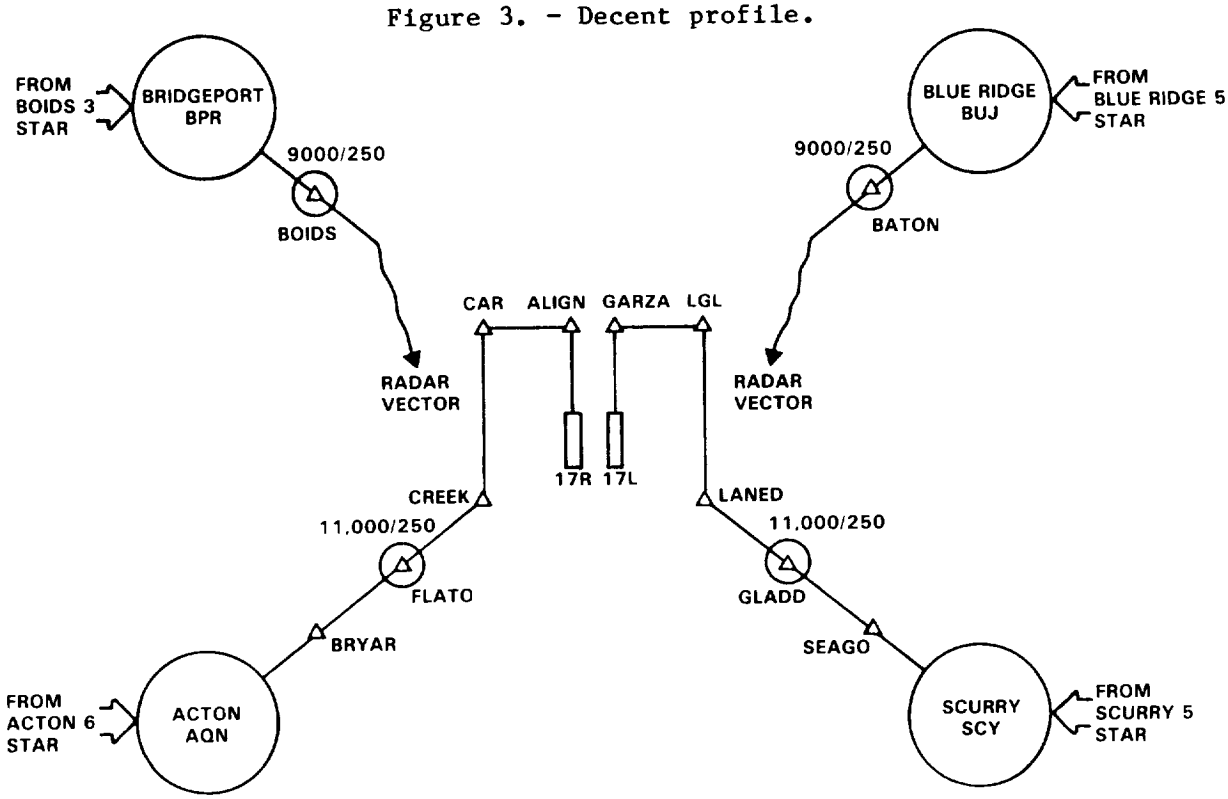

Figure 4. - Dallas/Fort Worth south flow.

shows the DFW south flow transitioning from the four metering fixes into Runway 17L and 17R.

For the procedure to function properly, aircraft delivery to the metering fixes must not exceed the airport's acceptance rate to avoid conflicts and delays. The basic logic for computing the metering fix arrival time for approaching airplanes is shown in figure 5. Based on the forecast winds aloft, filed TAS and radar position, the aircraft's estimated time of arrival (ETA) at the runway threshold is calculated. The ETAs are then adjusted to resolve conflicts and to ensure the airport acceptance rate is not exceeded. The re-computed runway arrival times are called the actual computed landing time (ACLT). Difference between the ACLT and the runway ETA is the delay the airplane must absorb in the en route airspace. The originally computed metering fix ETA is then adjusted to include the computed delay. This process is continually repeated until the aircraft is approximately 25 minutes from the metering fix at which time the metering fix ETA is frozen and becomes the assigned time slot for the airplane. The amount of delay and the final assigned metering fix time are then passed on to the controller for his use in delivering the airplane to the metering fix.

1.3 ARTCC/FMS Descent Model Comparison

The Fort Worth ARTCC method of estimating the metering fix arrival time was evaluated using the approach paths to runway 17L and 17R as shown in figure 6. The ATC algorithm estimates the flight time to the waypoint called TRANS based on the aircraft's ground speed computed at the ARTCC. Flight time between TRANS and the metering fix is then estimated by an empirical model which uses expected aircraft altitude, flight path and true airspeed. The same procedure is also used for computing the aircraft's runway threshold arrival time. The metering fix arrival time estimate (assuming no conflicts) is simply based on the summation of the flight time to TRANS and the flight time from TRANS to the metering fix.

FMS-derived descent trajectories for the L-1011 were calculated and the resulting time and spatial profiles compared with those offered by the ARTCC model. Figures 7 through 10 show the differences between the two techniques for each of the four STARs in use at DFW; a summary is presented in figure 11. Conditions for the comparison were for a descent from 32,000 feet to the metering fix at a speed schedule of 0.82/320/250. An aircraft weight of 300,000 pounds was used; no wind effects were introduced.

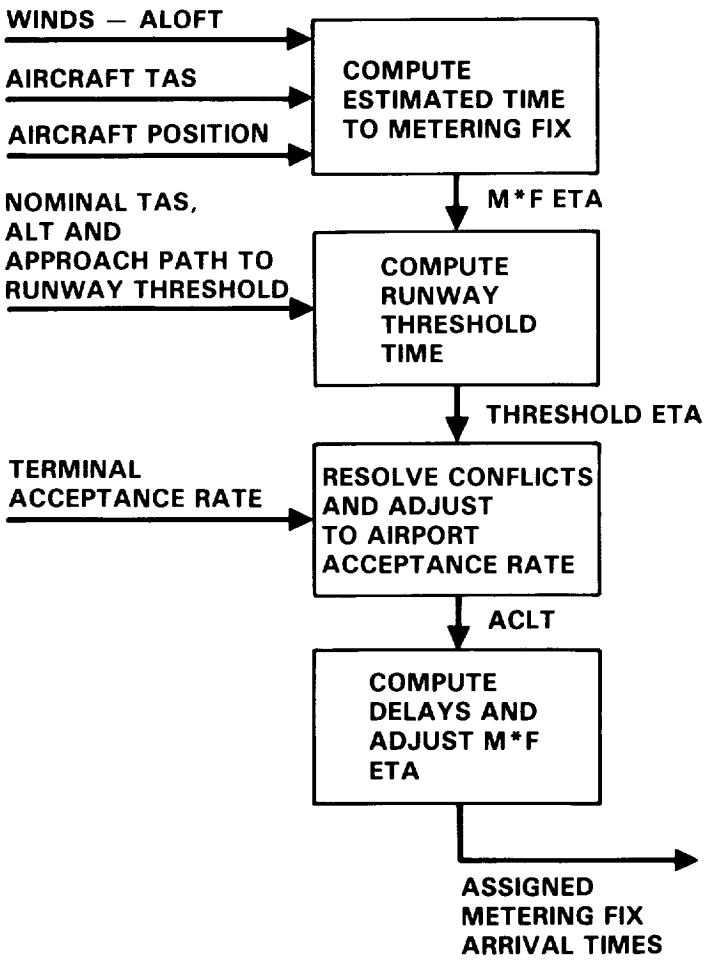

Figure 5. - ATC time-based algorithm.

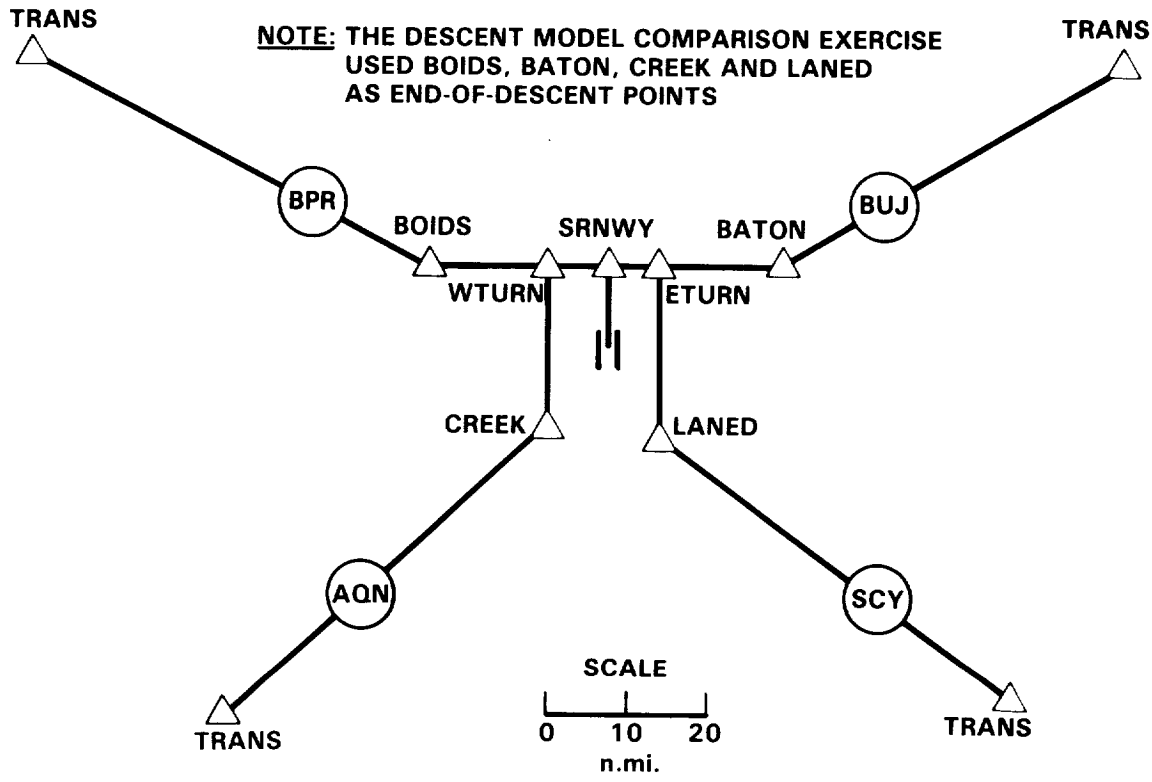

Figure 6. - DFW runways 17L and 17R.

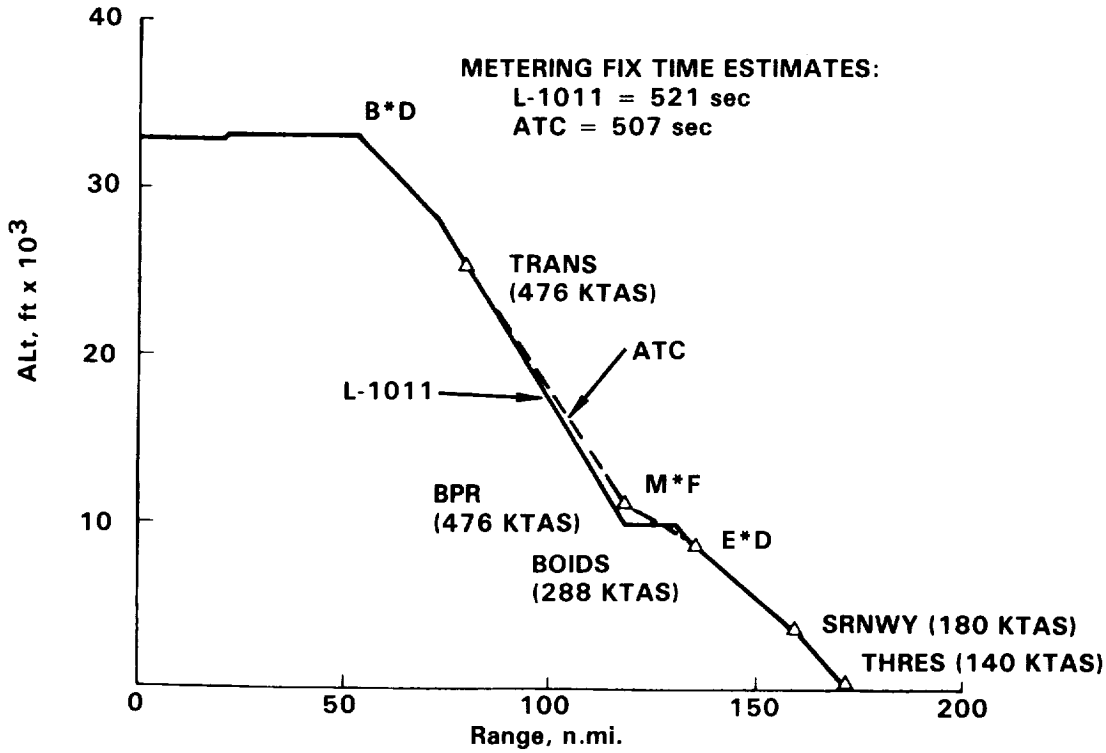

Figure 7. - DFW BPR descent profile.

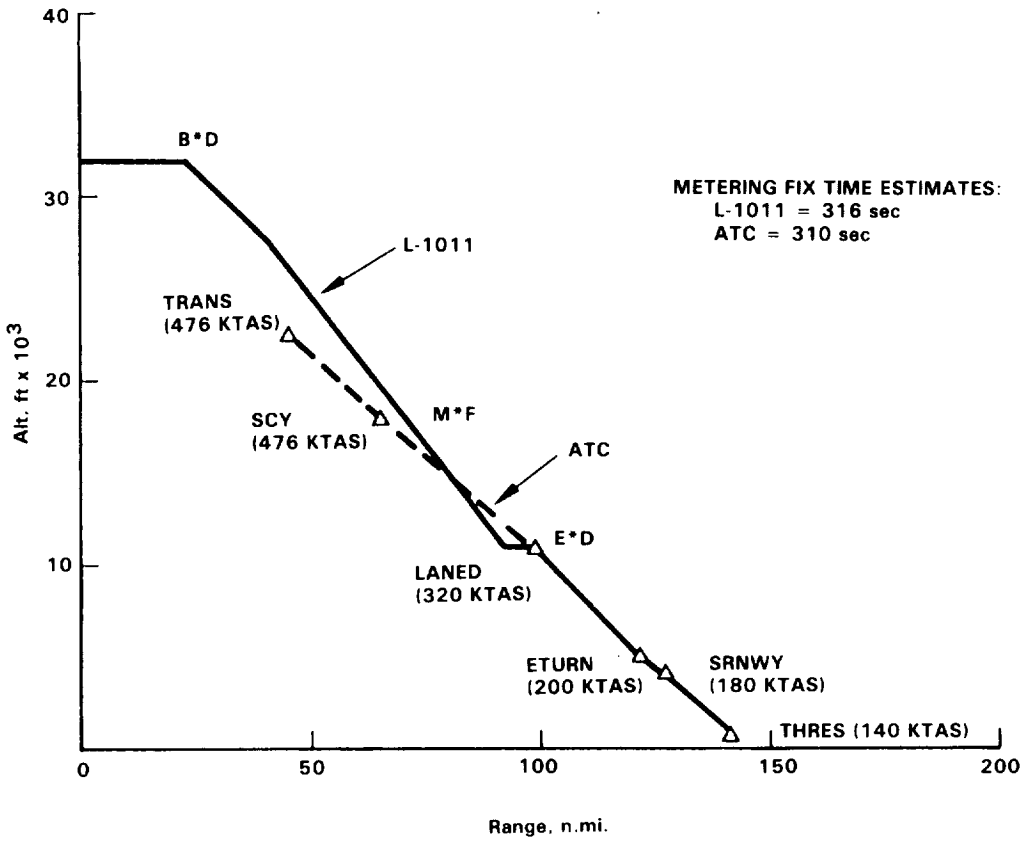

Figure 8. - DFW SCY descent profile.

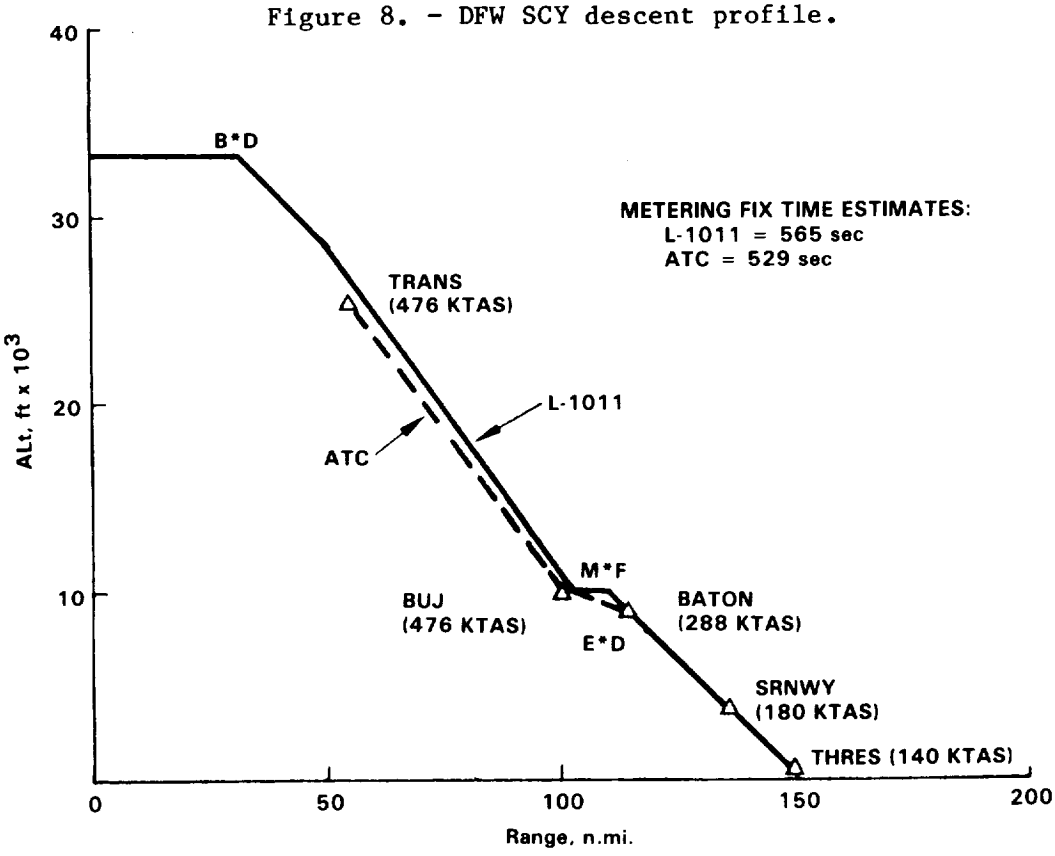

Figure 9. - DFW BUJ descent profile.

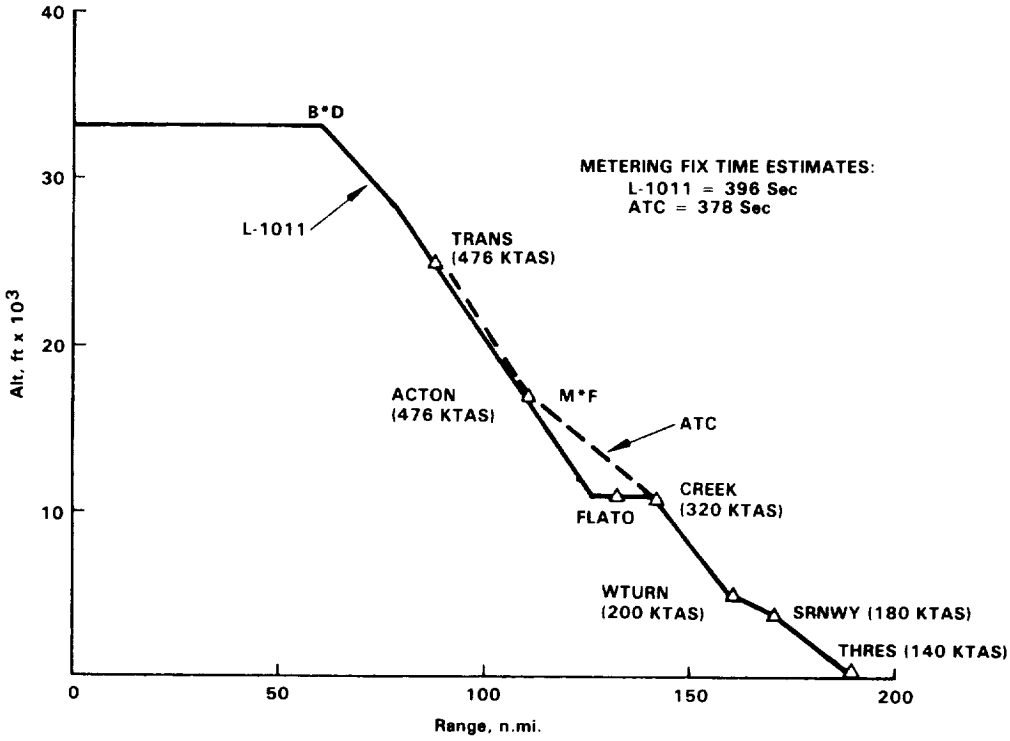

Figure 10. - DFW ACTON descent profile.

STAR	TIME DIFFERENCE (L-1011 – DFW)	ALTITUDE DIFFERENCE (L-1011 – DFW)
AQN	+ 18 sec	0 ft
SCY	+ 6 sec	+ 2,000 ft
BPR	+ 14 sec	– 1,500 ft
BUJ	+ 36 sec	+ 750 ft

ESTIMATION DIFFERENCES AT METERING FIX

Figure 11. - DFW and L-1011 FMS descent times and altitudes.

2. 4-D FMS DESIGN APPROACH

This section describes the development of the 4-D guidance and control algorithms and their mechanization using the existing L-1011 flight management system (FMS) hardware and software. The objective was to provide the L-1011 FMS with an automatic 4-D cruise and descent capability and flexible operational procedures compatible with the FAA's en route arrival metering system. The potential benefits offered by the 4-D FMS are enhanced safety resulting from reduced flight crew and controller workloads and increased fuel savings due to the execution of a precise, time-referenced optimal trajectory based on the specific performance of the aircraft.

2.1 The L-1011 Flight Management System

2.1.1 Basic operation.- The FMS is an extension of the area navigation (or RNAV) capability originally certified with the aircraft in 1971. It performs the basic RNAV functions of waypoint navigation and coupled guidance as well as the automatic selection of VORTAC stations, tuning of the aircraft's VOR/DME receivers, and the mixing of inertial, radio, heading and air data sensor inputs to provide optimal navigation accuracy and reversionary mode operation in the event of degradation. The system is comprised of a computer, a CRT control and display unit (CDU), and a CRT map display.

The flight management capabilities, mainly related to automatic control of engine performance for all phases of flight, are as follows:

- selection and performance of fixed or calculated optimum climb speed schedules
- selection and performance of desired engine pressure ratio (EPR) with automatic or manual derating
- calculation of optimum cruise conditions (i.e., altitude, speed, step-climb determinations) with automatic transitioning from climb to optimum or manually-specified cruise flight
- calculation of the descent trajectory required for optimum or manually-specified descent speed schedules with automatic initiation and termination of descent at a prescribed end-of-descent point, at the desired altitude and speed
- other capabilities such as estimated time en route to waypoints, engine-out drift down modes, calculation of flap holding speeds, reversionary airport fuel and point-of-no-return calculations based on the effects of current and forecast winds which can be entered into the system by the crew.

A description of the L-1011 FMS optimization algorithms is given in reference 2.

2.1.2 System interface.- The typical aircraft configuration is a dual system installation with the electronic map accepting inputs from either system as desired.

The functional interface of each system with the aircraft is summarized in figure 12. The major aircraft systems involved are the:

- inertial and radio navigation sensors
- heading reference system
- air data systems
- automatic flight control and flight director system pitch and roll channels
- automatic throttle
- related flight instruments

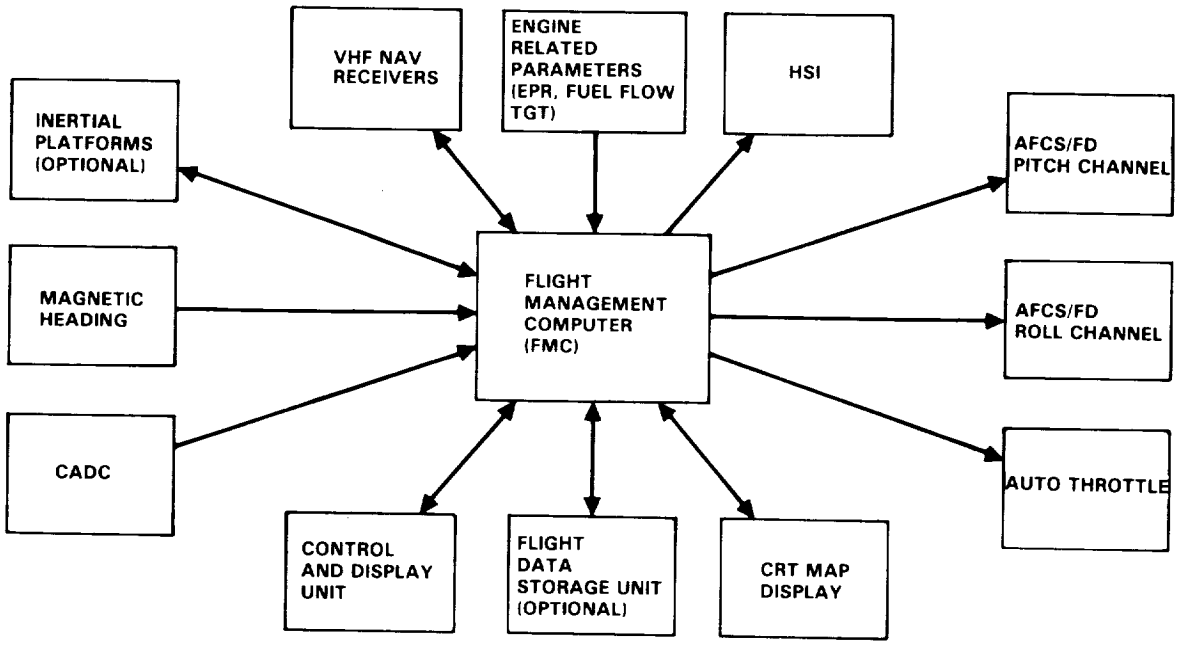

Figure 12. - Flight management system block diagram.

The detailed interface, shown in figure 13, illustrates that considerable redundancy exists for the air data and navigation functions. Single system failures are automatically dealt with and the most optimum operational mechanization is configured for the sensors available at any given time. The available navigation modes are:

- inertial/radio mix with up to three inertial systems and two each VOR/DME receivers
- inertial only (one to three inertial systems)
- radio only with submodes of
  - DME/DME
  - VOR/DME
- heading/air data

2.2 Accuracy Considerations

One result of the several workshops that were held with ARTCC personnel is a better understanding of the requirements for accuracy and flexibility that a 4-D system should have. An air traffic controller can deliver airplanes to a metering fix with an accuracy of one to two minutes. However, the 4-D accuracy objective adopted as a result of this study is plus or minus eight seconds for 95 percent of all arrivals. This may seem like more accuracy than necessary, particularly for today's ATC system, but there is good reason for its selection.

Equation 1 illustrates how the many errors associated with delivering an aircraft to a metering fix can easily add up to one minute's uncertainty. The terms under the radical sign are only reasonable estimates; however they do serve to illustrate the point. The two-sigma errors represented are as follows:

- wind error, 20 seconds - the uncertainty of metering fix arrival time resulting from unmodeled wind errors.
- radar error, 4 seconds - time error resulting from radar inaccuracies.
- linear flight path, 20 seconds - ARTCC computers estimate flight path times based on straight line segments and do not compensate for turn radius.

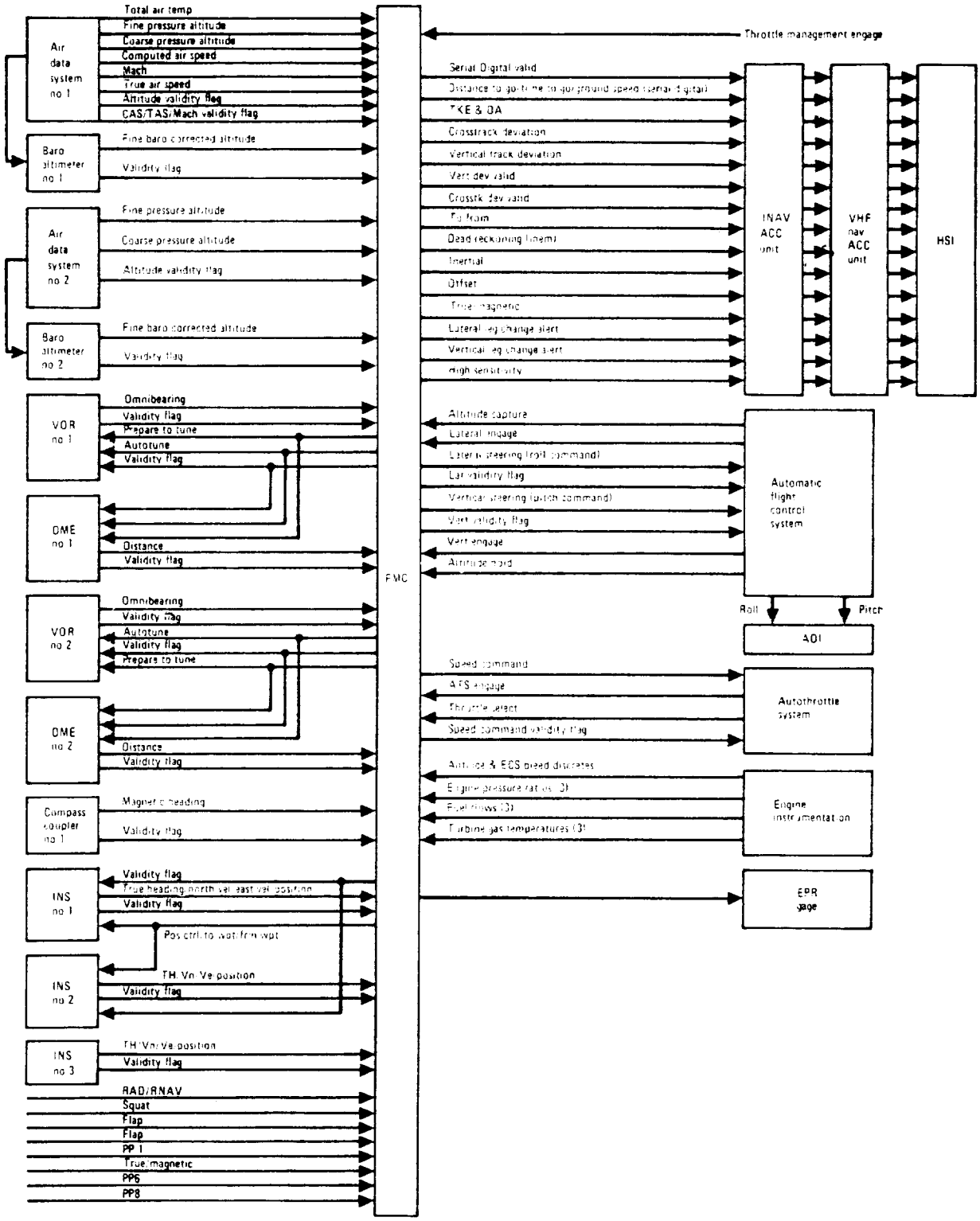

Figure 13. - FMS/Aircraft interface.

- communications lag, 10 seconds - represents the time lag caused by the voice communication process.

- aircraft performance model, 15 seconds - results from unmodeled aircraft performance errors (e.g., L-1011 vs B747) and their effect on ATC arrival time estimates.

- integral minute, 30 seconds - metering fix arrival times are issued for integral minute intervals.

- controller performance, 10 seconds - an estimate of the uncertainty introduced by the controller.

NOTE: all the above terms represent ATC-related errors

- aircraft open-loop response, 40 seconds - an estimate of how well an aircraft can perform an open-loop, high profile descent to the metering fix without time control.

The overall RSS error which results from considering the above various error sources is on the order of one minute, which agrees fairly well with the observations obtained from the workshop sessions and presented earlier.

Equation 2 illustrates how 4-D accuracy and flexibility can contribute to a considerable improvement in the metering fix delivery accuracy. The ATC-related errors from equation 1 contribute 46 seconds uncertainty, but can be compensated for with 46 seconds of time flexibility from the 4-D aircraft flexibility budget (which can be three to six minutes as discussed in Section 2.3). The 4-D aircraft operating closed-loop with a time control accuracy of eight seconds can therefore operate efficiently in today's ATC environment and arrive at the metering fix within a few seconds of the assigned time.

Equation 3 shows that even in tomorrow's ATC environment where most of the ATC-related errors approach zero, the need for closed-loop 4-D control still exists; some 40 seconds of uncertainty can result, mostly from open-loop descent performance. It can be easily seen that if this 40 second open-loop error term is replaced by the eight second closed-loop error term, the resulting uncertainty will again be approximately eight seconds; however, in this case, nearly the full time flexibility budget will be available to the aircraft for handling contingencies since ATC-related errors are very small.

PRESENT ATC WITHOUT 4-D

$$= \sqrt{\left[\left(\frac{\text{WIND}}{\text{ERROR}}_{20s}\right)^2 + \left(\frac{\text{RADAR}}{\text{ERROR}}_{4s}\right)^2 + \left(\frac{\text{LINEAR}}{\text{FLT PATH}}_{20s}\right)^2 + \left(\frac{\text{COMMUN}}{\text{LAG}}_{10s}\right)^2 + \left(\frac{\text{AIRCRAFT}}{\text{PERF MODEL}}_{15s}\right)^2 + \left(\frac{\text{INTEGRAL}}{\text{MINUTE}}_{30s}\right)^2 + \left(\frac{\text{CONTROLLER}}{\text{PERFORMANCE}}_{10s}\right)^2\right] + \left(\frac{\text{AIRCRAFT}}{\text{OPEN-LOOP RESPONSE}}_{40s}\right)^2}$$

ATC-RELATED ERRORS

$$= 61 \text{ SECONDS} \qquad (1)$$

PRESENT ATC WITH 4-D

$$= \sqrt{\left[(20s)^2 + (4s)^2 + (20s)^2 + (10s)^2 + (15s)^2 + (30s)^2 + (10s)^2\right] + \left[(8s)^2 - (48s)^2\right]}$$

48 SECONDS; 4-D FLEXIBILITY; 4-D ACCURACY

$$= 8 \text{ SECONDS (REMAINDER OF 4-D FLEXIBILITY BUDGET AVAILABLE FOR INTEGRATION PURPOSES)} \qquad (2)$$

(AIRCRAFT CLOSED-LOOP RESPONSE)

FUTURE ATC (MODE S, MITRE MODEL ETC) WITHOUT 4-D

$$= \sqrt{\left[(0)^2 + (4s)^2 + (0)^2 + (0)^2 + (0)^2 + (0)^2 + (0)^2\right] + (40s)^2}$$

$$= 40 \text{ SECONDS} \qquad (3)$$

Since ATC meters airplanes on an integral minute basis, it is possible for planes to pass the same metering fix point one minute apart as shown in figure 14. If their arrival dispersion is less than eight seconds, 95 percent of the time the airplanes will be spaced four miles or more from one another. It should be noted that as the arrival error gets worse the number of spacing commands the controllers downstream of the metering fix must perform becomes greater.

2.3 L-1011 4-D Flexibility Study

Flexibility is a must for 4-D flight; figure 15 lists the reasons why. There must be several minutes of arrival time variation possible without requiring a change to the flight path. This flexibility is necessary so that the arrival time of the airplane will coincide with the arrival time required by the air traffic controller. Flexibility is also needed to compensate for wind and performance modeling errors in the FMS computer; however, these will typically be quite small. The air traffic control ground system specifies the arrival of airplanes to the nearest integral minute, so the airplane must have at least 30 seconds of arrival time flexibility to fit. Additionally, the ground computer uses an arrival time estimation model which is not as exact as the FMS computation model. Delays caused by traffic or weather also require some flexibility.

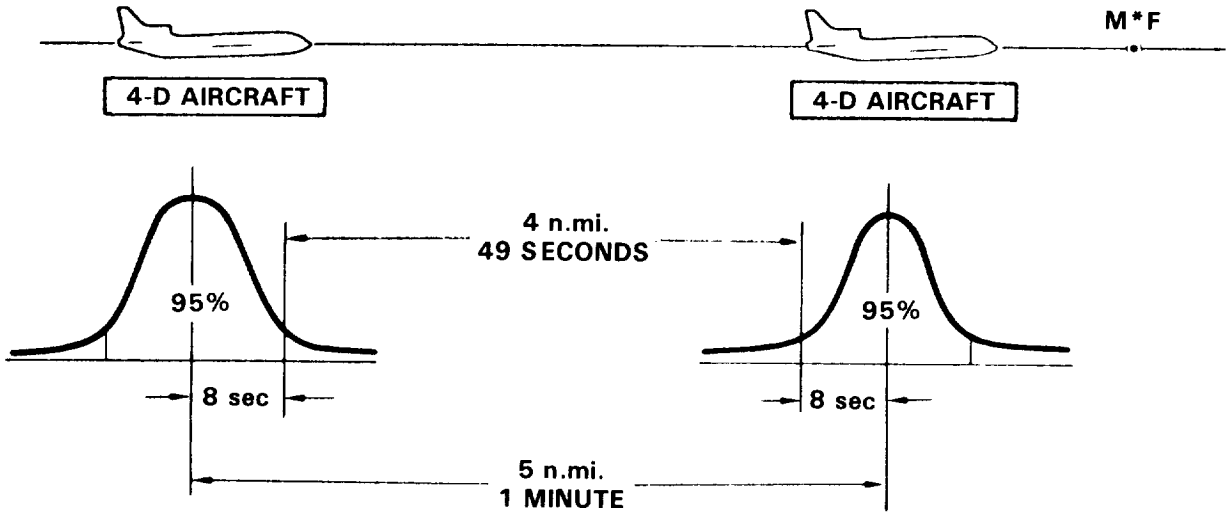

Figure 14. - Arrival dispersion.

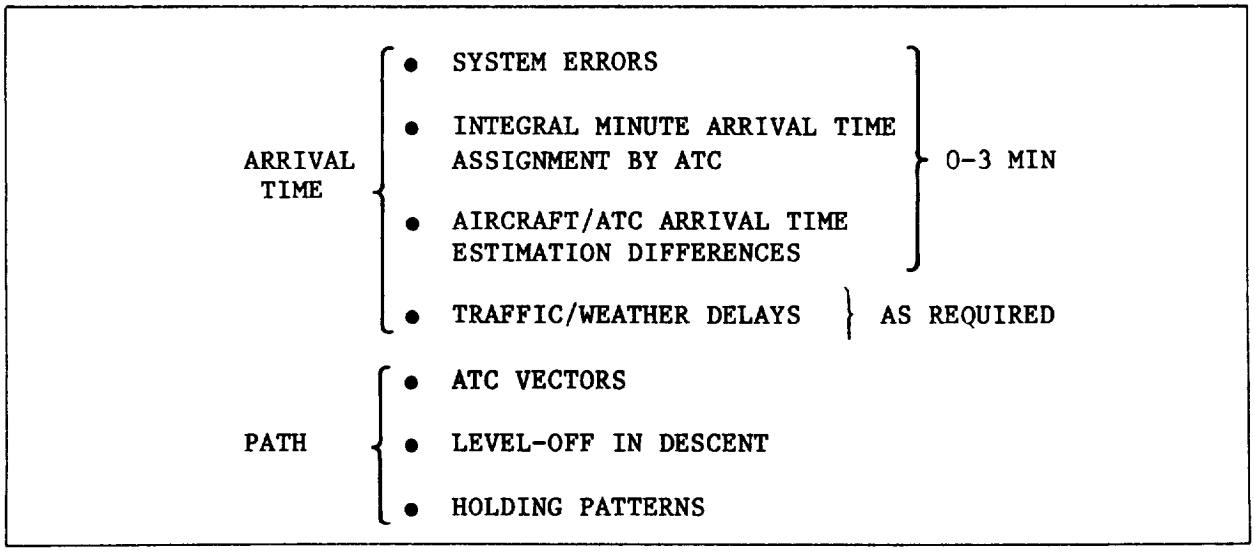

Figure 15. - Flexibility - a "must" for 4-D.

Besides arrival time flexibility, some path flexibility is also required. Figure 16 presents an example. After the airplane has been vectored off course because of traffic, the 4-D FMS must be capable of automatically re-engaging the descent, computing the new course back to the metering fix, and making good the original, or a newly-specified, arrival time.

Occasionally, airplanes are required to level off in their descent, for example when the high altitude air traffic controller hands the airplane off to the low altitude controller. This is shown in figure 17. When instructed to resume the descent, the 4-D system must be able to automatically re-engage and guide the airplane down through the metering fix at the pre-established time.

2.3.1 Descent time flexibility.- Figure 18 shows the L-1011-1 operating envelope in terms of altitude and true airspeed. High speed limits are the maximum operating speeds of 0.9 Mach and 375 knots CAS. The low speed limit is based on the 1.3 g buffet onset velocity with a descent weight of 380,000 lbs. The 1.3 g buffet onset speed criteria provides a 0.3 g maneuver margin before low speed initial buffeting occurs.

In calculating the descent time flexibility, safe speed limits within the operating envelope were selected. For the 4-D descent, the high speed limit was set at 0.86 mach and 365 knots CAS, and the low speed limit at 0.78 Mach and 240 knots CAS. These speed limits, together with five common descent schedules, are also shown in figure 18.

Delay time flexibilities for the five standard descents were calculated for the 300,000 and 360,000 pound aircraft and are shown in figures 19 and 20. Minimum speeds of 0.78 Mach and 240 knots CAS with a Mach to CAS transition altitude of 29,000 feet were used. The time flexibilities were calculated from the maximum altitude of 42,000 feet to an end-of-descent altitude of 10,000 feet. To determine time flexibility from a given aircraft altitude to a metering fix, the following equation can be used:

$$\Delta T = \Delta T_{ac} - \Delta T_{m*f} \qquad (4)$$

where ΔT_{ac} is the time flexibility from the aircraft altitude to 10,000 feet and ΔT_{m*f} is the time flexibility from the metering fix altitude to 10,000 feet. Since airspeed below 10,000 feet is normally restricted to 250 knots CAS, time flexibility below 10,000 feet was assumed to be zero.

Advance time flexibilities for the five standard descents were calculated using the maximum speeds of 0.86 Mach and 365 knots CAS for the 300,000 pound and the 360,000 pound aircraft as shown in figures 21 and 22.

Figure 16. - ATC vectors.

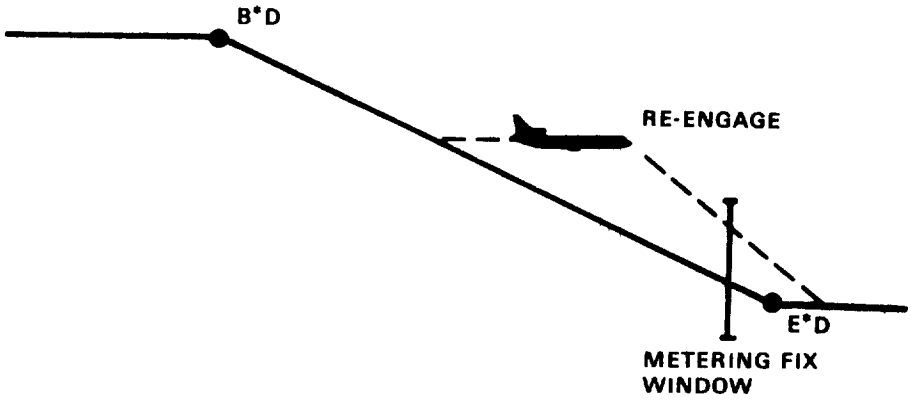

Figure 17. - Path flexibility.

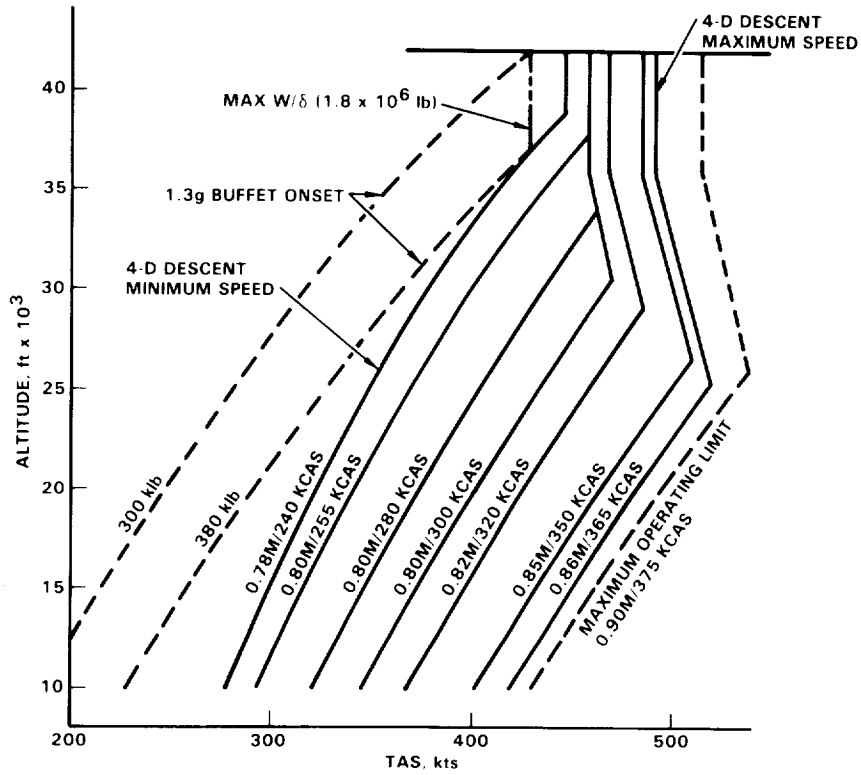

Figure 18. - L-1011-1 speed envelope.

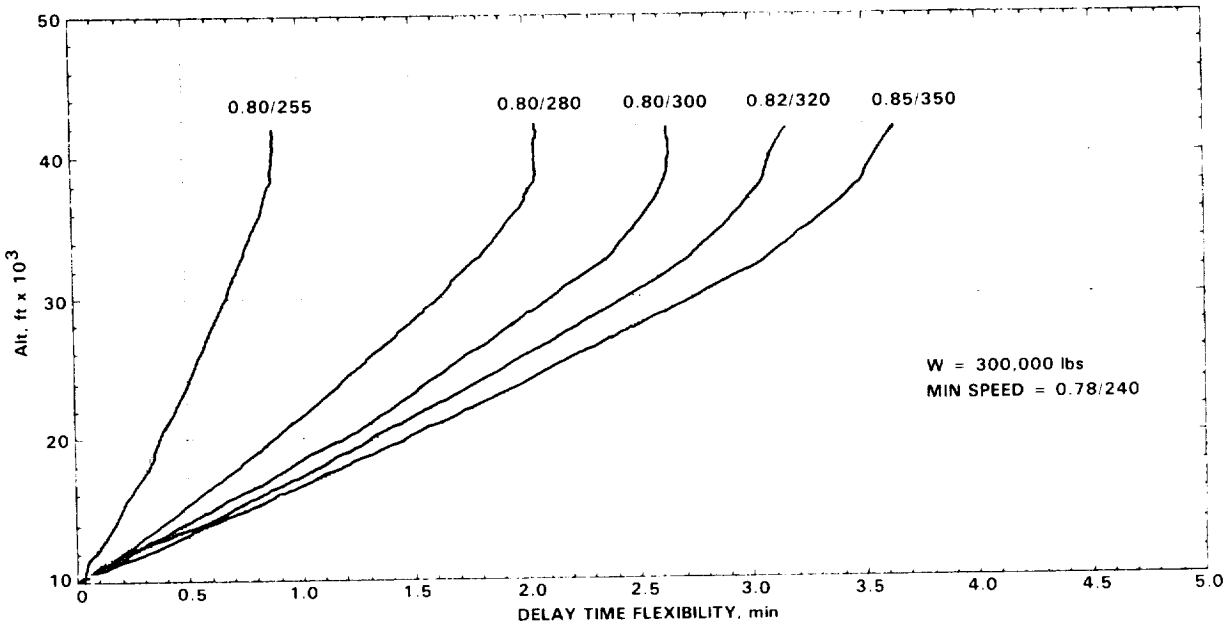

Figure 19. - Delay time flexibility in descent (300,000 lb weight).

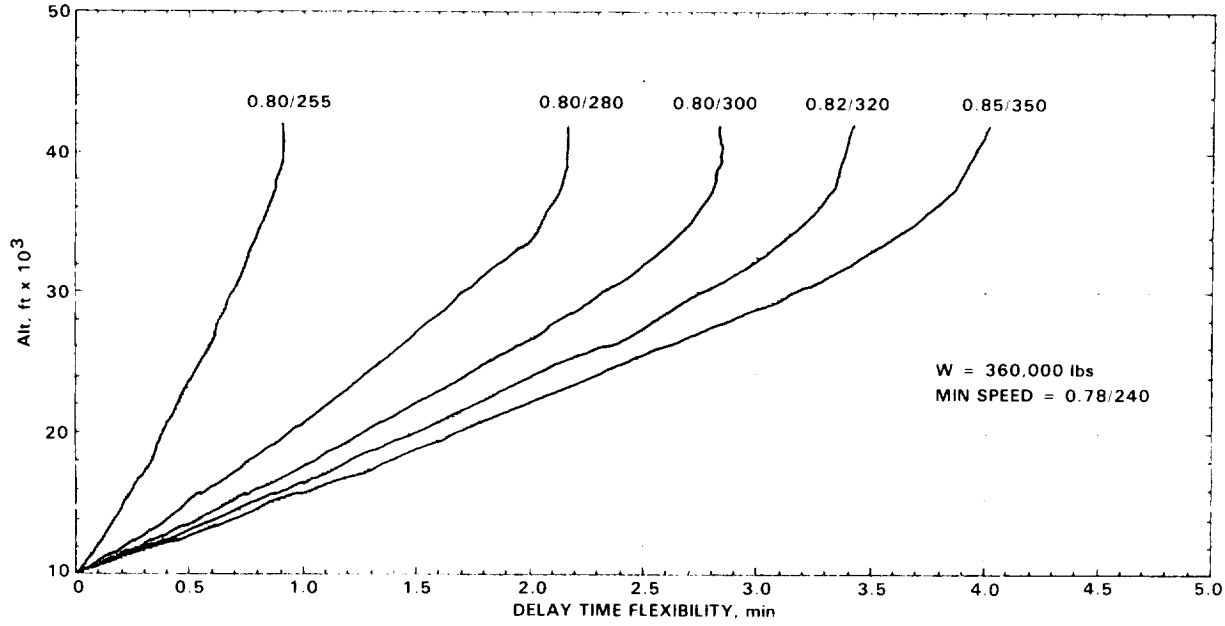

Figure 20. - Delay time flexibility in descent (360,000 lb weight).

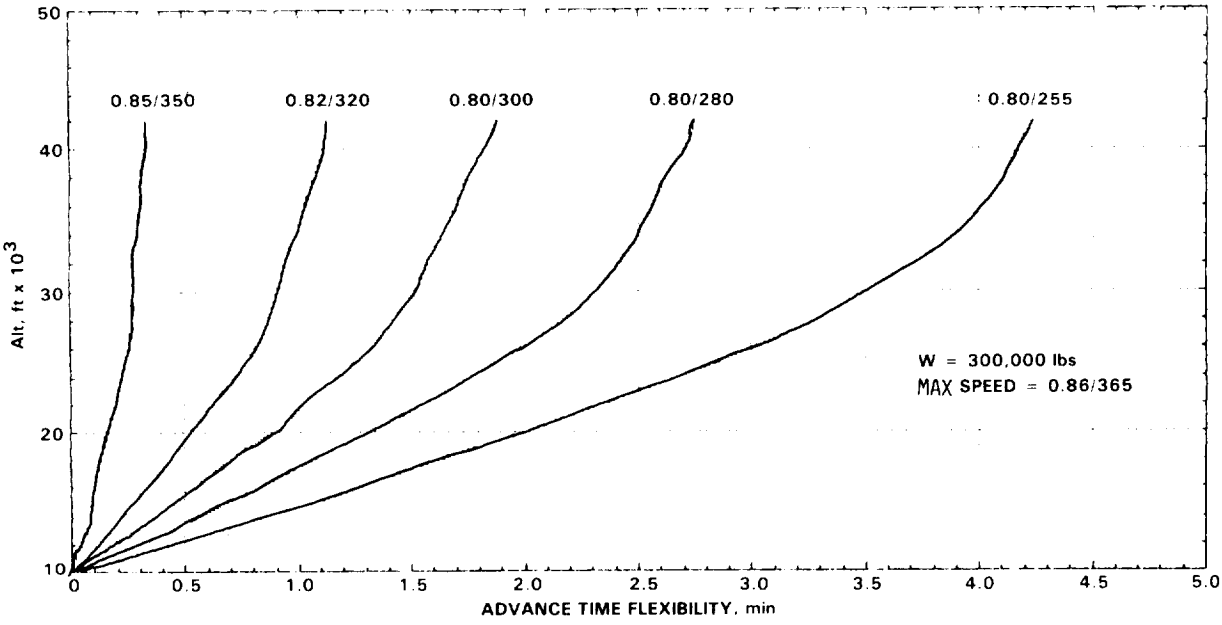

Figure 21. - Advance time flexibility in descent (300,000 lb weight).

2.3.2 Cruise time flexibility.- The cruise delay time flexibility can be calculated as a function of cruise distance by the equation

$$\Delta T = \frac{D}{Vmin} - \frac{D}{V_0} \qquad (5)$$

where D is the cruise distance, Vmin is minimum speed, and V_0 is the initial aircraft cruise speed.

Figure 23 shows the delay time flexibilities for various cruise altitudes using the initial speeds of 0.86 Mach and 0.82 Mach, and the minimum speed of 0.78 Mach.

2.3.3 Level-off flexibility.- The level-off flexibility is expressed in terms of maximum level-off distance and time where the aircraft can still return to the original metering fix by flying a steeper trajectory using a maximum spoiler deflection of 15 degrees. The maximum level-off distances and times for the 360,000 pound aircraft calculated for various descent speeds are as shown in figures 24 through 26. The effect of aircraft weight on the maximum distance is small and can be neglected.

2.4 Wind Modeling

For 4-D flight it is desired to maintain as much arrival time flexibility as possible. Inaccurate wind modeling, however, deteriorates this flexibility because the aircraft has to make airspeed changes to compensate for unmodeled wind errors. It was therefore decided that a more accurate wind model than that used in the production FMS was needed. This section discusses the development of a segmented wind model for descent and a cruise wind model, both of which consider the age and persistence of forecast winds.

2.4.1 Descent wind model.- Figure 27 depicts the actual wind profiles measured during four 4-D descents made in July 1979 off the coast of California. Each descent was made over the same course, the last descent occurring five and one-half hours after the first. The wind velocity persistence was seen to be consistent with statistical observations for winds in stable weather conditions.

A linear model, also shown on the graph, is routinely used in the production L-1011 FMS to characterize wind velocities for the descent. In the absence of other wind data, the linear model provides a fair estimate; however, in this case the model had a fairly large headwind error for most of the descent. Clearly, something better was needed to minimize these unmodeled errors.

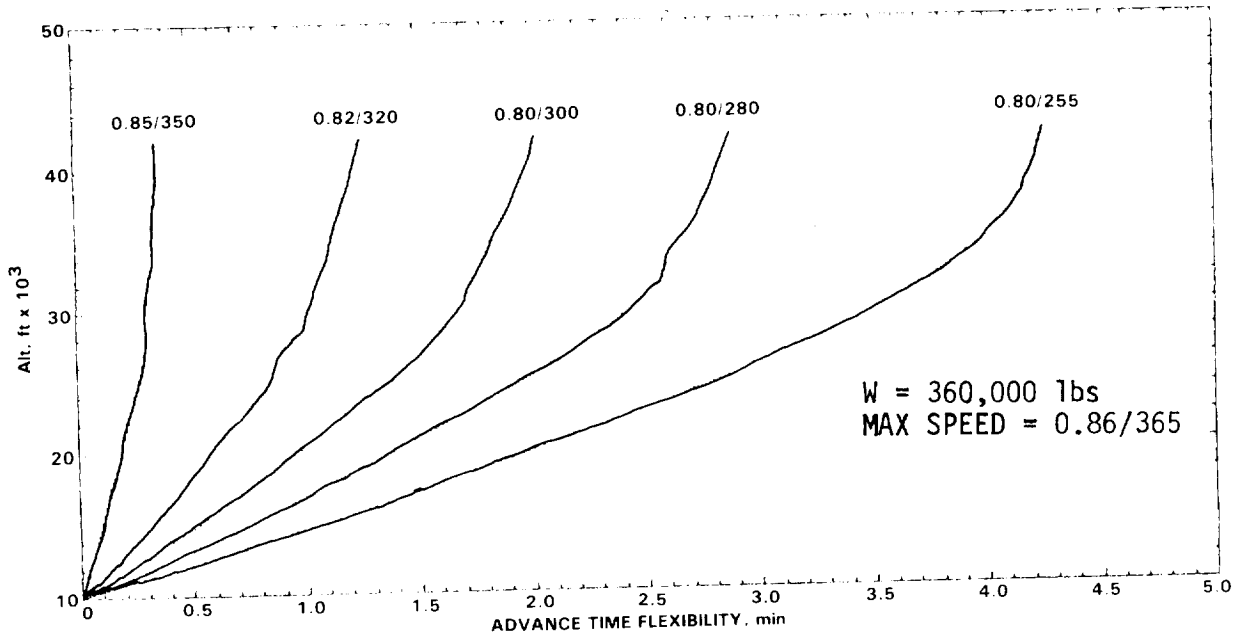

Figure 22. - Advance time flexibility in descent (360,000 lb weight).

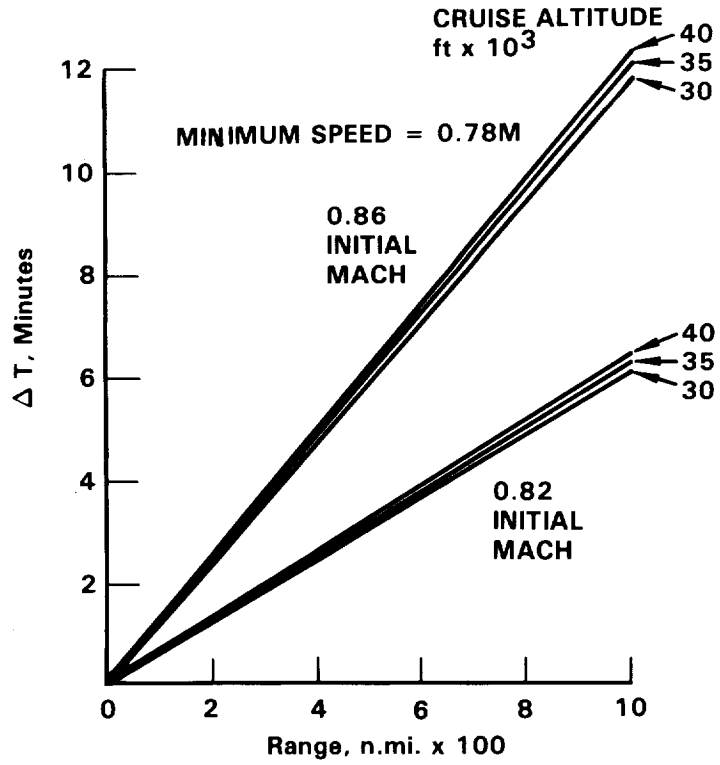

Figure 23. - Delay time flexibility in cruise.

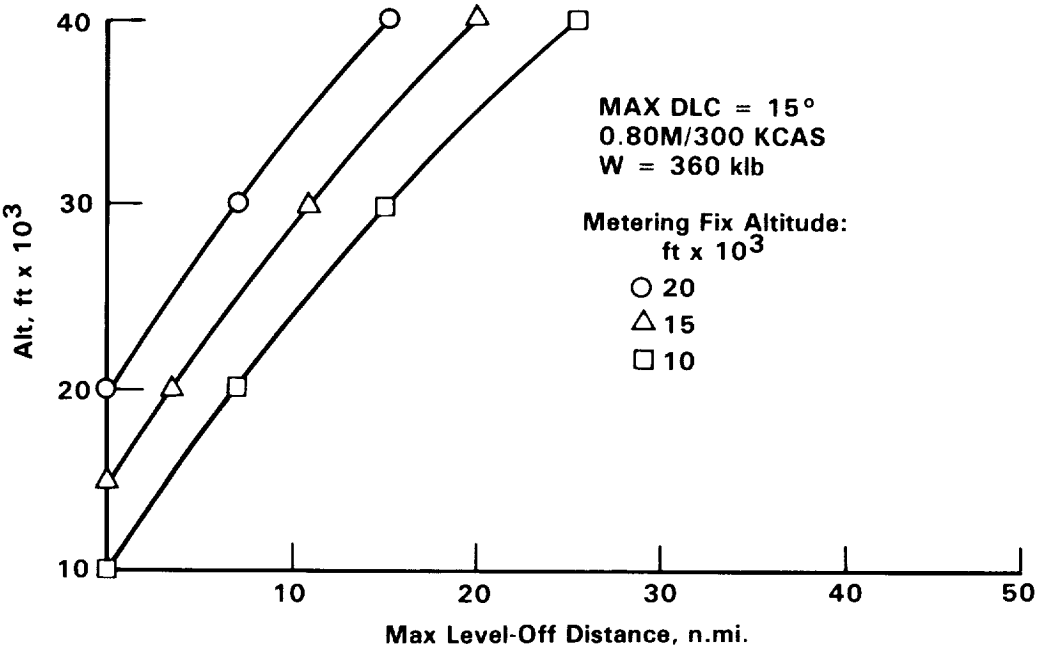

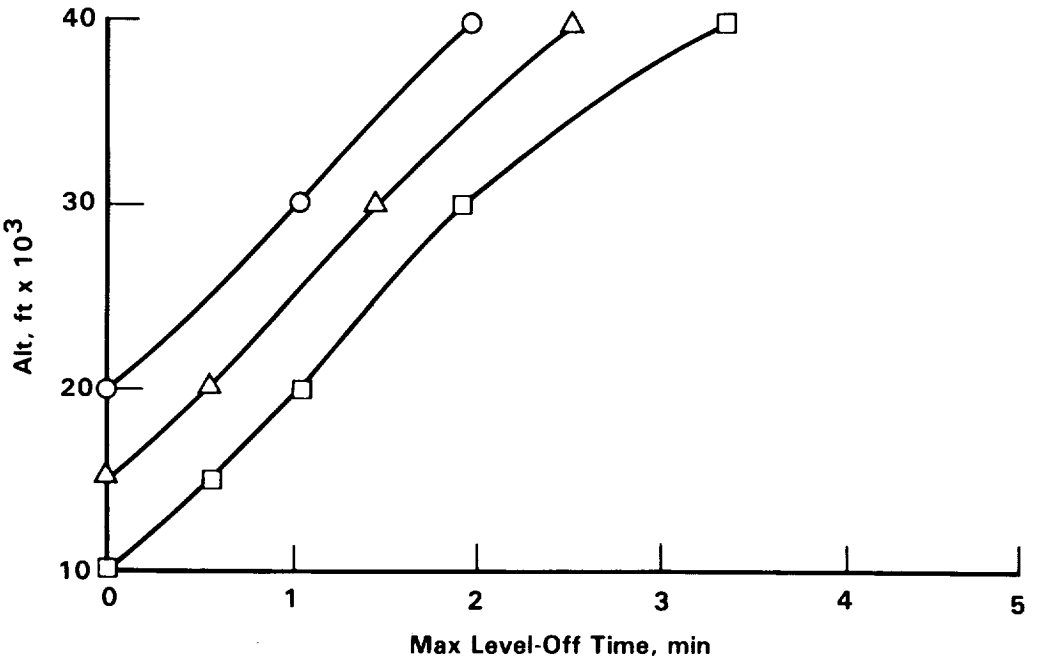

Figure 24. - Level-off flexibility (0.80M/300 KCAS descent).

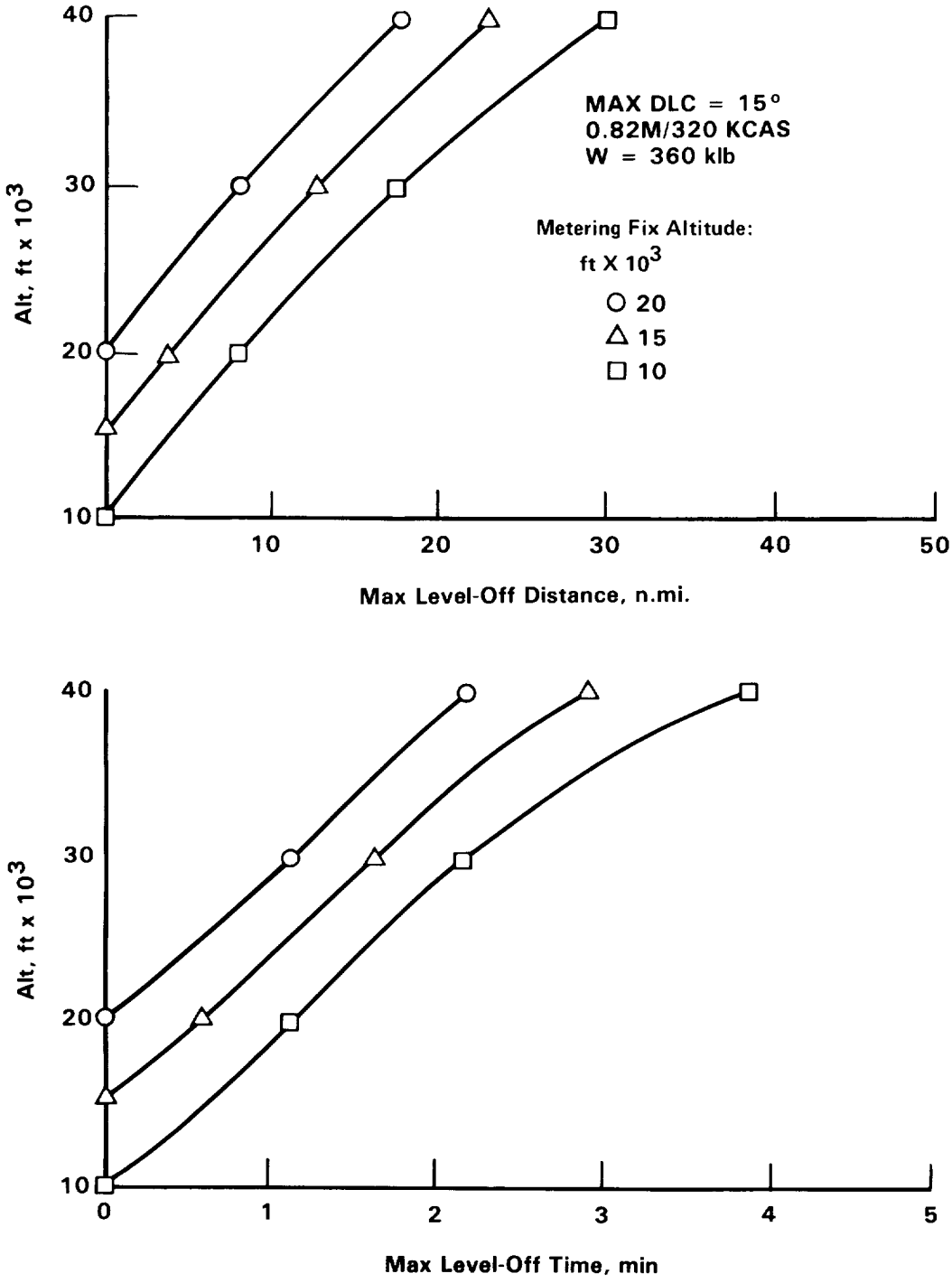

Figure 25. - Level-off flexibility (0.82M/320 CAS descent).

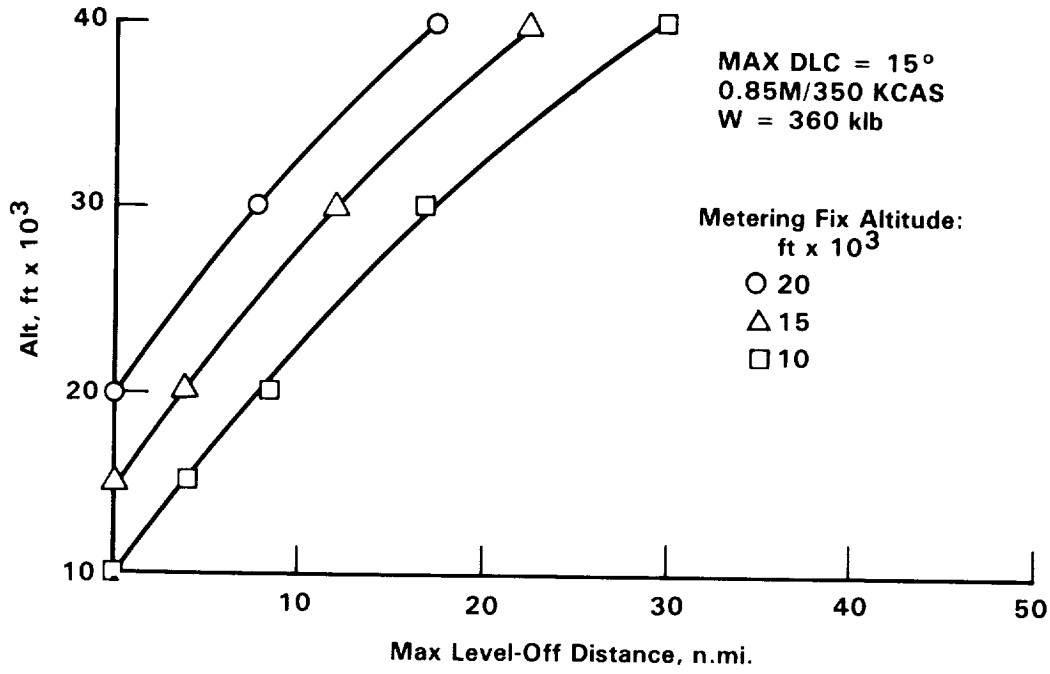

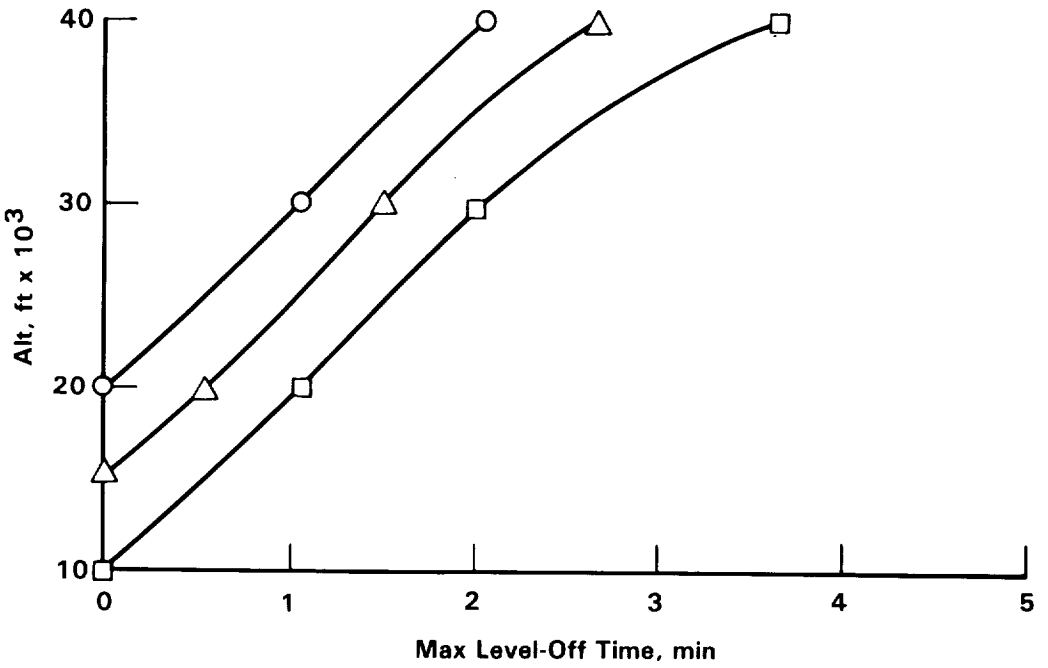

Figure 26. - Level-off flexibility (0.85M/350 KCAS descent).

To maximize 4-D flexibility, a segmented wind model capable of accepting reported wind velocity data for points at every 3000 feet of altitude was designed into the 4-D algorithm. By inspection of figure 27 it can be seen that such a model would be a good fit to the plotted wind velocities. As aircraft approach their destination airports the segmented wind velocities for their arrival route could be transmitted to them from preceding aircraft by means of a data link.

However, for the most part, only forecast wind data based on balloon observations are available today. Since these forecasts are based on observations as much as 12 hours old, their deviation from actual winds encountered in flight can be quite large. Figure 28 shows an example.

In this figure, the National Weather Service (NWS) forecast wind data are compared with the wind encountered during an L-1011 descent near Catalina Island in June 1981. Note the large wind error observed.

A more accurate wind model should utilize both the linear wind prediction technique and the forecast data. To do so, the statistical behavior of both, that is, the standard deviation of the linear model and the standard deviation of the forecast wind data must be known. Estimation theory can then be applied to blend the result of the two to derive a better prediction.

Reference 10 reported a method of calculating the standard deviation of forecast wind:

$$\sigma_{WF} = \sigma_{w} (2 - r)^{1/2} \qquad (6)$$

where σ_{WF} and σ_{W} are the forecast and climatological standard deviations respectively, and r is the lag correlation coefficient. The lag correlation coefficient (r) is the function of geographic location, altitude and the age of the forecast as illustrated in the examples of figure 29. To implement the equation into the FMS, the lag correlation coefficient is approximated by neglecting the altitude variable and by taking the average of all locations compiled in reference 10. The resulting model is shown in figure 30 and is given by the equation:

$$r = -0.023\ T + 1 \qquad (7)$$

where T is the age of the forecast.

The standard deviation of the linear wind model can be derived using linear regression and conditional probability theory. In reference 11, the standard deviation for winds at lower altitudes as predicted by the known wind velocity at cruise altitude was derived and is given by the equation:

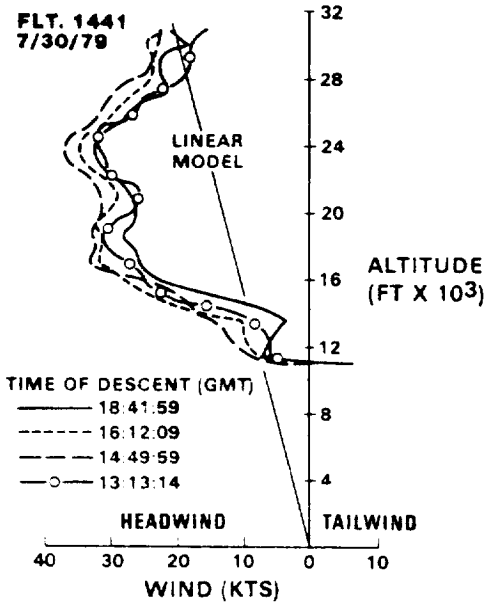

Figure 27. - Descent winds.

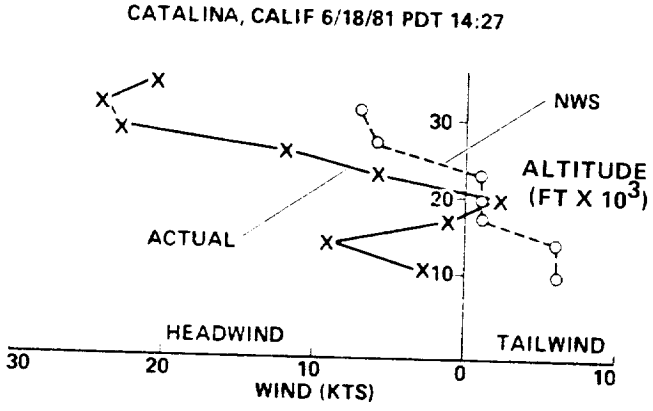

Figure 28. - Actual wind vs. NWS forecast winds.

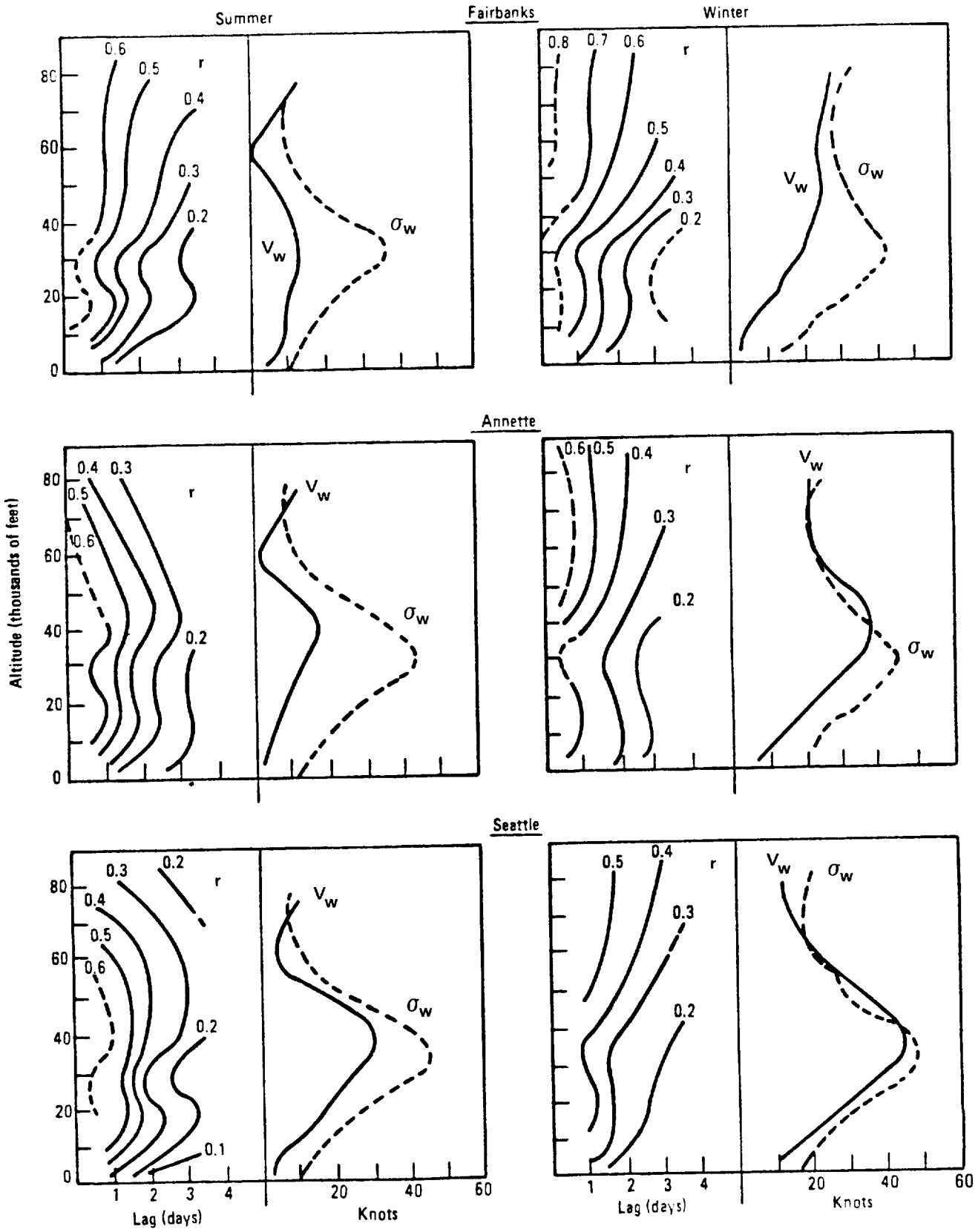

Figure 29. - Wind persistence data.

$$\sigma_{WL_i} = \sigma_{W_i} (1 - \rho^2_{ij})^{1/2} \qquad (8)$$

where σ_{W_i} is the climatological standard deviation at altitude level i, and ρ_{ij} is the correlation coefficient of wind at level i on level j. The correlation coefficient (ρ) for several geographical locations at different times of the year were compiled by NASA from earlier studies as given in references 12 and 13. Because of the large volume of data, ρ_{ij} was averaged by inspection and is shown in figure 31. The following equation is used to approximate ρ_{ij} as a function of cruise altitude (H_c) and descent altitudes (H_i).

$$\rho_i = -3.1 \times 10^{-5} H_i + 3.115 \times 10^{-9} H_i^2$$

$$+(1.165 \times 10^{-9} H_i - 7.231 \times 10^{-14} H_i^2)H_c \qquad (9)$$

To blend the forecast wind and linear wind, an estimation technique was used. The estimated wind velocity at altitude level i based on the two predictions is given by:

$$VW_i = \frac{\sigma^2_{WLi}}{\sigma^2_{WLi} + \sigma^2_{WFi}} VWF_i + \frac{\sigma^2_{WFi}}{\sigma^2_{WLi} + \sigma^2_{WFi}} VWL_i \qquad (10)$$

where VWF_i is the forecast wind velocity at altitude i and VWL_i is the wind velocity at altitude i as predicted by the linear wind model. Substituting equation (8) and (9) into equation (10), obtains:

$$VW_i = \frac{(1 - \rho^2_i)\ VWF_i + 2\ (1-r)VWL_i}{(1 - \rho^2_i) + 2(1 - r)} \qquad (11)$$

where r is given by equation 7, ρ_i is given by equation 9.

An example of the descent wind model is illustrated in figure 32, where the age of the forecast varied from 2 to 12 hours.

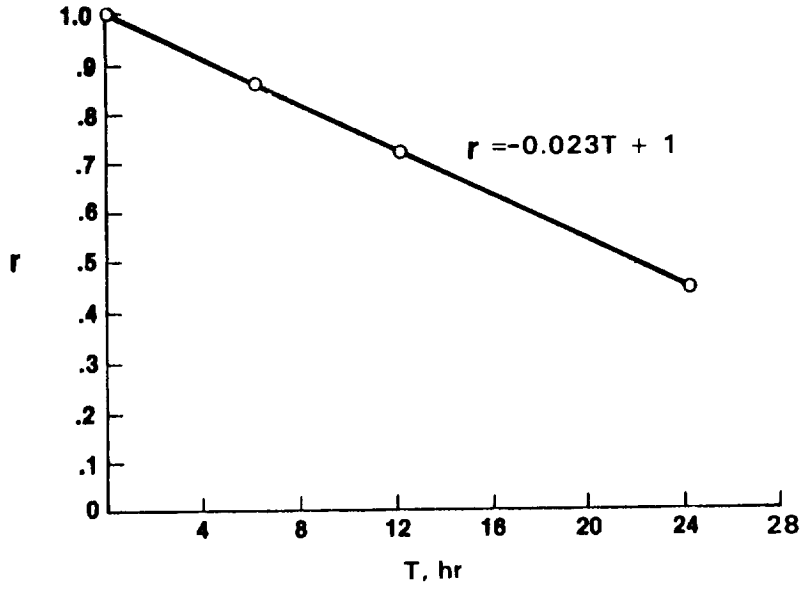

Figure 30. - Lag correlation coefficient of forecast wind.

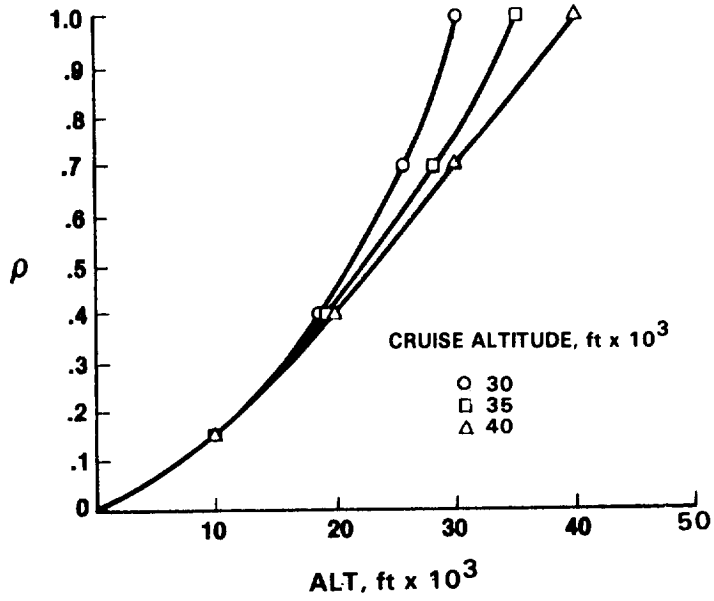

Figure 31. - Interlevel correlation coefficient of wind velocities.

To illustrate how this descent wind model will improve the accuracy of descent wind prediction, equation 11 was applied to the data of figure 28. Substituting the NWS forecast data and the linear wind predictions into equation 11, and using the age factor of 12 hours, the improved wind profile was calculated to be as shown in figure 33. When compared with the actual wind data, the improved method shows the least errors as compared to the linear wind method and the NWS forecasted data.

2.4.2 Cruise wind model.- The purpose of the cruise wind model is two-fold: (1) to provide a smooth transition between forecast waypoint wind velocities used by the guidance algorithms as the aircraft approaches the waypoint, and (2) to provide a more accurate wind estimation for each waypoint based on wind forecasts, and measurements made by on-board equipment. A simple wind model which can be easily incorporated into the FMS was developed based on spatial and time variabilities of wind velocity as reported in reference 14. The standard deviation of a wind forecast for a given location can be approximated by:

$$\sigma_t = 4\sqrt{T} \tag{12}$$

where T is the age of the forecast in hours. The variability of wind depends also on the distance between observation points. The standard deviation of wind velocity at a given waypoint predicted by on-board measurement is given by:

$$\sigma_{d_i} = 1.3\,\Delta D_i \tag{13}$$

where ΔD is the direct distance between the current aircraft position and the waypoint at which the wind is to be predicted. The estimated wind at waypoint i based on the two sources of measurement is given by:

$$VWP_i = \frac{\sigma_{d_i}^2}{\sigma_{d_i}^2 + \sigma_t^2} VWF_i + \frac{\sigma_t^2}{\sigma_{d_i}^2 + \sigma_t^2} VWM \tag{14}$$

where VWF_i is the forecast wind for waypoint i, and VWM is the measured wind at the current aircraft position. Substituting equations 12 and 13 into equation 14 results in:

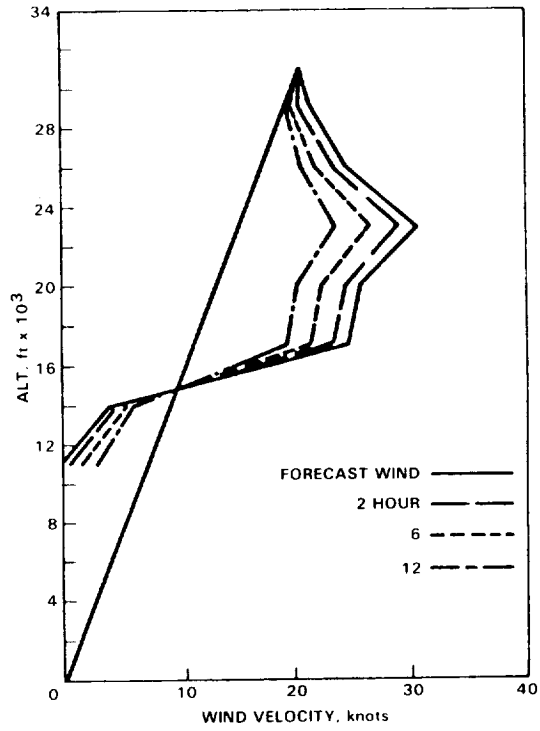

Figure 32. - Wind persistence model.

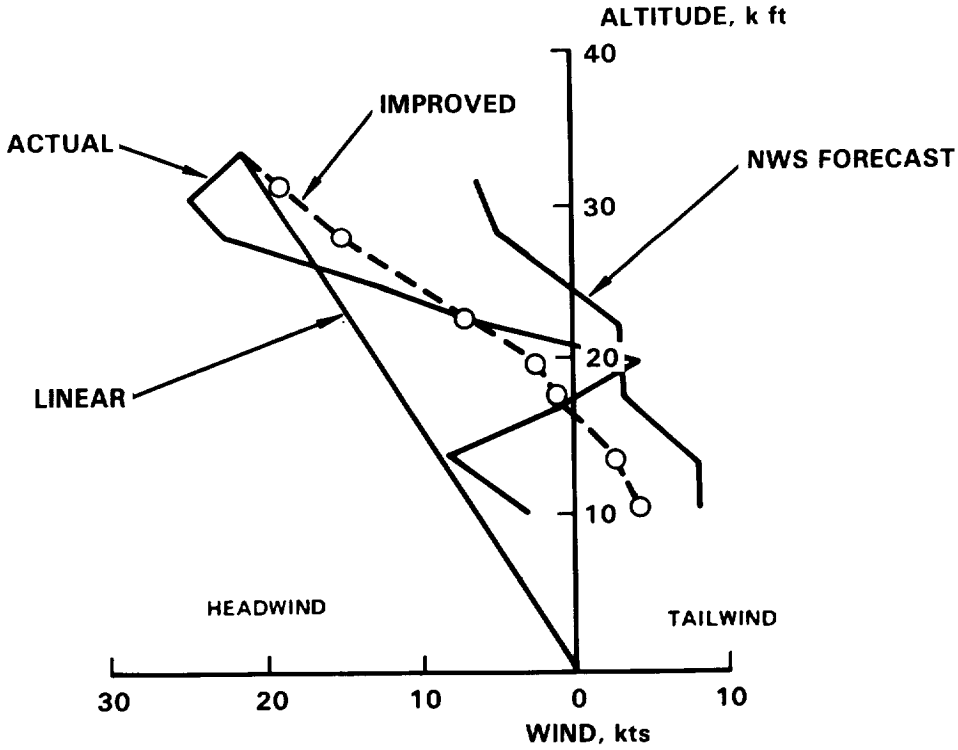

Figure 33. - Improved wind model vs. linear and forecast winds.

$$VWP_i = \frac{1.69\ (\Delta D_i)^2\ VWF_i + 16\ T\ VWM}{1.69(\Delta D_i)^2 + 16\ T} \tag{15}$$

Before this equation is applied, measured wind and forecast wind must be first resolved into north-south and east-west components by the following equations:

$$VWMx = VWM\ SIN\ (\psi WM)$$
$$VWMy = VWM\ COS\ (\psi WM)$$
$$VWFx_i = VWF_i\ SIN\ (\psi WF_i)$$
$$VWFy_i = VWF_i\ COS\ (\psi WF_i)$$

Using equation 14, the north-south and east-west components of the estimated wind at waypoint i are given by:

$$VWPx_i = \frac{1.69\ (\Delta D_i)^2\ VWFx_i + 16\ T\ VWMx}{1.69\ (\Delta D_i)^2 + 16\ T} \tag{16}$$

$$VWPy_i = \frac{1.69(\Delta D_i)^2 VWFy_i + 16\ T\ VWMy}{1.69\ (\Delta D_i)^2 + 16\ T} \tag{17}$$

The predicted wind heading with respect to true north for waypoint i is given by:

$$\psi WP_i = TAN^{-1}\ \frac{VWMx_i}{VWMy_i} \tag{18}$$

Figure 34 illustrates the effect of applying the cruise wind model.

2.5 4-D Guidance Algorithms

The 4-D guidance algorithms are those that provide the computation of a time-referenced flight path for guiding the aircraft to a metering fix under

ATC-imposed time and spatial constraints. These algorithms must support the tasks of selecting correct cruise and descent airspeed schedules, and generating airspeed, altitude, and range (longitudinal distance) commands for closed-loop control to make good the arrival time and spatial profile requirements.

The computational process of the guidance algorithms is illustrated in figure 35. The metering fix time assignment is given by ATC with the aircraft still at cruise altitude and some distance before the beginning-of-descent point (B*D). Upon receiving the time assignment, and using ATC published ground track and end-of-descent (E*D) airspeed restrictions, an iterative process is initiated to compute an airspeed profile. The profile consists of a constant Mach or CAS in the cruise region and one of several standard Mach/CAS schedules in the descent region. In addition to the required airspeeds, the B*D required time-of-arrival (RTA) and a 4-D descent trajectory defined by a table of altitude, range and time are generated and stored. This information is then used by the closed loop control laws for automatically guiding the aircraft to the metering fix, arriving at the ATC-imposed time objective.

In this section, the development of the 4-D descent trajectory model is described followed by a detailed treatment which relates the airspeed, ground track trajectory, wind, and flight time for the cruise region. The resulting descent and cruise algorithms are then combined to form a guidance algorithm for 4-D operation.

2.5.1 4-D descent trajectory modeling.- This section describes briefly the 4-D descent trajectory modeling techniques developed for the prototype 4-D descent demonstration. A more complete description of the descent trajectory equations can be found in reference 9. Methods for improving the accuracy of the model are also discussed and evaluated; these include:

- improved wind decay correction factor for the segmented wind model of section 2.4.1, and
- fine tuning the model to include the latest descent performance data of the test vehicle (L-1011 S/N 1001 with extended wing).

2.5.1.1 Computation of the 3-D descent profile: The FMS 3-D descent profile is generated in six segments, back-computed from the specified end-of-descent point (E*D), as shown in figure 36. The profile is established by sequential build-up of incremental ranges (Δr_i) and altitudes (Δh_i) for each of the six segments. Δh is set to a constant value of 500 feet except for the level flight segments and for segments transitioning to or from level flight. The corresponding Δr's are then computed as a function of Δh using prestored

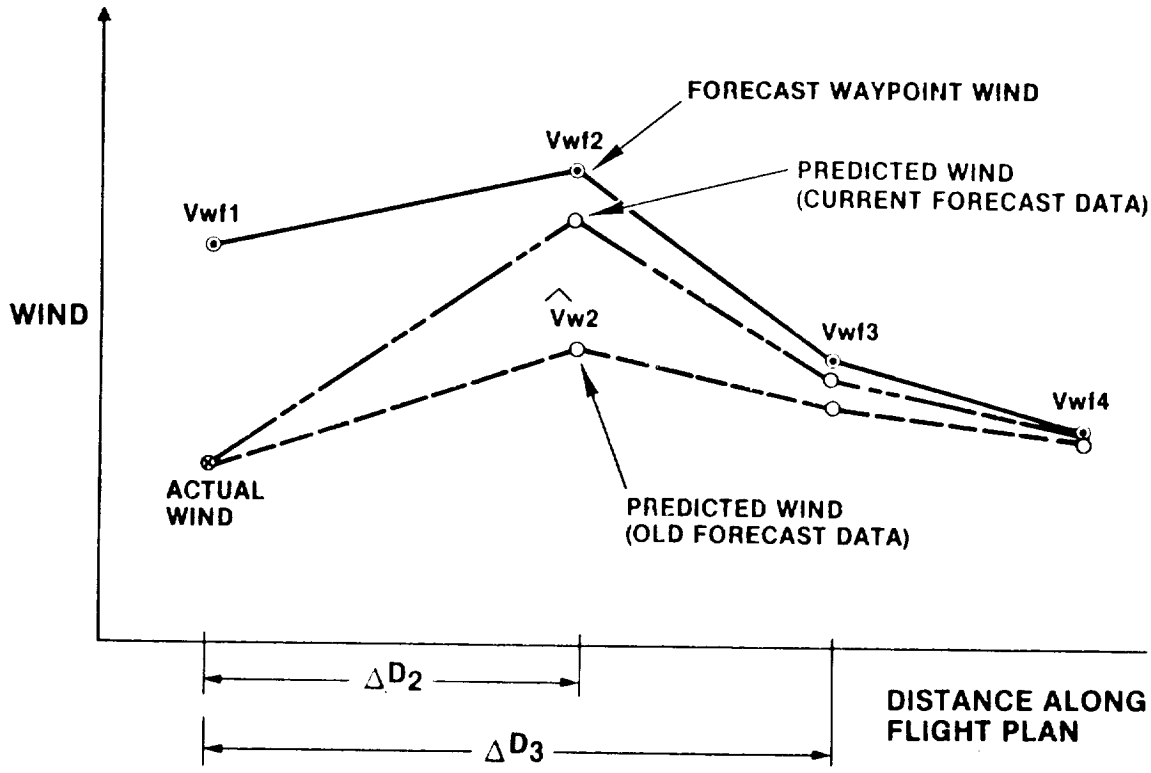

Figure 34. - Cruise wind prediction model.

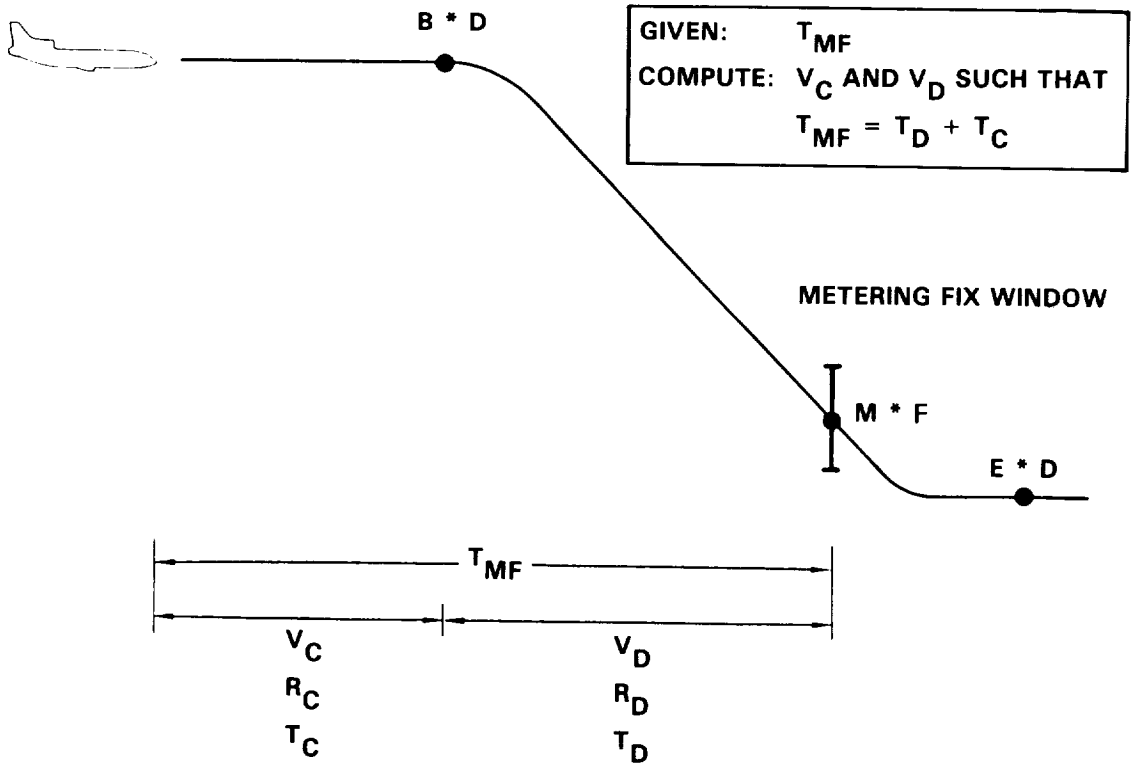

Figure 35. - 4-D guidance computational process.

polynomials determined from L-1011 aerodynamic data. The point at which the back-computed profile intersects cruise altitude is the beginning-of-descent point, or B*D. The calculated position of B*D is then automatically entered as a waypoint by the FMS computer program into the flight plan previously selected by the crew. The descent profile and the position of B*D are continually updated in flight to reflect current predictions of the descent entry initial conditions. The definition of B*D as a waypoint allows the program to calculate and display other desirable flight plan-related information, such as estimated time-of-arrival (ETA), course, distance, and time en route to B*D.

2.5.1.2 Computation of metering fix arrival time: In order to predict the time of arrival at the metering fix (M*F), the total time-in-descent is first computed. Then the ETA at M*F can be obtained by simply adding the time-in-descent between M*F and B*D to the estimated time-of-arrival at B*D:

$$\text{M*F ETA} = \text{B*D ETA} + \text{time-in-descent between M*F and B*D} \tag{19}$$

Total time-in-descent is determined by first calculating an incremental time (Δt_i) required to descend through each $\Delta h_i/\Delta r_i$ segment of the trajectory; the total time-in-descent is then the summation of these incremental times or

$$\text{Time-in-descent} = \Sigma \Delta t_i \tag{20}$$

The basic relationships used in the Δt_i computation are as depicted in figure 37.

With wind velocity (VW_i), true-air speed (VT_i), Δh_i and Δr_i given at the i-th altitude level, ground speed VGS_i and Δt_i are then computed:

$$VGS_i = VT_i \cos \gamma_i + VW_i$$

$$\Delta t_i = \frac{\Delta r_i}{1/2\ (VGS_i + VGS_{i+1})} \tag{21}$$

$$= \frac{2\Delta r_i}{(VT_i + VT_{i+1}) \cos \gamma_i + VW_i + VW_{i+1}} \tag{22}$$

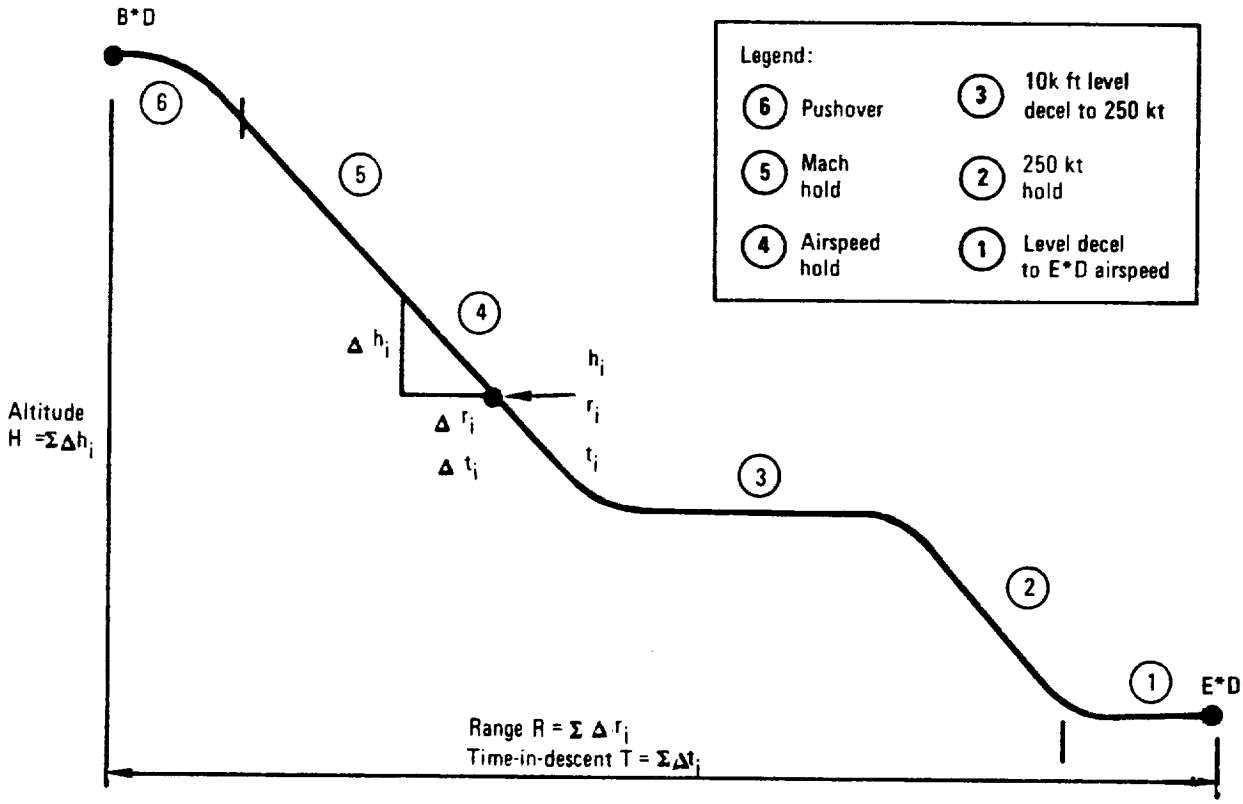

Figure 36. - Computation of 4-D descent profile.

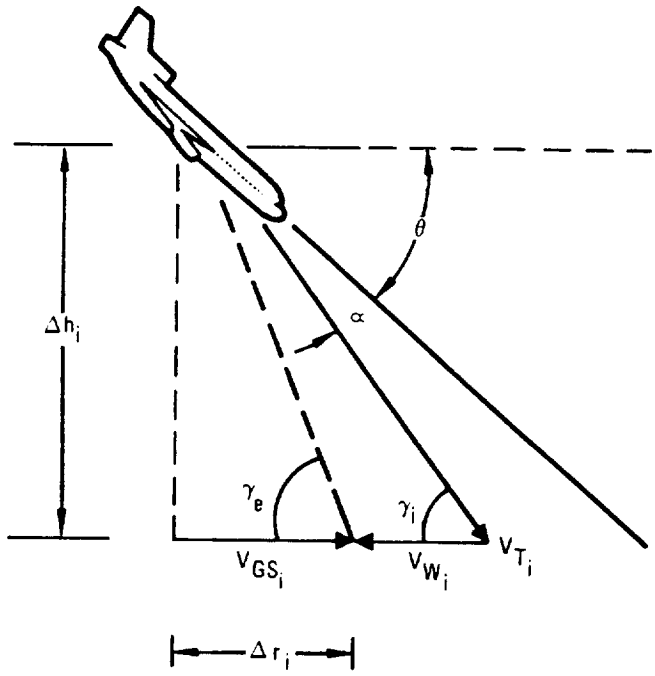

Figure 37. - Incremental segment relationships.

where Cos γ_i is approximated by the earth referenced path angle γ_e:

$$\text{Cos } \gamma_i \approx \text{Cos } \gamma_e = \frac{\Delta r_i}{\sqrt{\Delta h_i^2 + \Delta r_i^2}} \tag{23}$$

This approximation, used because the wind-referenced path angle γ_i was not calculated by the existing FMS software, results in an open-loop error of 2 seconds or less, and therefore had negligible effect on the closed-loop performance of the system.

2.5.1.3 Wind decay correction: The production FMS descent trajectory algorithm only accepts a linear wind profile. Wind decay effects are estimated by a constant correction coefficient averaged over the entire descent profile. In order to take maximum advantage of the segmented wind profile developed earlier, the FMS algorithm was modified by using a more accurate wind decay correction coefficient taking into consideration each region of the descent trajectory.

The FMS descent trajectory is generated by computing incremental ranges every 500 feet by the equation

$$\Delta R = \Delta R_0 (1 + \frac{VW}{VTAS})(1 + \text{Kws } \frac{dVW}{dh}) \tag{24}$$

where ΔR_0 is the zero wind incremental range which is the function of various parameters such as weight, temperature, and speed schedule. ΔR_0 is then corrected for the effects of wind and wind-decay by the terms

$$(1 + \frac{VW}{VTAS}) \qquad \text{and}$$

$$(1 + \text{Kws } \frac{dVW}{dh}) \tag{25}$$

respectively. Currently, Kws is set to a constant average value of 29 ft/knot over the entire descent. For a more accurate result, Kws was evaluated over each of the three regions of the descent as follows:

- Constant Mach region, altitude greater than 36,090 ft

$$Kws = \frac{Mach \times C \times K}{g} \tag{26}$$

- Constant Mach region, altitude less than or equal to 36,090 ft

$$Kws = \frac{Mach \times C \times K}{g}\left(\frac{1}{1 - .133\ Mach^2}\right) \tag{27}$$

- Constant CAS region

$$Kws = \frac{Mach \times C \times K}{g}\left(\frac{1}{1 - .133\ Mach^2 + \left(\frac{Mach^2}{5} + 1\right) - \left(\frac{Mach^2}{5} + 1\right)^{-5/2}}\right) \tag{28}$$

where C is speed of sound, g is equal to 32.2 ft/sec^2, and K is equal to 1.688 ft/sec/kt.

These equations were computed over the entire descent region for all descent speeds and are given in figures 38 through 40. For implementation into the FMS software, the results were curve fitted using the following expressions:

- Constant Mach region, altitude greater than 36,090 ft

$$Kws = 50.76\ Mach - .0132 \tag{29}$$

- Constant Mach region, altitude H less than or equal to 36,090 ft

$$Kws = -.2039\ \frac{H}{1000} + 68.72\ Mach - 3.264$$

- Constant CAS region

$$Kws = .2596\ \frac{H}{1000} + .06168\ CAS + 5.515$$

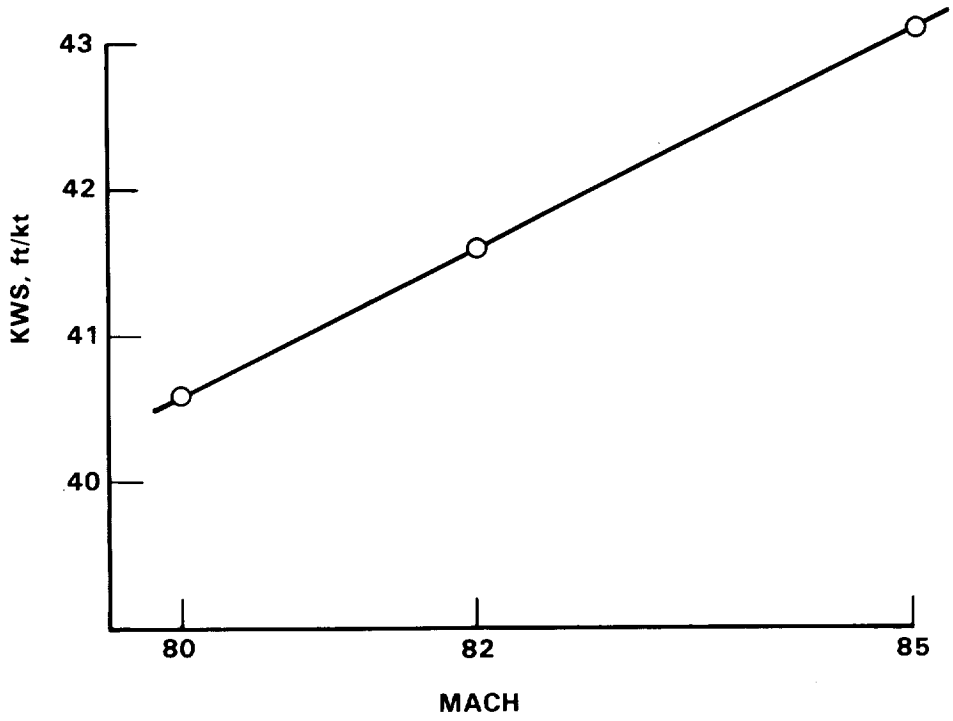

Figure 38. - Wind decay correction factor, constant Mach region, altitude > 36,090 ft.

2.5.1.4 Addition of low-speed descent profiles: Three descent speed schedules are used in the existing production FMS software: 0.80 Mach/300 kts IAS, 0.82/320, and 0.85/350. The flexibility analysis of Section 2.3 indicated that an additional one to two minutes of time flexibility can be obtained by adding slower descent speed schedules. The two additional schedules selected were 0.80/280 and 0.80/255.

2.5.1.5 3-D descent trajectory modeling improvement: The flight tests conducted with the prototype system were performed with less-than-optimal modeling of the aircraft's propulsion and aerodynamic characteristics (reference 9). Most descents were flown with a mixed engine configuration of both RB.211-22B and RB.211-524B4 engines which have differing thrust ratings. Other errors were introduced because the flight test aircraft had recently been fitted with extended wing tips to support the development and flight test of the Active Control System. These factors contributed trajectory modeling errors because the descent trajectory model used was for an L-1011-200 production aircraft having a standard wingspan and a full complement of the higher thrust -524B4 Rolls Royce engines.

For better matching of descent performance with the test vehicle, theoretical descent trajectories were first calculated by the Lockheed L-1011 Mission Analysis Program. Aerodynamics data for L-1011 S/N 1001 with extended wing and propulsion data for the -22B engine and the -524B engines were used.

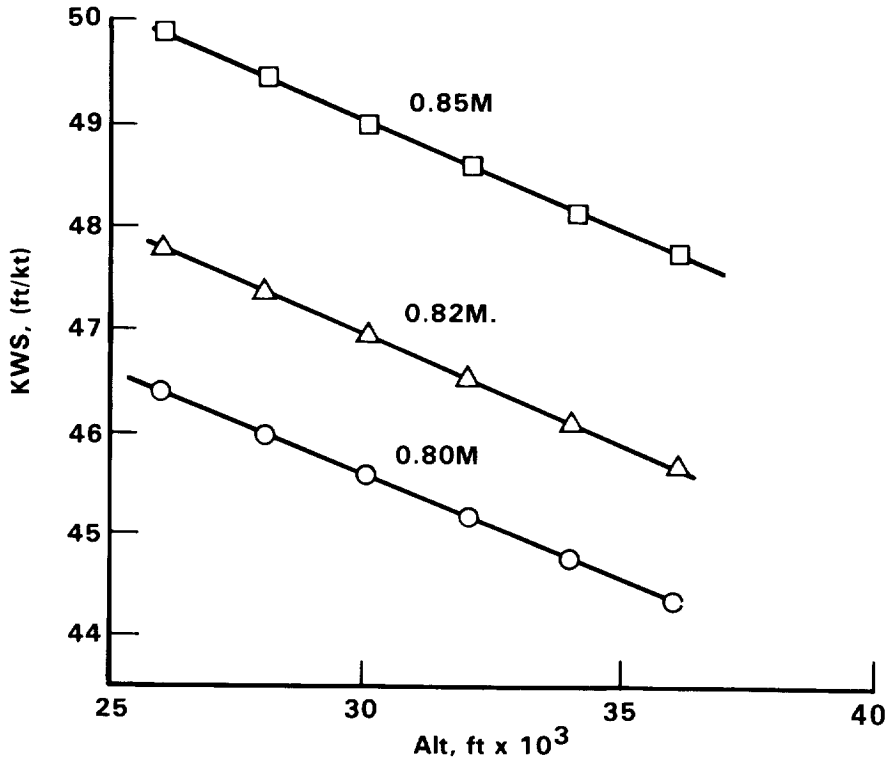

Figure 39. - Wind decay correction factor, constant Mach region, altitude $\leq$ 36,090 ft.

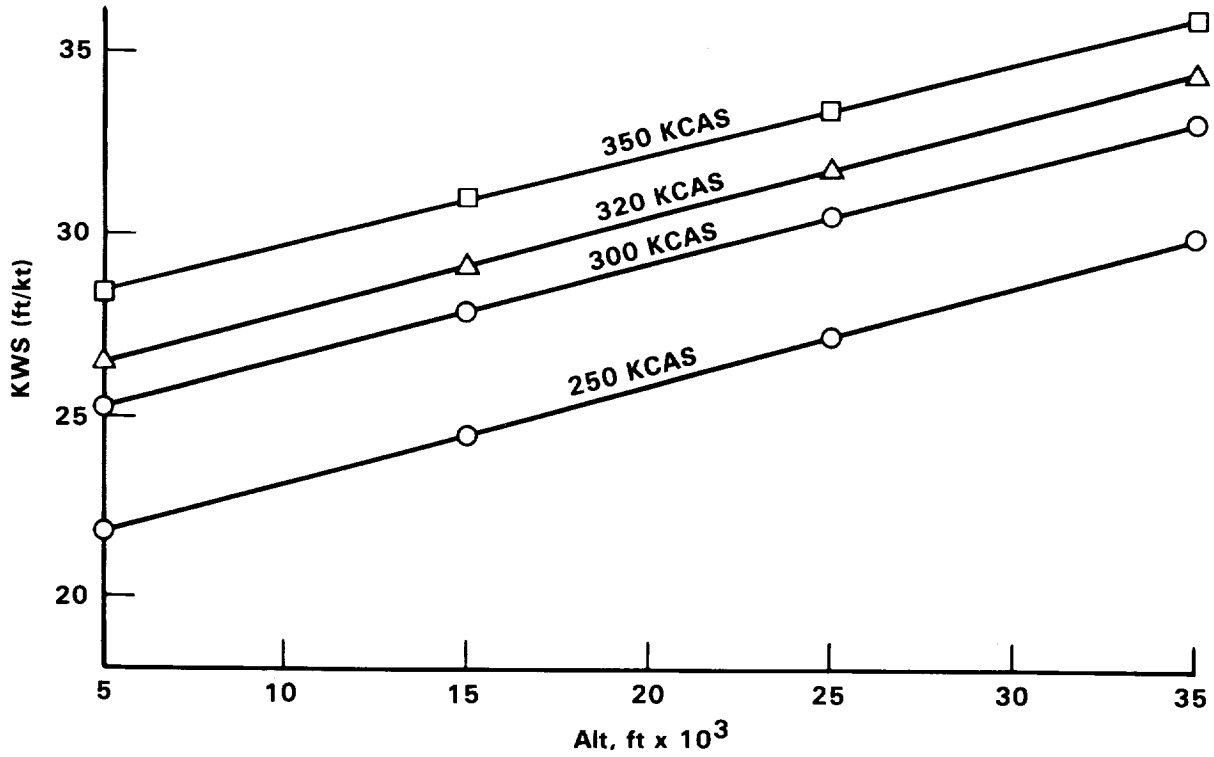

Figure 40. - Wind decay correction factor, constant CAS region.

The resulting trajectories were then curve fitted by an existing program. The polynominal coefficients were input into a computer program developed to simulate the FMS descent profile software. The resulting errors between the theoretical trajectories and the curve fitted trajectories were found to be small, generally less than 5 percent. Differences between the descent performance for the -22B and -524B4 engine were found to be small; figure 41 show a typical comparison. Differences in descent times and ranges between the two engine types were generally within curve fitting errors; therefore, no efforts were made to curve fit the descent trajectories for the newer -524B engines.

In August 1981, three open-loop descents of 0.80/255/250, 0.82/320/250 and 0.85/350/250 were flown on the L-1011 test vehicle to validate the theoretical descent performance. Descent conditions matching the flight test data were then input into the simulation program and the results compared against the flight test data as shown in figure 42 through 44. The performance errors are summarized in table I. The errors are small and should be correctable with the closed-loop control laws.

2.5.2 4-D cruise guidance algorithm.- The metering fix time assignment is usually "frozen" by ATC when an aircraft is at cruise altitude and some 50 to 100 n.mi. before beginning its descent. To achieve maximum time flexibility and optimal fuel operation, it is always desirable to deal with arrival time assignments as soon as they are known (to leave open other alternatives for dealing with the unknown). An algorithm to accurately relate cruise airspeed, ground track trajectory and elapsed flight time is therefore needed.

In this section, an algorithm is presented for determining the airspeed needed to fly the ATC restricted ground track in a specified elapsed time. The algorithm is based on the research reported by Foudriat (reference 15) where a general solution using an elliptic integral approximation which relates flight time, aircraft airspeed, and ground distance on straight-line and circular-arc trajectory segments was developed. The solution is applicable to both constant and accelerating aircraft flight with the presence of constant wind and wind-shear. Here, Foudriat's procedure is simplified by neglecting the accelerating flight and wind-shear equations. The omission of acceleration equations greatly simplified the algorithm and was justified by a study concluding that the resulting airspeed errors were generally small with the typical cruise distance for 4-D descent operations; the resulting time errors can be nulled by the feedback control laws presented in Section 2.6.3. Quantitative wind-shear information is generally not available for flight planning and was therefore not considered in this study.

2.5.2.1 Ground track description: For the application of the 4-D cruise algorithm, the flight plan is presented as an N-segment ground track as illustrated in figure 45. Each segment can contain a straight-line portion and a circular arc portion representing the aircraft's turn radius. When a segment does not contain a circular-arc portion, the turn radius is set equal to zero; likewise, the straight-line distance is set equal to zero when a segment does

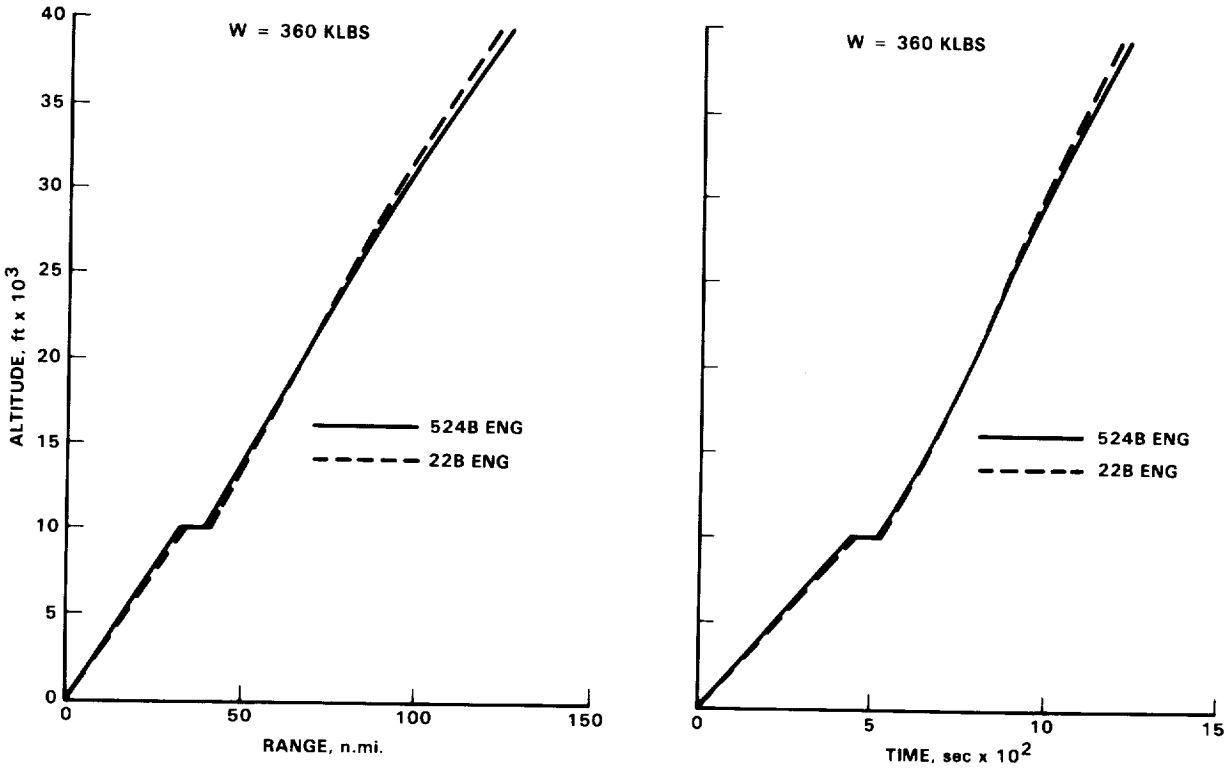

Figure 41. - 22B and 524B engines descent performance comparison.

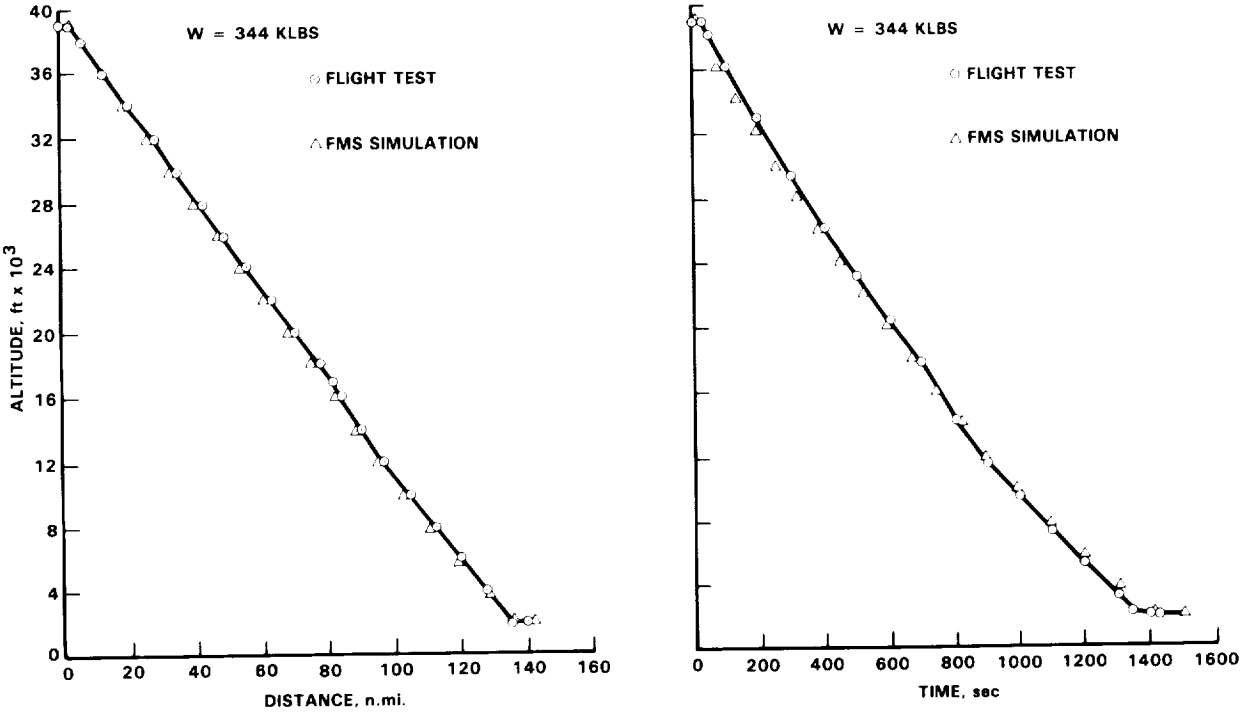

Figure 42. - Theoretical and flight test descent profile comparison, 0.8/255/250 descent.

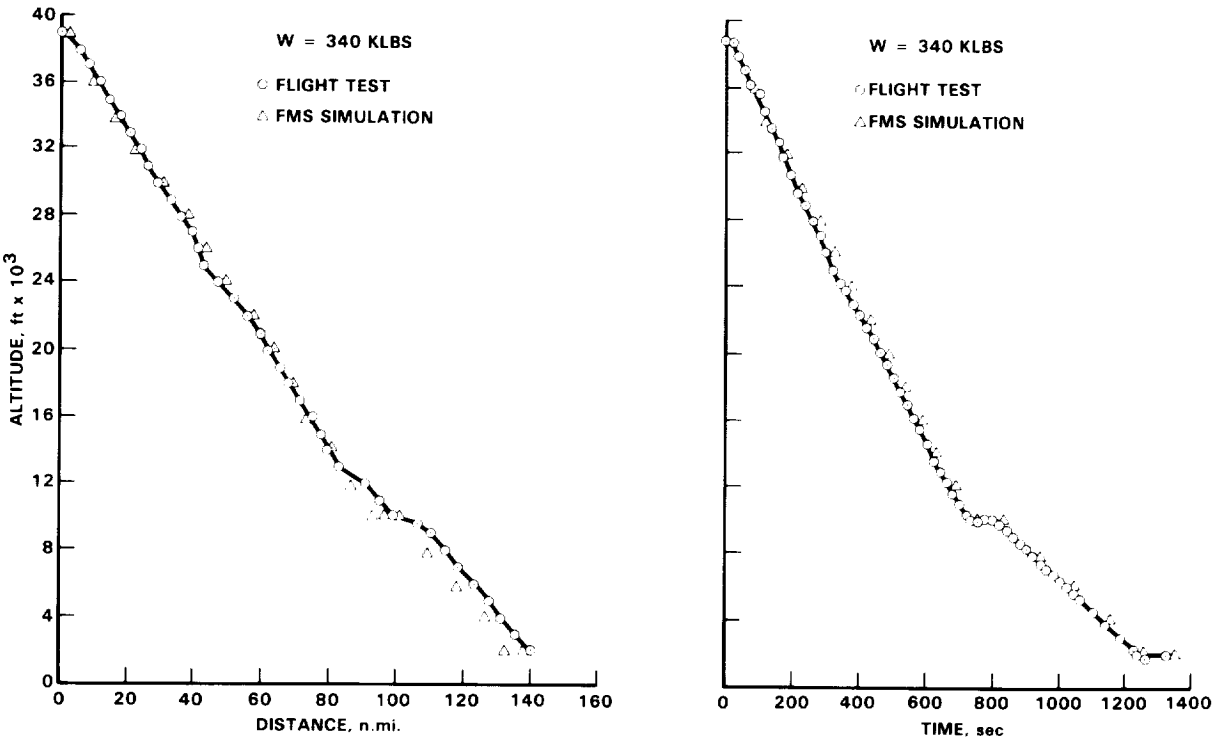

Figure 43. - Theoretical and flight test descent profile comparison, 0.82/320/250 descent.

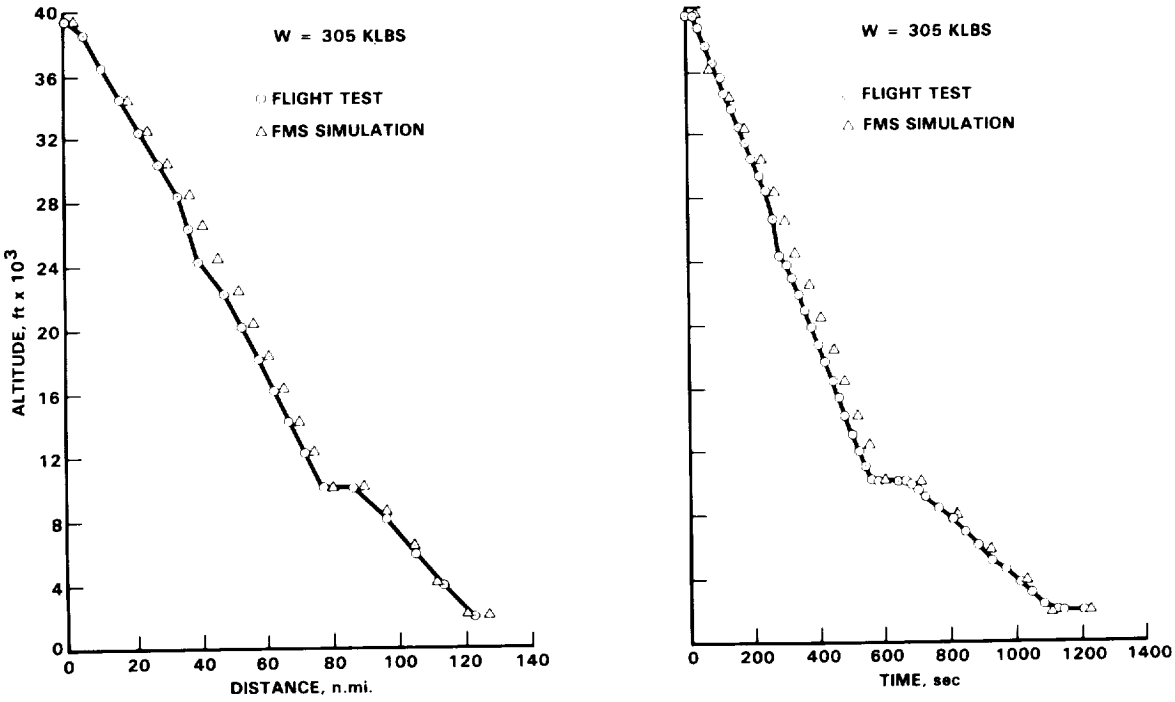

Figure 44. - Theoretical and flight test descent profile comparison, 0.85/350/250 descent.

TABLE I. - FLIGHT TEST AND FMS DESCENT MODEL COMPARISON

Descent Schedule	Total n.mi. Range	Total Time, sec	Time Error Std Deviation, sec	Range Error n.mi. Std Deviation
0.80/255/250	139	1508	24.5	1.71
0.82/320/250	138	1350	19.3	3.80
0.85/350/250	127	1218	32.3	3.30

not contain a straight-line portion. Each segment begins and ends with a waypoint. The first waypoint in the cruise flight plan is the current aircraft position; the last waypoint is the beginning of descent (B*D).

The following ground track parameters are required for the cruise algorithm:

(1) D distance for straight-line portion,

(2) R turn radius for circular-arc portion,

(3) ψg ground track heading

(4) VWP predicted wind speed at waypoints,

(5) ψWP predicted wind heading at waypoints,

(6) VW wind speed along straight-line portion, and

(7) ψW wind heading along straight-line portion

Using the latitude and longitude coordinates of each waypoint, the total distance between waypoints and the ground track heading (ψg) of each leg are calculated by the FMS computer's navigation software. The turn radius (R) and the straight-line distance (D) can be calculated by computing the track capture anticipation distance Dcap as shown in figure 46. The straight-line distance D_i and D_{i+1} (for the i-th and i+1-th waypoints) are calculated by subtracting Dcap from the total distance between the waypoints as shown. Calculation of Dcap is obtained from production FMS software and is given by the equation:

$$Dcap = \frac{Vg^2 \ COT(Bmax)}{Kg} \ TAN \ \frac{\Delta\psi g}{2} + \frac{Vg \ t}{3600} \qquad (32)$$

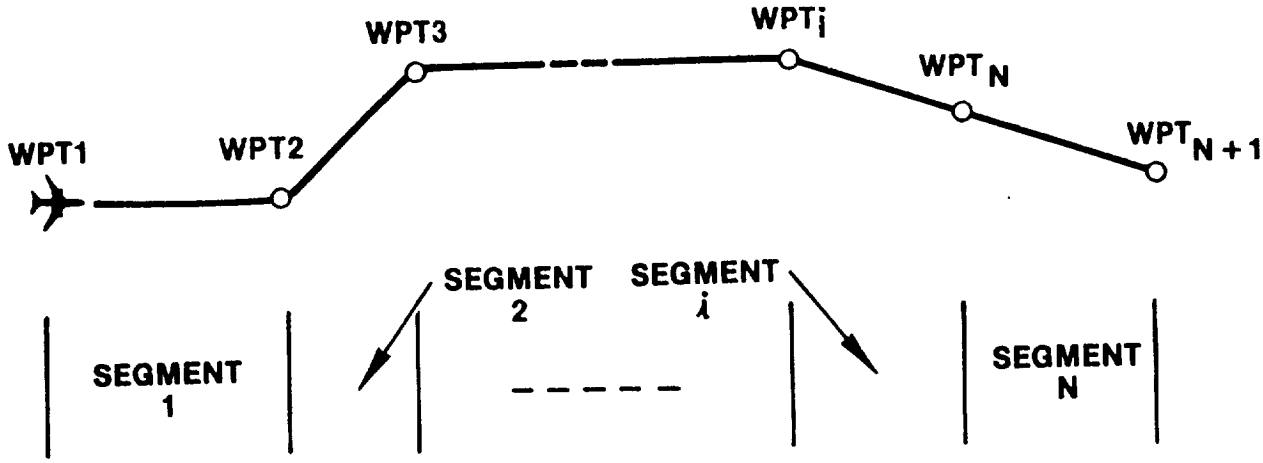

Figure 45. - Ground track trajectory representation.

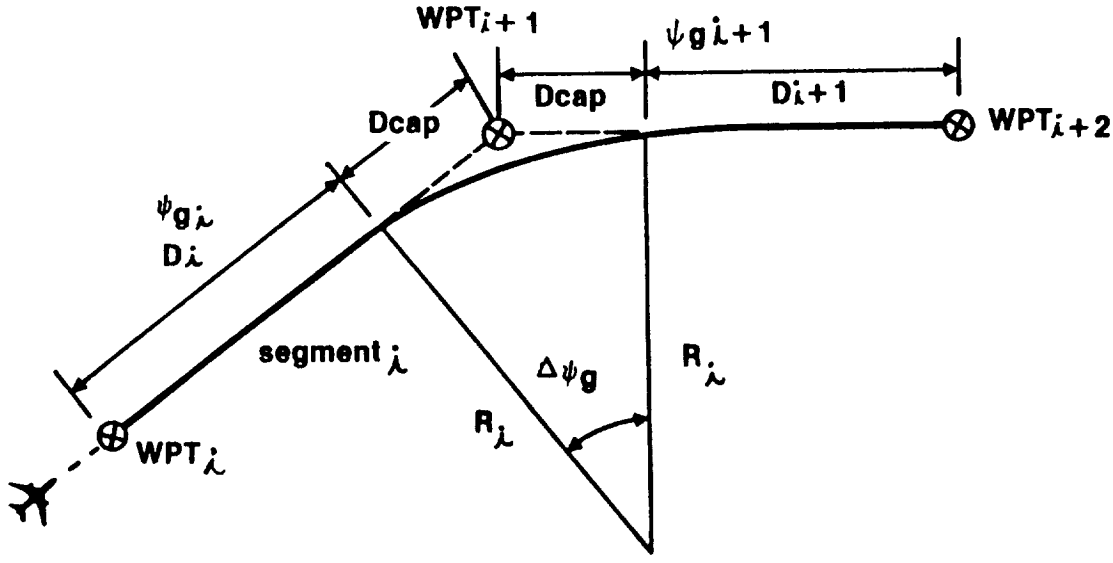

Figure 46. - Computation of straight-line distance and turn radius.

Turn radius is given by:

$$R = \frac{Dcap}{TAN\ (\Delta\psi g/2)} \tag{33}$$

where:

Vg = predicted ground speed, knots

$Bmax$ = maximum bank angle, 20 degrees for cruise flight

$\Delta\psi g = \psi g_{i+1} - \psi g_i$

$g = 32.2\ ft/sec^2$

t = 15 seconds forced additional time

$$K = \frac{3600^2\ (sec/hr)^2}{6076\ \ (ft/n.mi)} = 2132.95\ sec^2\text{-}nm/ft/hr^2$$

The wind speed (VWP) and direction (ψWP) at each waypoint are predicted by the cruise wind model developed in Section 2.4.2. Wind speed (VW) and direction (ψW) for the straight-line portion of a segment is derived by averaging the wind velocities of its associated waypoints as illustrated in figure 47.

From figure 47, the north-south and east-west components of the wind at a waypoint are given by:

$$VWPy = VWP\ COS\ (\psi WP) \tag{34}$$

$$VWPx = VWP\ SIN\ (\psi WP) \tag{35}$$

The north and east components of the wind along straight-line segment i are obtained by:

$$VWx_i = (VWPx_{i+1} + VWPx_i)/2 \tag{36}$$

$$VWy_i = (VWPy_{i+1} + VWPy_i)/2 \tag{37}$$

The wind speed at segment i is given by:

$$VW_i = \sqrt{(VWx_i^2 + VWy_i^2)} \tag{38}$$

The wind heading of segment i is given by:

$$\psi W_i = TAN^{-1} \frac{VWx_i}{VWy_i} \tag{39}$$

2.5.2.2 Equations relating constant airspeed flight: The relationship between ground velocity, wind velocity and aircraft airspeed is illustrated in figure 48. The ground speed of an aircraft in the presence of wind is given by the equation:

$$Vg = Vu \left\{[1 - A^2 \, SIN^2 \, (Z)]^{1/2} + A \, COS \, (Z)\right\} \tag{40}$$

where:

$$A = \frac{VW}{Vu}$$

$$Z = \psi g - \psi W$$

Vu = true airspeed

Time required to traverse distance D_i in the straight-line portion of segment i is given by:

$$t_i = 3600 \frac{D_i}{Vg_i} \tag{41}$$

Substituting Vg_i from equation 2.5.1 results in:

$$t_i = \frac{3600 \, D_i}{Vu} f_2(A_i, Z_i) \tag{42}$$

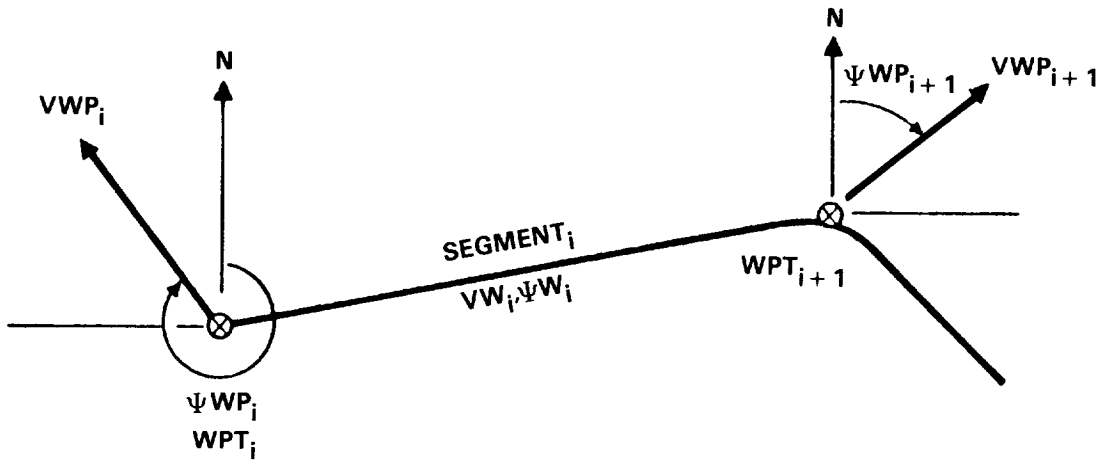

Figure 47. - Wind average for straight-line segment.

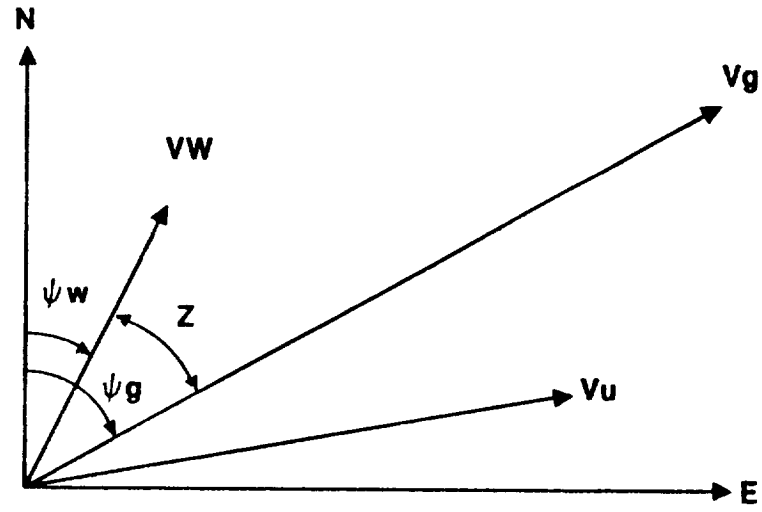

Figure 48. - Ground speed vector.

where:

$$f_2(A_i, Z_i) = \frac{1}{[1-A_i^2 \ SIN^2 \ (Z_i)]^{1/2} + A_i \ COS(Z_i)} \tag{43}$$

$$A_i = \frac{VWi}{Vu}$$

$$Z_i = \psi g_i - \psi W_i$$

During circular flight, the heading change rate is given by:

$$\frac{d\psi gi}{dt} = \frac{57.3}{3600} \left(\frac{Vg_i}{R_i}\right) \tag{44}$$

Substituting Vg from equation 39 and integrating to obtain t'_i:

$$t'_i = \frac{3600}{57.3} \left(\frac{R_i}{Vu}\right) \int_{\psi g_i}^{\psi g_{i+1}} \frac{d\psi_g}{[1 - A_i^2 \ SIN^2 \ (Z_i)]^{1/2} + A_i \ COS \ (Z_i)} \tag{45}$$

Rearranging variables:

$$t'_i = \frac{3600}{57.3} \left(\frac{R_i}{Vu}\right) \int_{Z_i}^{Z_{i+1}} \frac{[1-A_i^2 \ SIN^2 \ (Z)]^{1/2} + A_i \ COS \ (Z)}{(1 - A_i^2)} \ dZ \tag{46}$$

The integral is in the form of an incomplete elliptic integral of the second kind. The approximate solution of this integral is given by:

$$f_1 \quad (A_i, Z_{i+1}, Z_i) =$$

$$\left\{ \frac{1}{1-A_i^2} \ (1 - \frac{A_i^2}{4} - \frac{3}{64} A_i^4) \ \frac{Z}{57.3} - A_i SIN(Z) + \frac{1}{8} (A_i^2 + \frac{A_i^4}{4}) \ SIN(2Z) - \right.$$

$$\left.\frac{A_i^4}{256}\,\mathrm{SIN}(4Z)\right\}\Bigg|_{Z_i}^{Z_{i+1}} \tag{47}$$

The time required to traverse a circular-arc under constant airspeed is given by:

$$t'_i = \frac{3600}{57.3}\left(\frac{R_i}{Vu}\right) f_1\,(A_i,\ Z_{i+1},\ Z_i) \tag{48}$$

where:

$$Z_{i+1} = \psi g_{i+1} - \psi WP_{i+1}$$

$$Z_i = \psi g_i - \psi WP_{i+1}$$

$$A_i = \frac{VWP_{i+1}}{Vu}$$

$f_1\,(A_i,\ Z_{i+1},\ Z_i)$ is as given by equation (47)

Note: The wind speed (VWP) and wind heading (ψWP) in the above expressions are the wind at the (i+1)th waypoint.

2.5.2.3 Iterative process for computing required airspeed: Total time required to traverse all N segments of a cruise trajectory is the summation of all t_i's given by equation 47 for straight-line flight and by equation 48 for circular-arc flight; i.e.:

$$Tc = \sum_{i=1}^{N}\left[\frac{3600\ D_i}{Vu}\ f_2\,(A_i,\ Z_i) + \frac{3600}{57.3}\left(\frac{R_i}{Vu}\right) f_1\,(A_i,\ Z_{i+1},\ Z_i)\right] \tag{49}$$

When time Tc is specified, constant airspeed Vu can be obtained by an iterative process. Solving for Vu from the above expression, the (k+1)th iterative solution of Vu is given by the equation:

$$Vu^{(k+1)} = \frac{3600}{Tc}\sum_{i=1}^{N}\left[D_i f_2(A_i^{(k)},\ Z_i) + \left(\frac{R_i}{57.3}\right) f_1(A_i^{(k)},\ Z_{i+1},Z_i)\right] \tag{50}$$

where:

Tc = required flight time in seconds

The variables A and Z and the functions f_1 and f_2 are defined in equations 43 and 47.

A computer program was developed to evaluate the convergent property of equation 50. The simplified logic flow chart of the program is shown in figure 49. The test trajectory and wind condition are summarized in table II, and illustrated in figure 50. The time required to traverse the ground trajectory was set to 1300 seconds. The algorithm took three iterations to converge from the initial airspeed of 458.0 knots to 480.9 knots. The rapid convergence rate illustrated by the test trajectory concludes that the algorithm is suitable for application of real-time 4-D flight guidance and control.

2.5.3 Algorithm for computing descent and cruise airspeeds.- For 4-D operation as illustrated in figure 51, the airborne flight management algorithm must be able to select the required cruise and descent speeds to satisfy the following requirements:

- ATC published ground track
- B*D location and required time of arrival (RTA)
- 4-D descent trajectory as defined by a table of altitude, range and time
- metering fix arrival time
- E*D location
- E*D airspeed

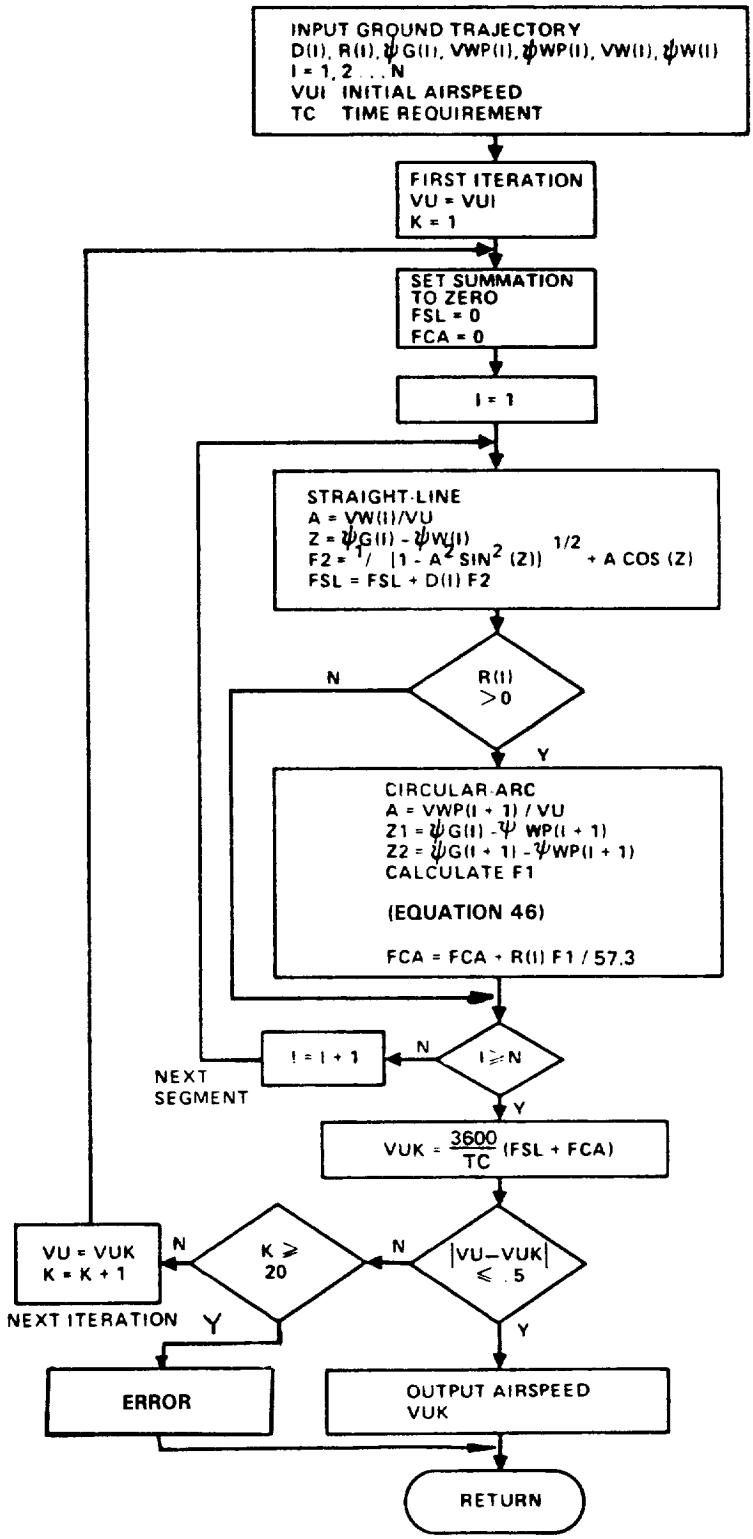

Figure 49. - Logic flow for cruise speed determination.

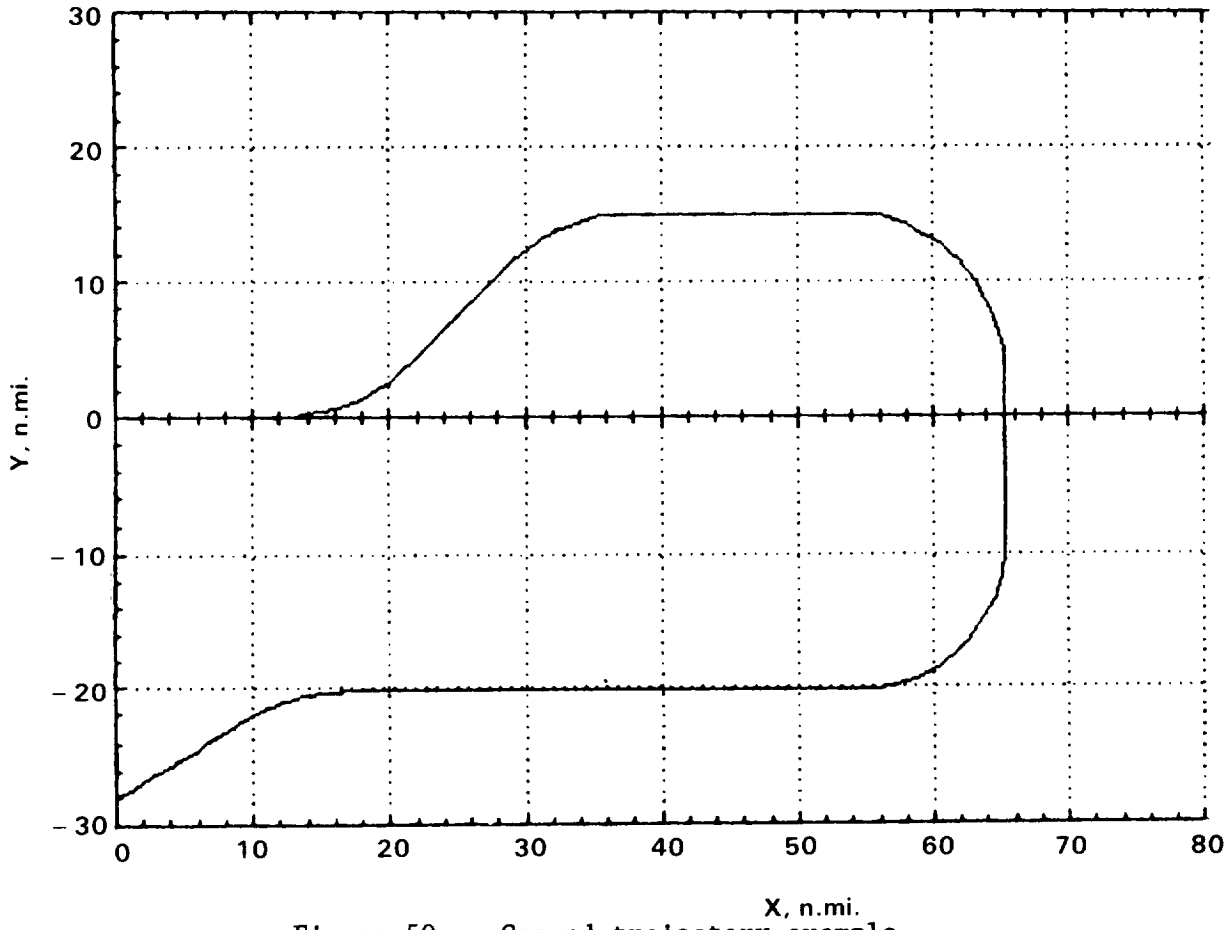

Figure 50. - Ground trajectory example.

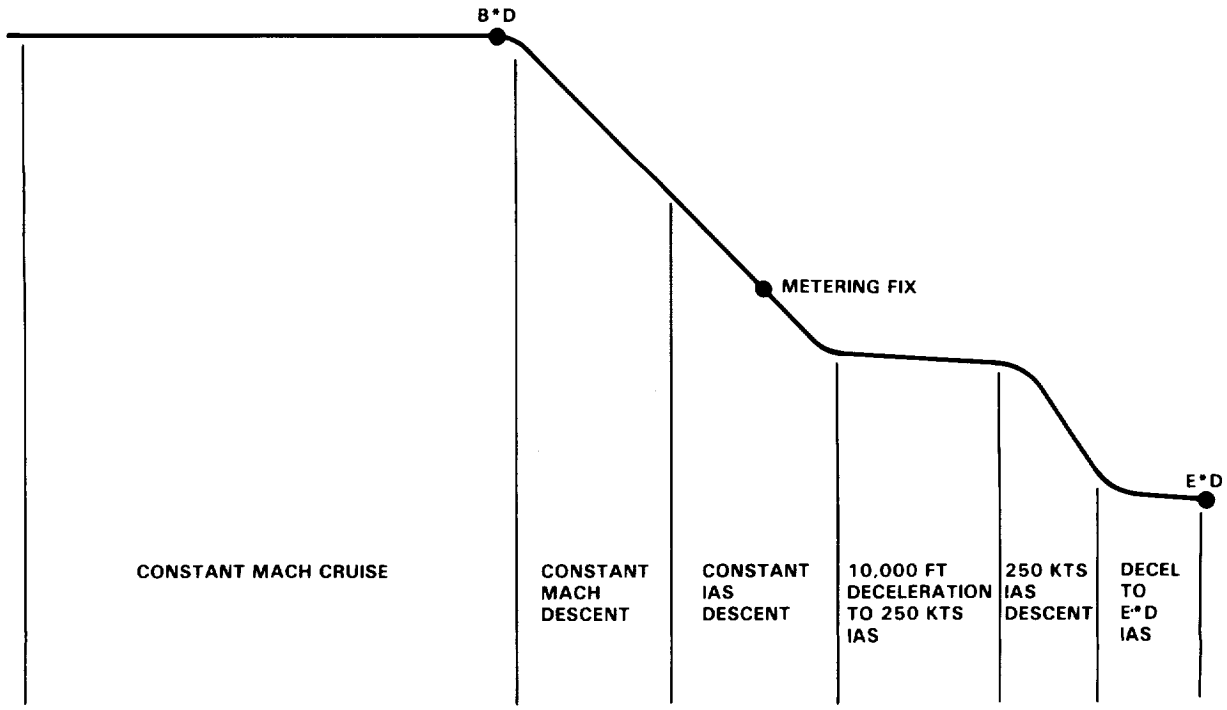

Figure 51. - 4-D profile descent vertical plane geometry.

TABLE II. - TEST TRAJECTORY

Segment	Straight-Line Distance (n.mi.)	Turn Radius (n.mi.)	Ground Heading (deg)	Wind Speed (kts)	Wind Heading (deg)
1	17.5	15.0	90	20	45
2	21.2	15.6	45	30	50
3	32.5	13.2	90	40	80
4	35.0	12.2	180	50	110
5	27.5	0	270	60	120
6	25.0	15.7	270	50	150
7	14.6	0	239	40	180
8	0	0	239	30	180

Figure 52 shows the logic flow of the algorithm. Descent and cruise speeds are computed iteratively when the metering fix arrival time is specified.

The algorithm begins by calculating the necessary ground track parameters and the descent and cruise wind predictions. Minimum and maximum flight times to the metering fix are then computed using the aircraft's maximum and minimum descent and cruise airspeeds (0.85/355/250 and 0.80/255/250 for descent, and 0.86 Mach and 0.78 Mach for cruise). The ATC specified flight time to the metering fix is then tested by the inequality

$$Tmax \geq Tmf \geq Tmin \tag{51}$$

to ensure that cruise and descent airspeeds are within the operational limits of the aircraft. The iterative process begins with the initial descent airspeed schedule of 0.82/320/250. B*D location and descent time Td are calculated. The cruise time requirement is then determined by:

$$Tc = Tmf - Td \tag{52}$$

Knowing B*D location and the cruise time requirement, cruise airspeed is calculated by the methods developed in Section 2.5 and shown in Figure 52. The resulting cruise speed is then tested against the inequality

$$.78 \text{ Mach} \leq Vc \leq .86 \text{ Mach} \tag{53}$$

If this inequality is satisfied, the process has converged and the computation ends.

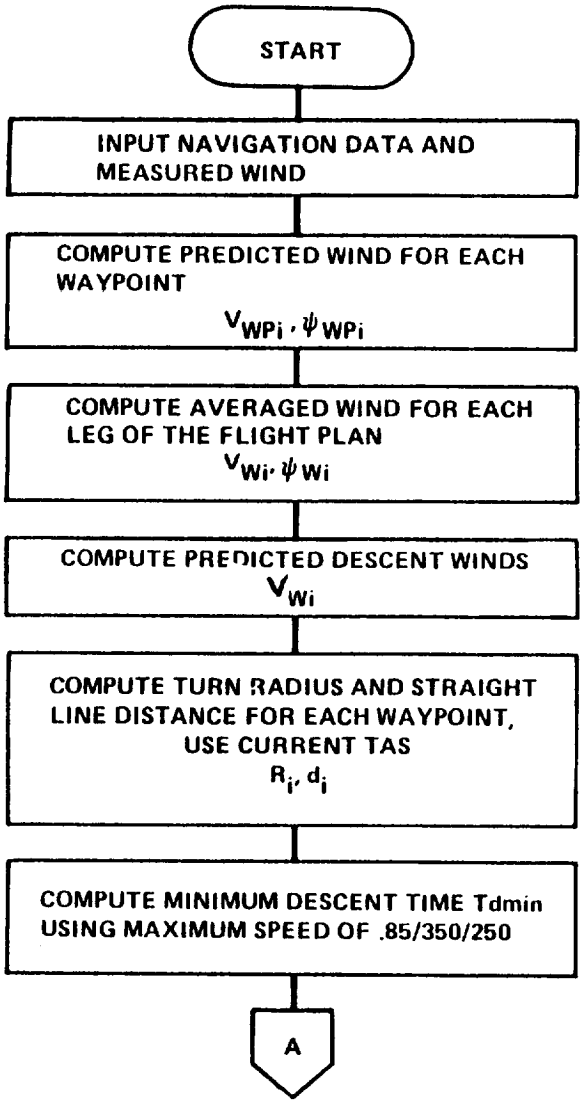

Figure 52. - Descent and cruise airspeed logic flow chart.

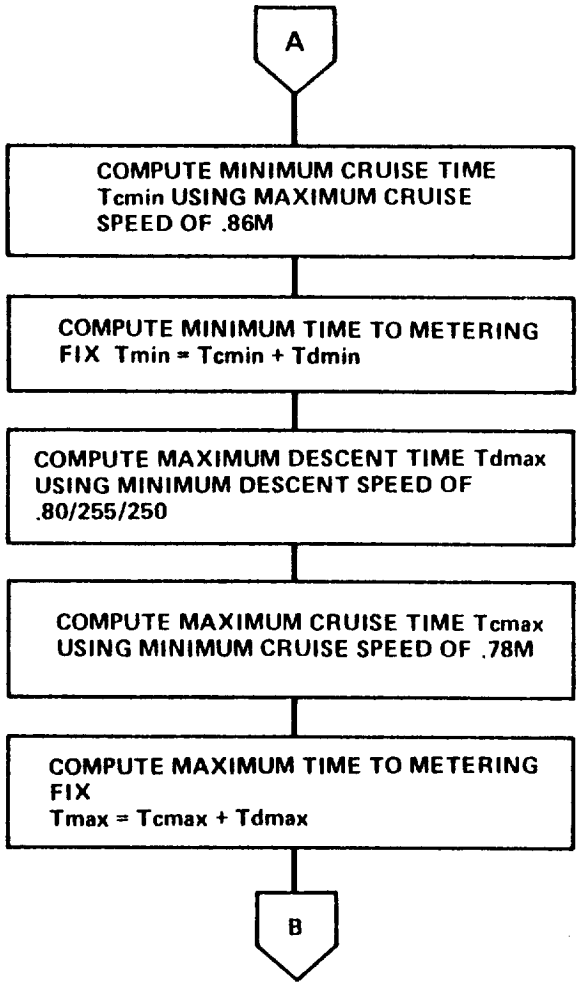

Figure 52. - Continued.

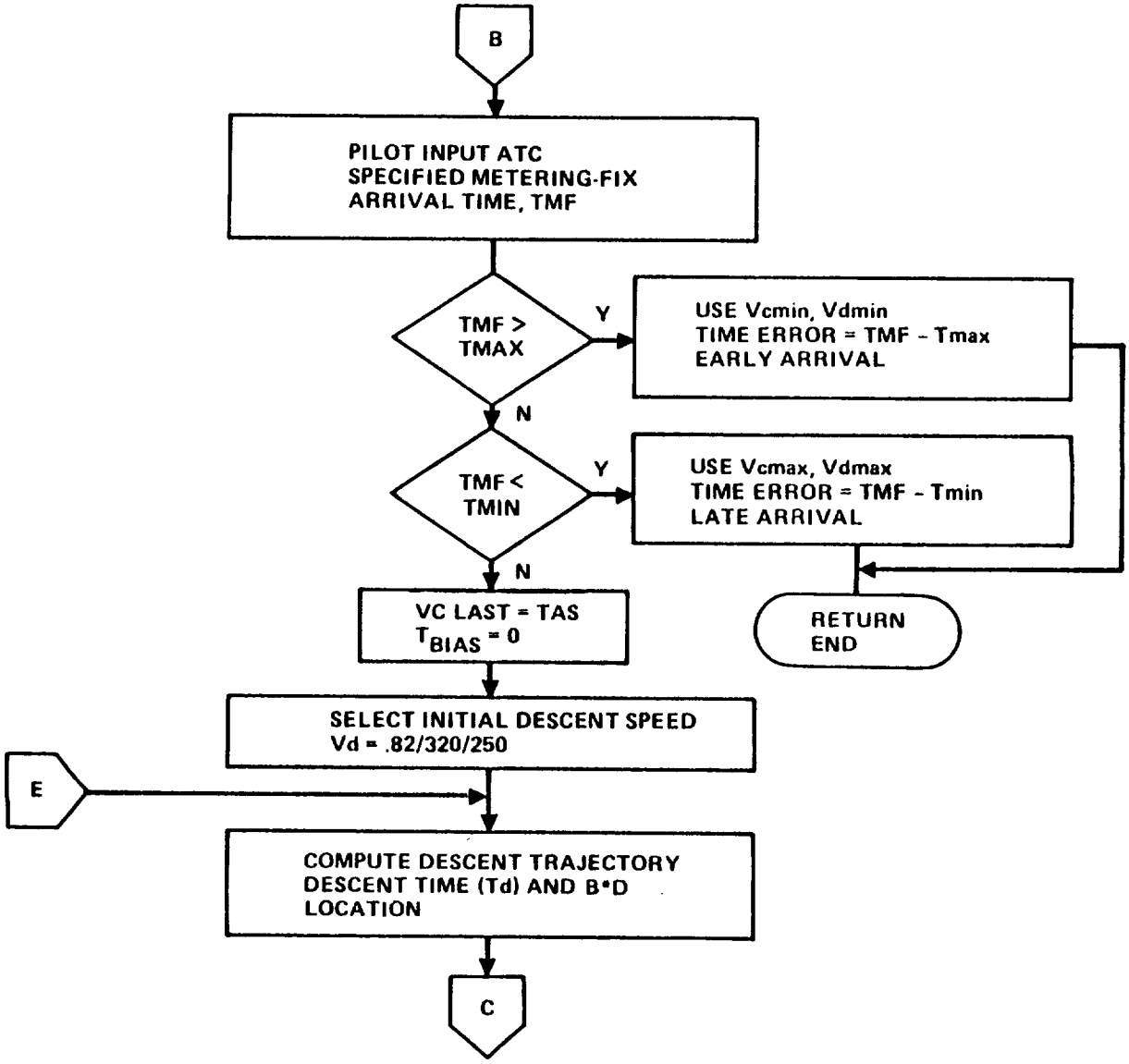

Figure 52. - Continued.

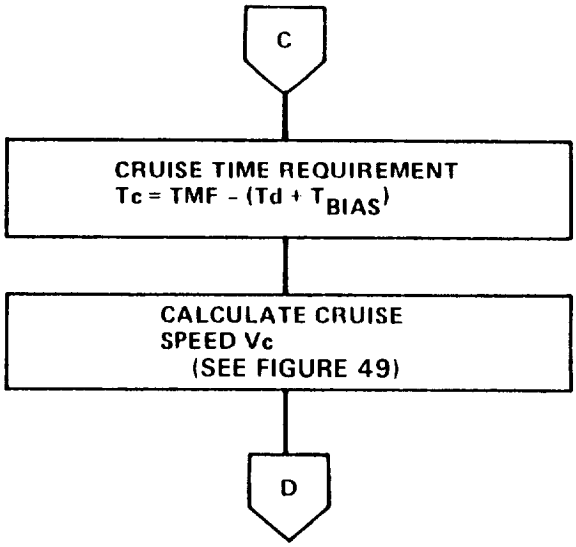

Figure 52. - Continued.

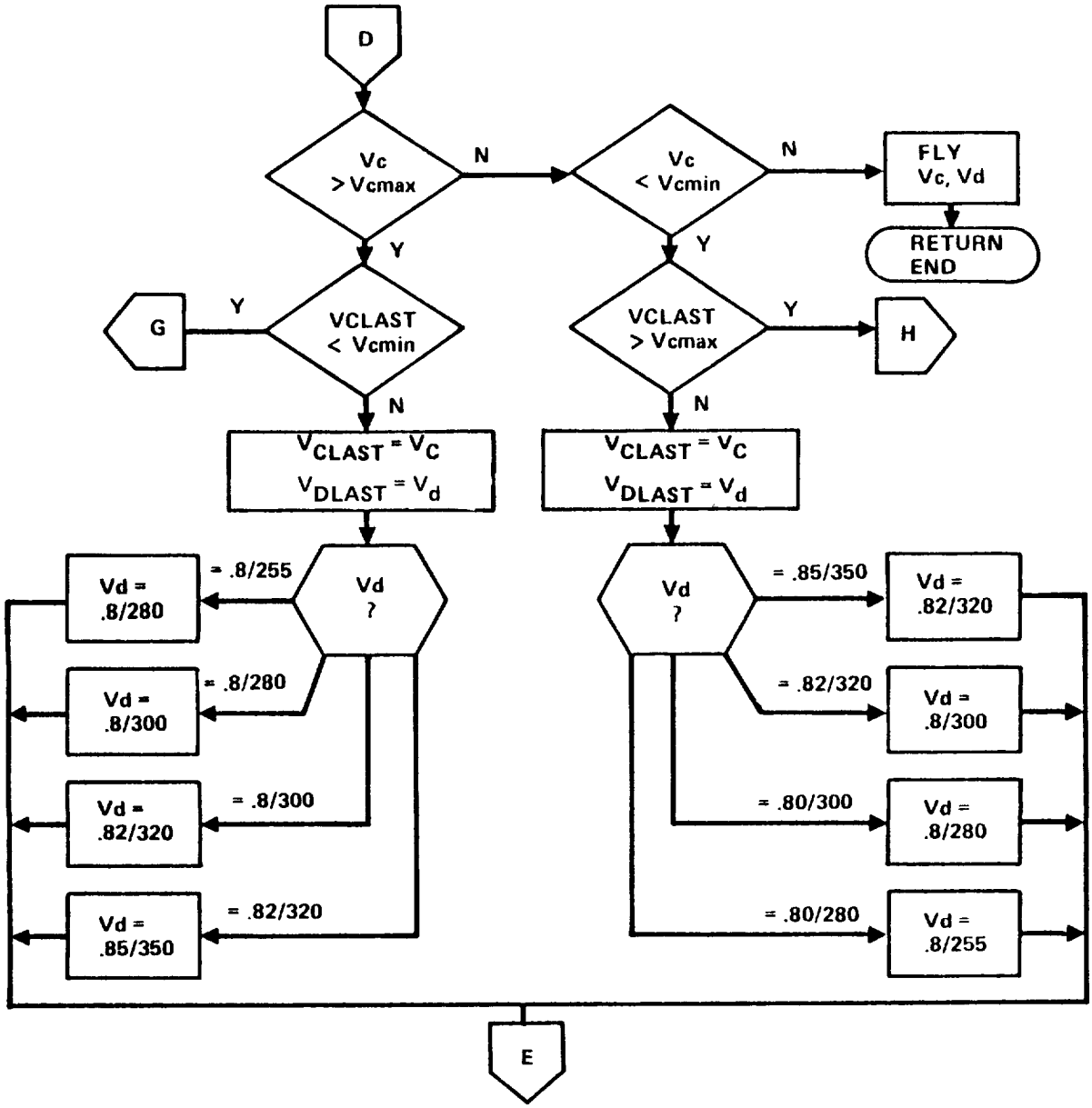

Figure 52. - Continued.

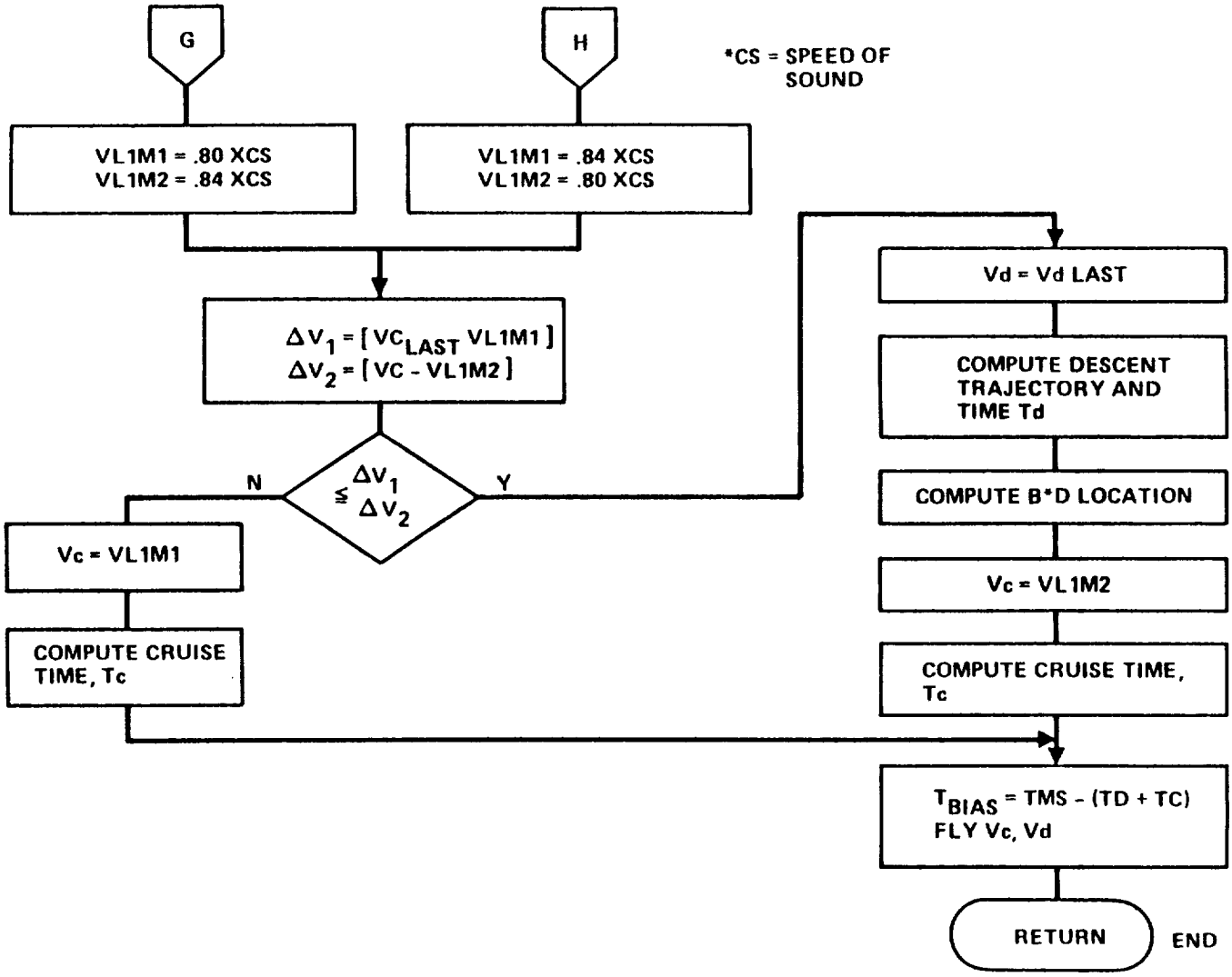

Figure 52. - Concluded.

If the resulting cruise airspeed does not satisfy the inequality, the descent speed is then adjusted to the next higher or lower speed schedule depending on whether the cruise speed is above or below the speed limits. The cruise speed is then recomputed until the inequality of equation 53 is satisfied.

Because only standard descent schedules are available, the iterative process can be oscillatory when the aircraft position is too close to B*D (less than 15 n.mi.). This situation is illustrated in figure 53. In this case, the cruise speed for the first iteration is below the minimum limit, and above the maximum limit when the descent speed is reduced for the second iteration. When this situation occurs, the descent speed causing the least deviation from the speed limits is used. Cruise speed is set to 0.80 Mach or 0.84 Mach depending upon whether the cruise speed is below or above the limits of the associated descent speed. Descent time, Td, and cruise time, Tc, are calculated and used to compute descent time bias, Tbias, using the equation:

$$Tbias = Tmf - (Td + Tc) \tag{54}$$

The time bias is usually small (less then 20 seconds), and can be absorbed by the closed-loop descent control laws which act through the aircraft pitch axis and are described in later sections.

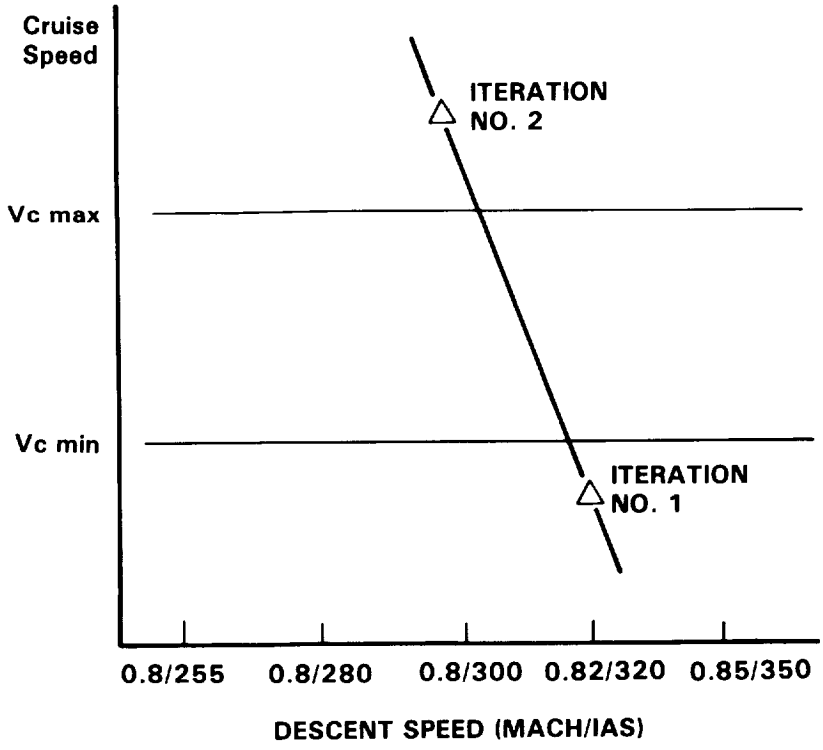

Figure 53. - Cruise and descent airspeed selection.

2.5.4 Range command generator for cruise guidance.- A range command generator was developed for cruise guidance of the aircraft to B*D. Required range as a function of time is calculated by the algorithm when the cruise airspeed is known. Instantaneous time error can then be determined by the equation:

$$\text{time error} = \left(\frac{\text{aircraft range - required range}}{\text{aircraft ground speed}}\right) 3600 \tag{55}$$

Since FMS ground track is used for generation of the range commands, this algorithm applies only when FMS ground track steering is engaged. This is necessary because aircraft range in the above equation is assumed to be along the FMS ground track.

The logic flow chart for generating the range command is shown in figure 54.

The following tasks are performed at the first entry of the algorithm: (1) initialization, (2) read and store required ground track parameters from the cruise table, (3) input required cruise airspeed (VUREQ) as determined by the airspeed algorithm and, (4) calculate required ground speed (VGREQ) for each segment.

Incremental distance (DELDIS) for each computational cycle (DT = 0.1 second) is computed. In the straight-line portion of a segment, incremental distance is determined by:

$$\text{DELDIS} = \frac{\text{VGREQ(I)}}{3600}\,\text{DT} \tag{56}$$

In the circular-arc portion,incremental distance is determined from the heading rate (SYD) by the equation:

$$\text{DELDIS} = \frac{\text{SYD} * \text{DT}}{57.3}\,\text{R(I)} \tag{57}$$

Heading rate is determined by the predicted ground speed during the turn (VGCA), predicted wind at the waypoint (VWP), predicted wind heading at the waypoint (SYWP), and predicted heading during the turn (SY). Range command (RGCMD) is computed by summing the previous RGCMD with the incremental distance (DELDIS).

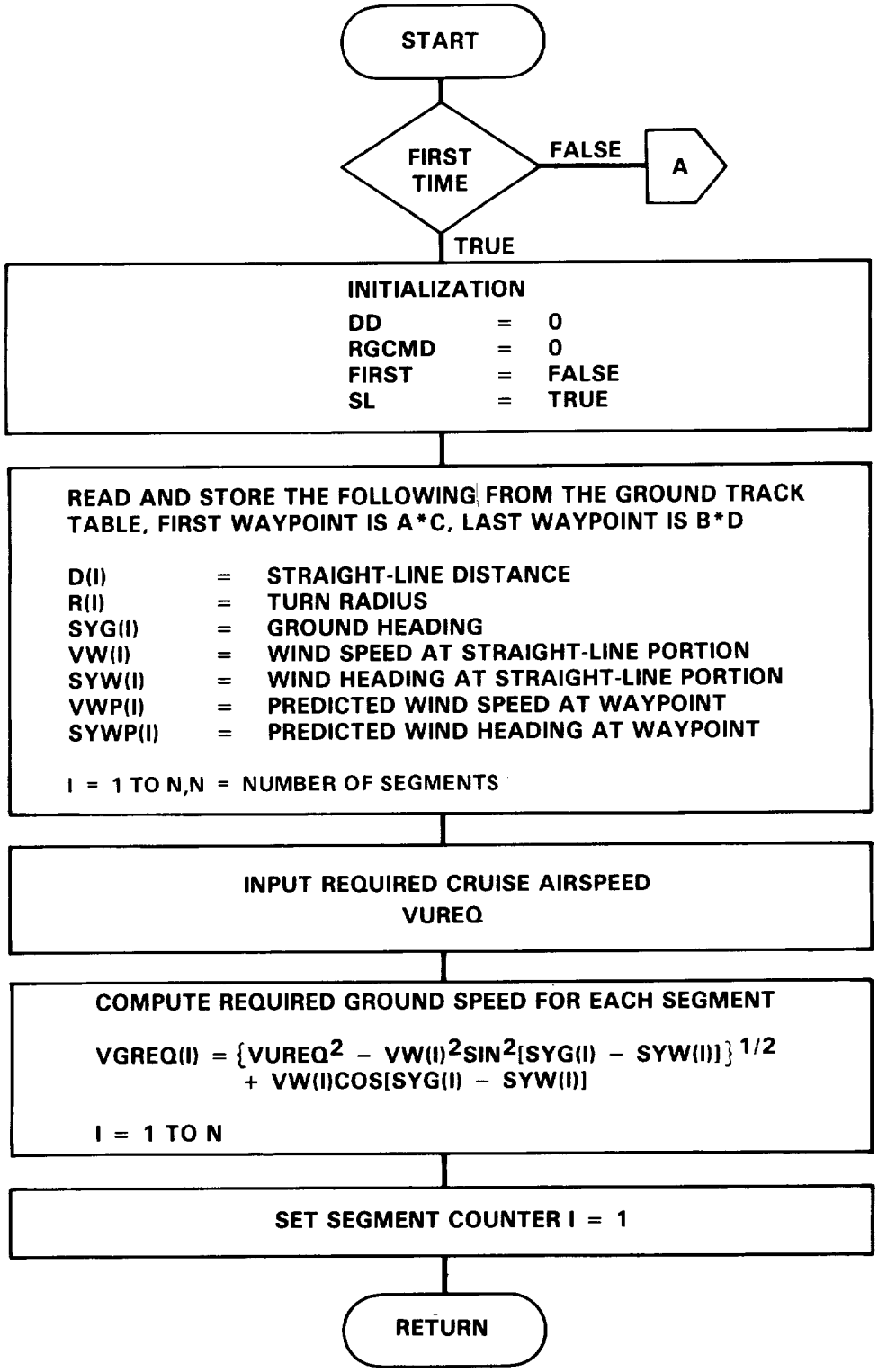

Figure 54. - Logic flow chart for range command generator.

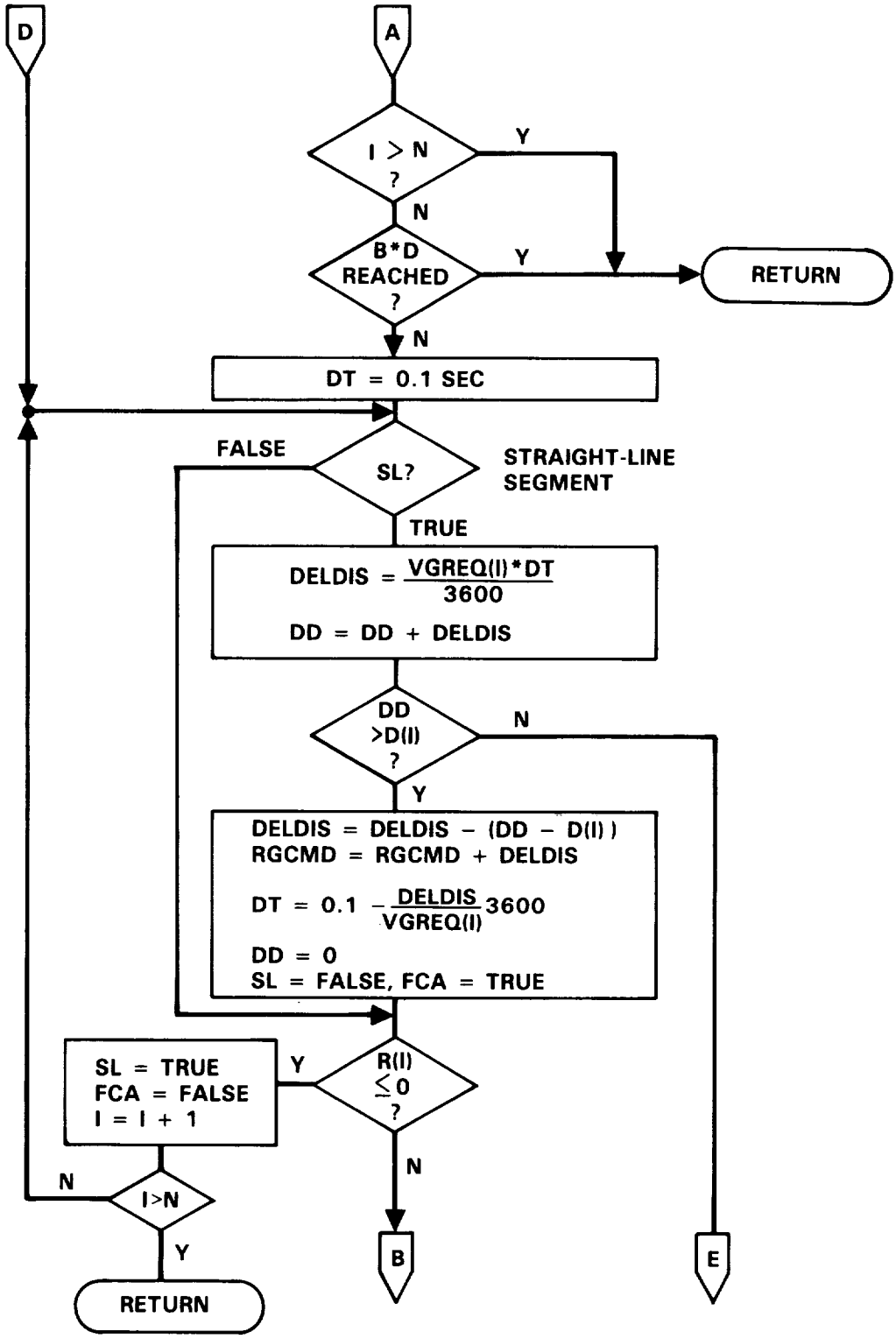

Figure 54. - Continued.

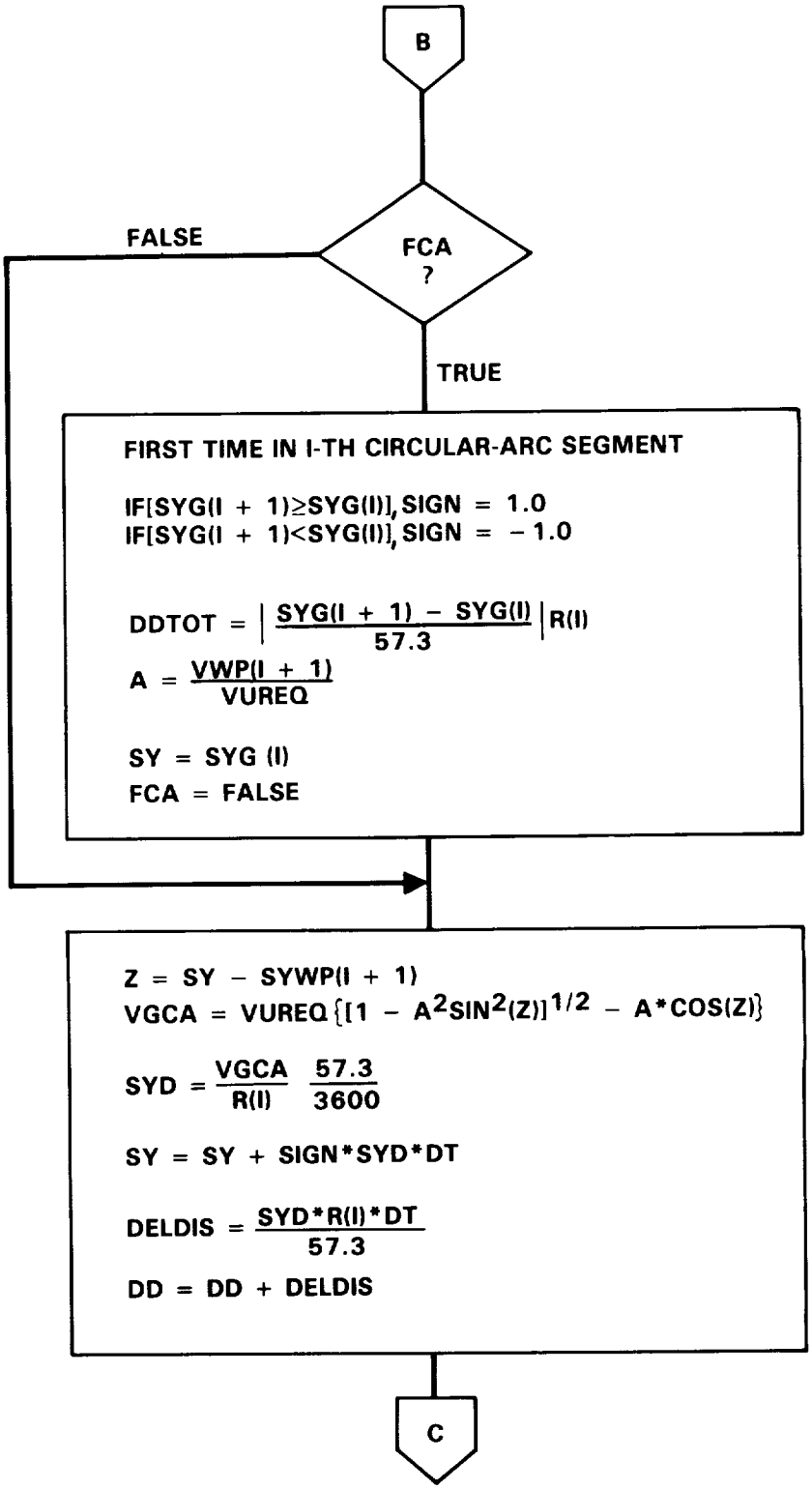

Figure 54. - Continued.

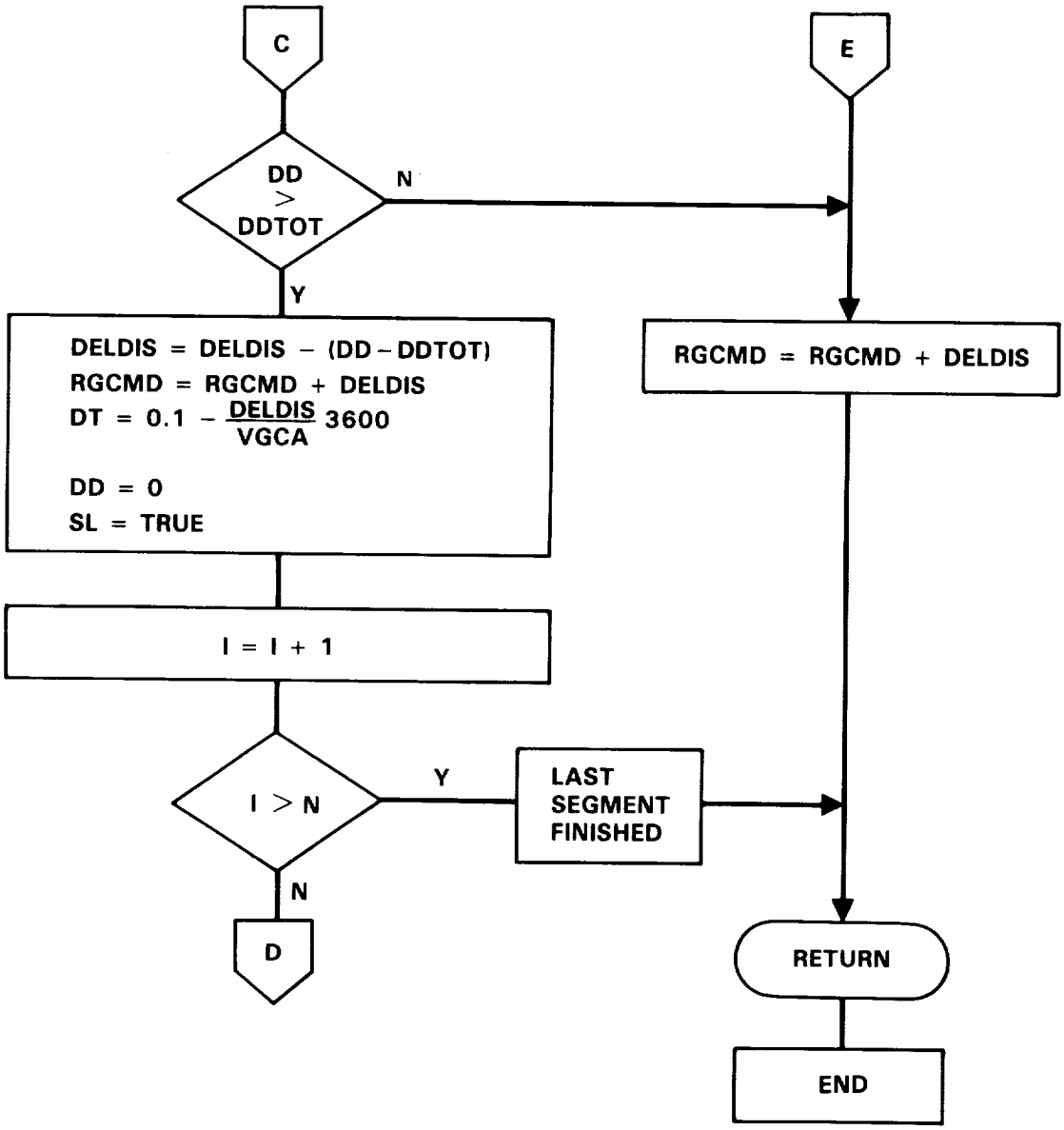

Figure 54. - Concluded.

Logic for switching to a new flight segment is provided by the variable DD. When DD is greater than the straight-line distance of the I-th segment, the existence of a circular-arc on the segment is determined by testing the turn radius (R). If a circular-arc exists in the segment, the computation proceeds to calculate range command in the circular-arc portion; otherwise, the segment counter (I) is incremented by one and the computation proceeds to the next segment.

2.6 4-D Control Laws Development

In Section 2.5, 4-D guidance algorithms were developed to compute an ideal trajectory to guide the aircraft to the metering fix at its specified time. In this section, feedback control laws to track the ideal trajectory for spatial and time control are presented. The design procedure used to arrive at the final control laws and the analytical simulation results are described.

2.6.1 Descent control laws development.- The total descent process is shown in figure 55. The 4-D descent control laws developed in this study are for the Mach and IAS regions above 10,000 feet, the level-off mode and the vector mode. The push-over mode, 10,000 feet deceleration mode, and the E*D deceleration mode were taken from the existing production FMS software; no development work was required.

The automatic 4-D descent control concept is shown in figure 56. The technique chosen was to:

- Precompute an ideal 4-D trajectory which is defined by a table of time, range and altitude.
- For the current aircraft position (current range), compute the required altitude from the ideal trajectory; spoilers and engine thrust are used for altitude error control.
- For the current time, compute the required range; speed changes through the pitch autopilot are used for range error control.

The sections which follow describe the analyses performed to derive the final descent control laws.

2.6.1.1 Feedback variables study: It was decided to apply speed changes for range error control for two reasons: since the existing production FMS used speed control through the pitch channel of the autopilot during descent, this minimized development risk and software changes; the same approach used in the prototype 4-D descent was satisfactory and resulted in accurate time control.

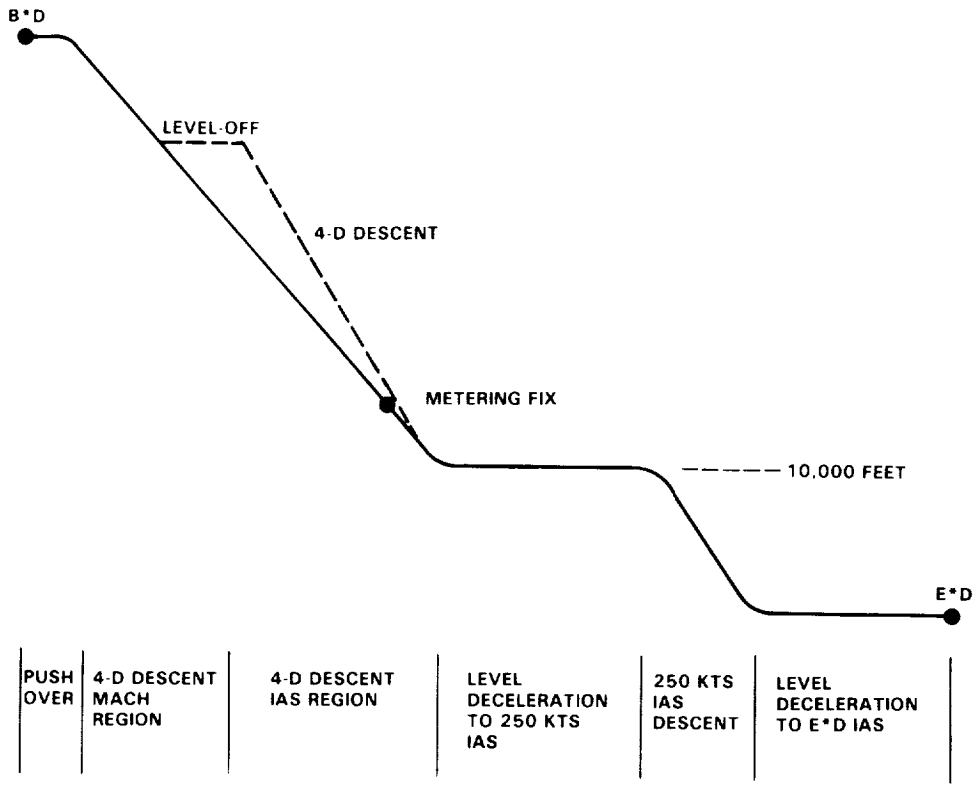

Figure 55. - 4-D descent mode.

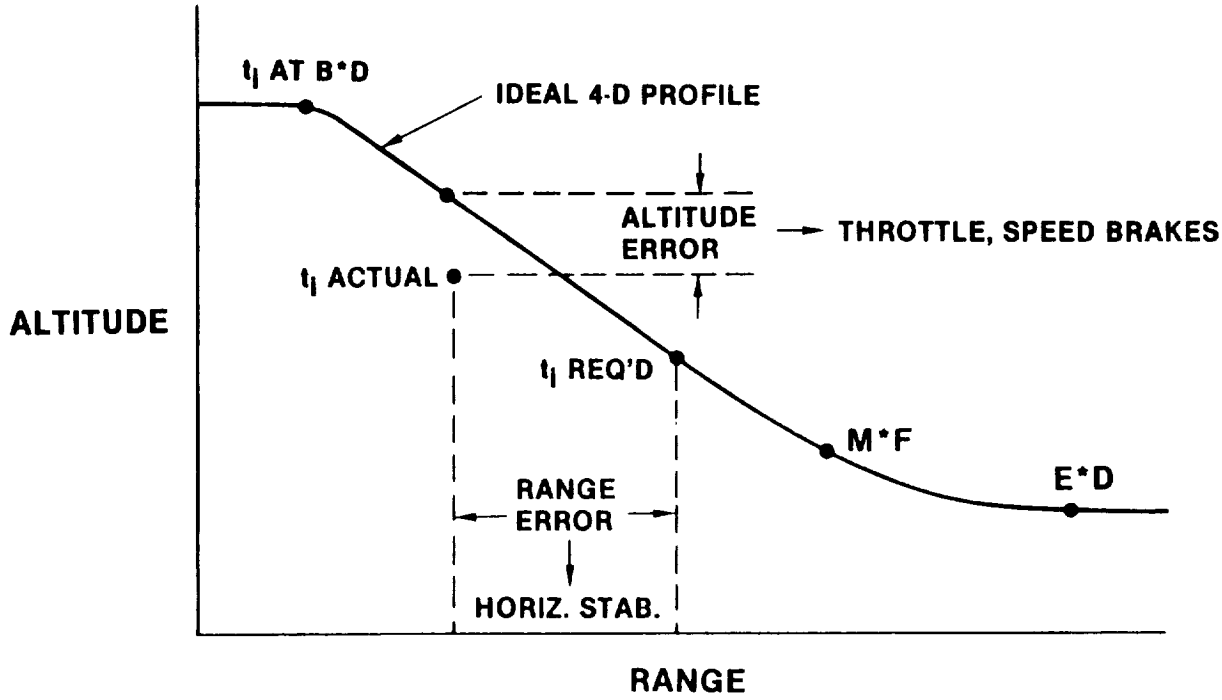

Figure 56. - 4-D descent control variables.

FMS descents are normally performed with engines at idle and all spoilers stowed. Three concepts of using engine thrust and/or direct lift control (DLC - spoiler surfaces No. 1 through No. 6) for altitude error control were considered:

1. Descent with aircraft surfaces at a "clean" configuration, altitude deviations from ideal profile are controlled by DLC for the "too high" case and by engine thrust for the "too low" case.

2. Bias DLC at 8 degrees trailing edge up; DLC is then modulated for altitude error control. When DLC is fully retracted, engine thrust can be applied for the extreme "too low" case. This concept is similar to the technique used in the L-1011 Autoland,® where DLC is successfully utilized for glide path control during final approach and landing.

3. Same as concept 2, except DLC is active in only the IAS region.

The effects of the three descent concepts are illustrated in figure 57. The clean configuration uses the least fuel because cruise distance is minimal. However, engine cyclings are required to control the aircraft when it deviates below the precomputed trajectory due to unexpected winds or windshears. To minimize engine wear, a concept using DLC surfaces for spatial profile control was considered. For aircraft deviations below the nominal trajectory, DLC is retracted from midposition to reduce aircraft drag and bring the aircraft back up to the trajectory; engine thrust is required only when DLC authority is exceeded. Since the added DLC drag results in a steeper nominal trajectory, a new descent model would be required. Also, the steeper descent results in a longer cruise distance and therefore requires extra fuel as compared to the clean configuration. In an attempt to reduce this fuel penalty and still take advantage of DLC control, a third concept of using DLC only in the constant IAS region was considered.

In order to arrive at a final configuration, theoretical fuel consumptions for each of the three methods were computed using a performance computer program developed in this study. Results are shown in figure 58. The fuel penalties due to added cruise distance are 188 pounds (28 gallons) for the descent using DLC in the IAS region and 233 pounds (35 gallons) for the descent using DLC for the entire descent.

To assess the fuel requirement for active altitude error control, flight test results of the prototype 4-D descent experiments and simulations were used. The prototype descent experiments were conducted using the clean configuration with engine thrust and spoilers deployed manually by the crew. As shown in figure 58, an average of 446 pounds of fuel was used. This seems high initially but a review of the flight test data showed that engine thrust was applied most of the descent mainly due to the mismatch of performance between the theoretical FMS descent profile and the test vehicle. Also

® A registered trademark of Lockheed Corporation.

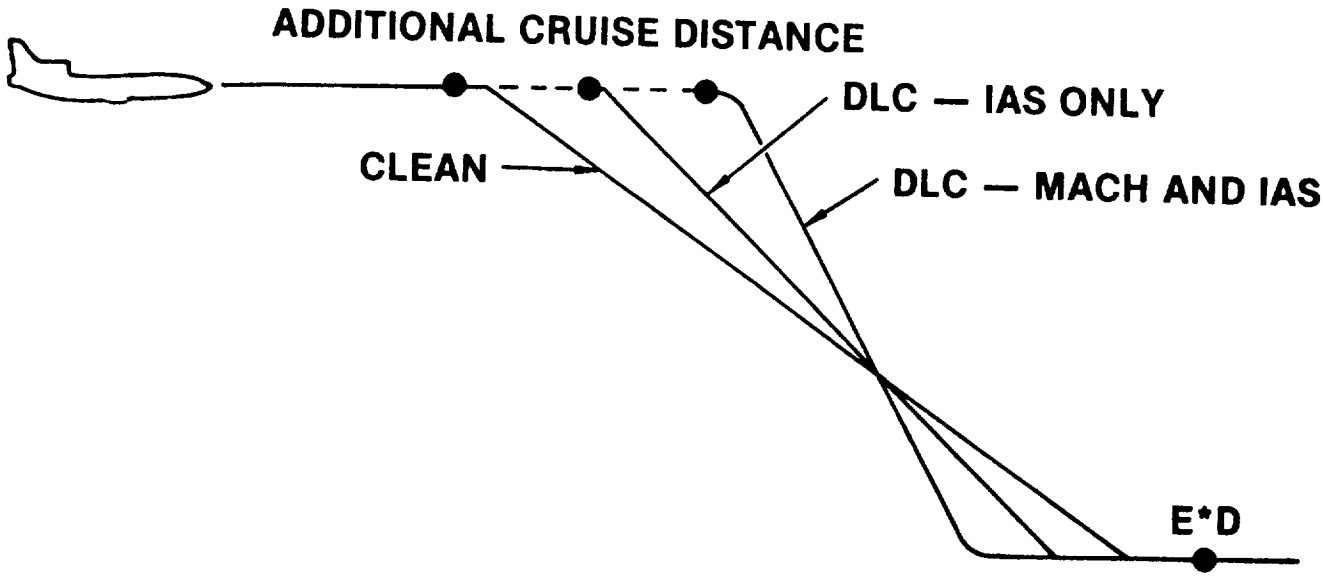

Figure 57. - DLC effects on descent distance.

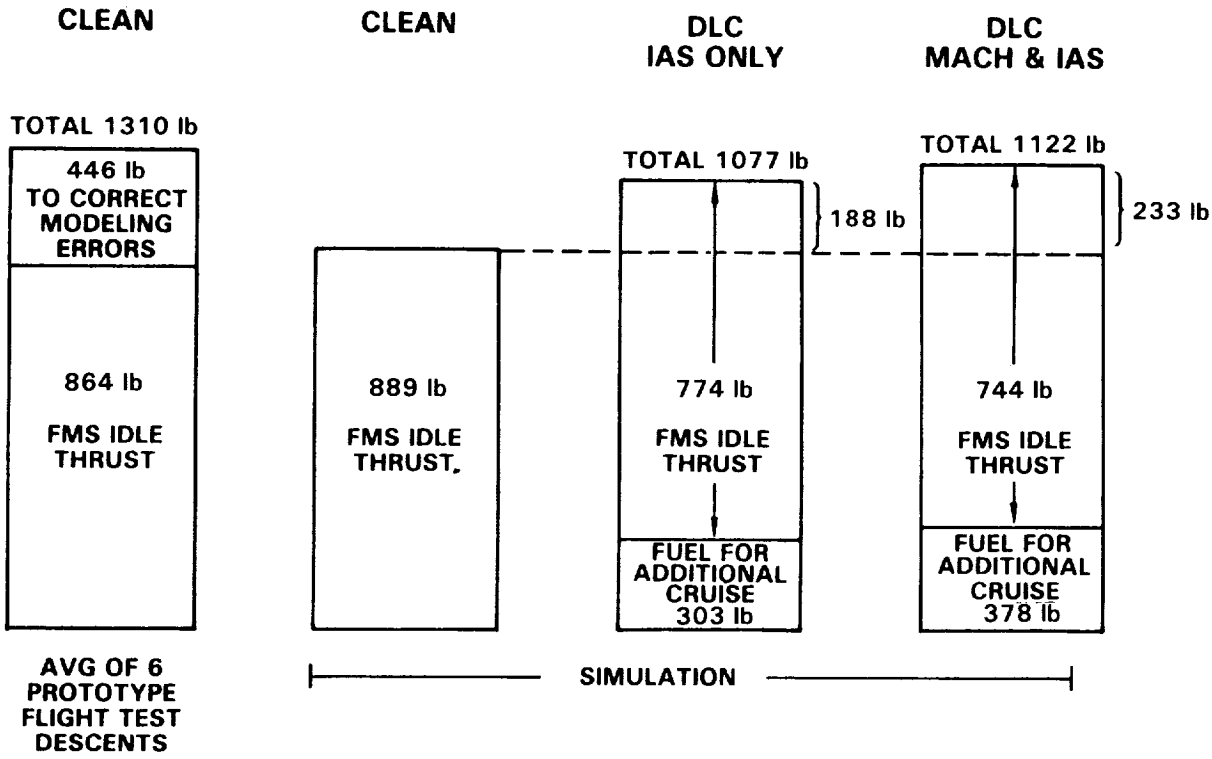

Figure 58. - Fuel used in descent - clean vs. DLC.

additional thrust was required due to the head wind errors resulting from use of the linear decay wind estimation method.

The same flight test conditions were simulated by computer using the winds encountered during the test flights but with a better descent trajectory model. As shown in figure 59, 100 less pounds of fuel were required for altitude error control. The same simulation was then repeated using the segmented wind model to eliminate the head wind errors. Fuel burned for the entire descent was 250 pounds less than the descent using the linear wind technique; the same amount of fuel for altitude error control was observed.

Using the biased DLC method, it is anticipated that fuel required for the altitude control will be halved to 50 pounds. However, the added cruise distance could result in 188 to 233 pounds of fuel penalty as shown again in figure 58. The penalty will outweigh the benefit of the fuel savings achieved using DLC.

The conclusion of this study is that with more accurate wind and descent trajectory predictions, less fuel will be required for altitude error control and the 188 to 233 pounds of additional fuel required for the added DLC cruise distance will become less attractive. The clean configuration descent method was therefore chosen for detailed control law synthesis.

2.6.1.2 Root locus analysis: Having established the feedback variables and the approach of altitude and range error control, the next step was to design the feedback gains. A root locus technique was used to design the feedback gains of the DLC loop for altitude error control and the airspeed loop for range error control. The Lockheed-developed interactive computer program called the Advanced System Analysis Program (ASAP) was used. The program is operated by the control systems designer from an interactive computer graphics terminal and contains standard root locus, Bode, Nyquist, and other linear analysis tools used in the synthesis and analysis of feedback control systems.

The results of the root locus analysis provided insight into the system's stability characteristics and therefore valuable intuitive understanding of the system behavior during nonlinear simulation in the time domain for final control law configuration development. The same analysis was not performed for the engine loop for altitude error control because of the small saturation limits used to eliminate excessive engine cyclings.

Figure 60 is the basic analytical block diagram with the significant control system dynamics represented by Laplace transfer functions. The airframe was modeled with rigid body longitudinal equations of motion with aerodynamic derivatives calculated at flight idle descent conditions. The system functions included are the autopilot Mach and IAS hold, horizontal stabilizer servo systems, and the DLC servo systems; the outer loops analyzed were the DLC and the airspeed loops. Four descent flight conditions at a c.g. of 25% MAC were evaluated as given in table III. The design of loop gains was concentrated using the typical descent flight condition number 1. The

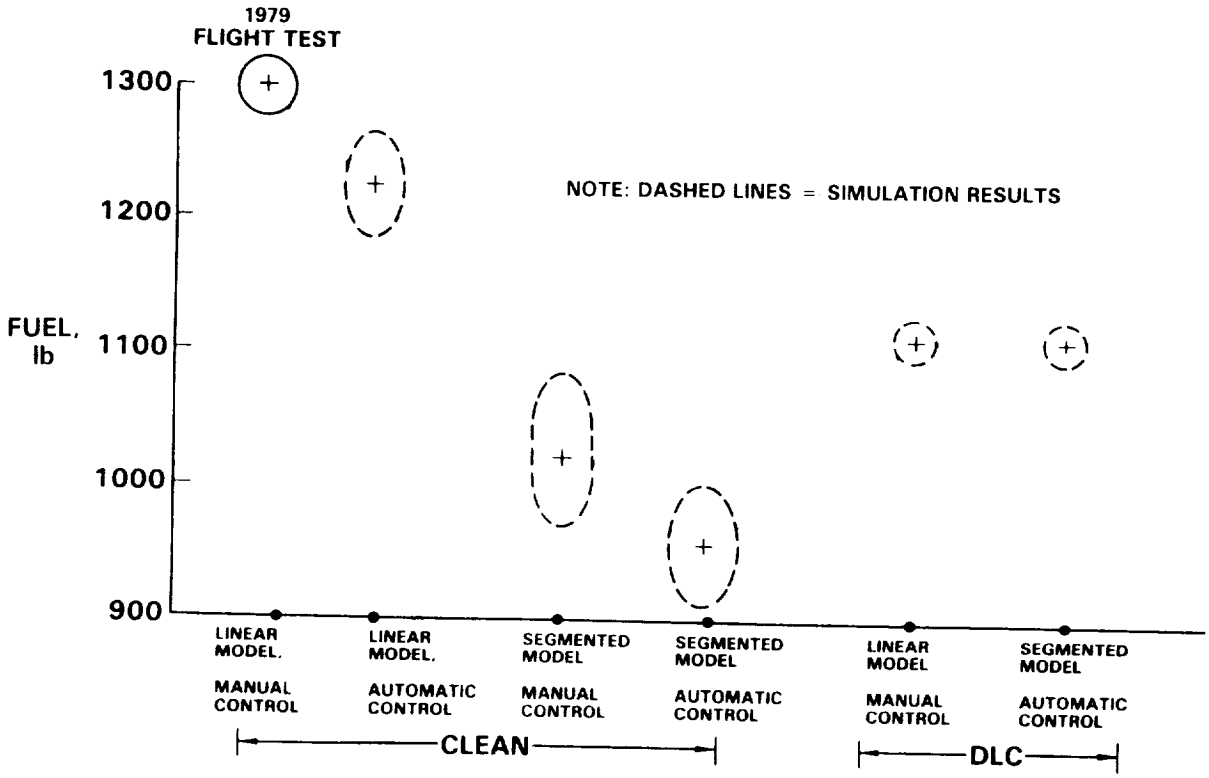

Figure 59. - 4-D descent control trade-off.

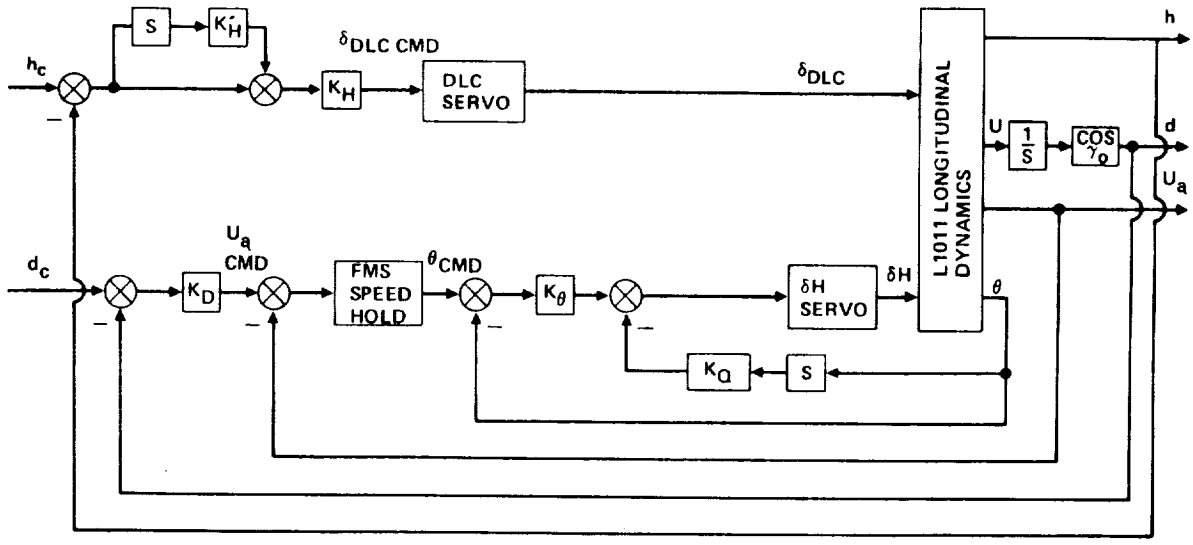

Figure 60. - 4-D descent control system block diagram for linear analysis.

TABLE III. - ROOT LOCUS ANALYSIS FLIGHT CONDITIONS

Flight Condition	$Altitude_3$ (ft x 10^3)	$Weight_3$ (lb x 10^3)	Speed (IAS/Mach)
1	25	300	320 kts
2	25	360	320 kts
3	25	360	350 kts
4	35	360	0.82 Mach

resulting gains were then re-evaluated using the other three flight conditions to verify that no adverse stability problems resulted due to the variation of flight conditions.

DLC loop stability is shown in the root locus plot of figure 61. The system's open loop phugoid mode, which is the free airplane phugoid modified due to closures of the autopilot inner loops and the FMS airspeed loop, is located at 0.3 radian/second with damping ratio of 0.3. Closure of the DLC loop for altitude error control destabilizes the system by causing the phugoid to drift to the right-hand plane as shown by the root loci. The system becomes oscillatory at the DLC gain (K_H) of 0.3 degree per foot. A nominal gain of 0.1 degree per foot having a phugoid damping ratio of 0.27 was selected; this is three times smaller than the unstable gain of 0.3 degree per foot and should therefore provide sufficient stability margin.

Distance error loop stability is shown on the root locus plot of figure 62. Closure of this loop virtually has no effect on the phugoid mode; increasing the loop gain (K_D) therefore should not contribute to phugoid instability. The only effect this loop has is on a very low frequency complex pole located at 0.03 radian per second with high damping ratios of 0.7 to 0.58 when the loop gain was varied from 10 to 30 knots/n.mi.. Therefore, a wide range of range error feedback gains can be used without significantly affecting the system's stability. An altitude-scheduled range error gain was selected as shown in figure 63 based on the results of this study. The gain is increased from 15 knots IAS/n.mi. at the higher altitude region (30,000 feet) to 30 knots IAS/n.mi. at the lower altitude region (18,000 feet). The lower airspeed gain was used because it is desirable to have less airspeed variations at higher altitudes. The higher gain is required at lower altitudes to achieve more accurate arrival times at the metering fix. For the Mach region, a constant gain of 0.005 Mach per nautical mile was selected which roughly corresponds to 5 knots per nautical mile.

2.6.1.3 Engine feedback loop synthesis: The main concerns about using engine thrust for altitude error control are to minimize engine cyclings and application of excessive thrust. As a result, small engine thrust limits ($\pm$0.1 EPR) and an altitude error dead-zone were used. Because of these elements, classical control analysis techniques were not applicable. The

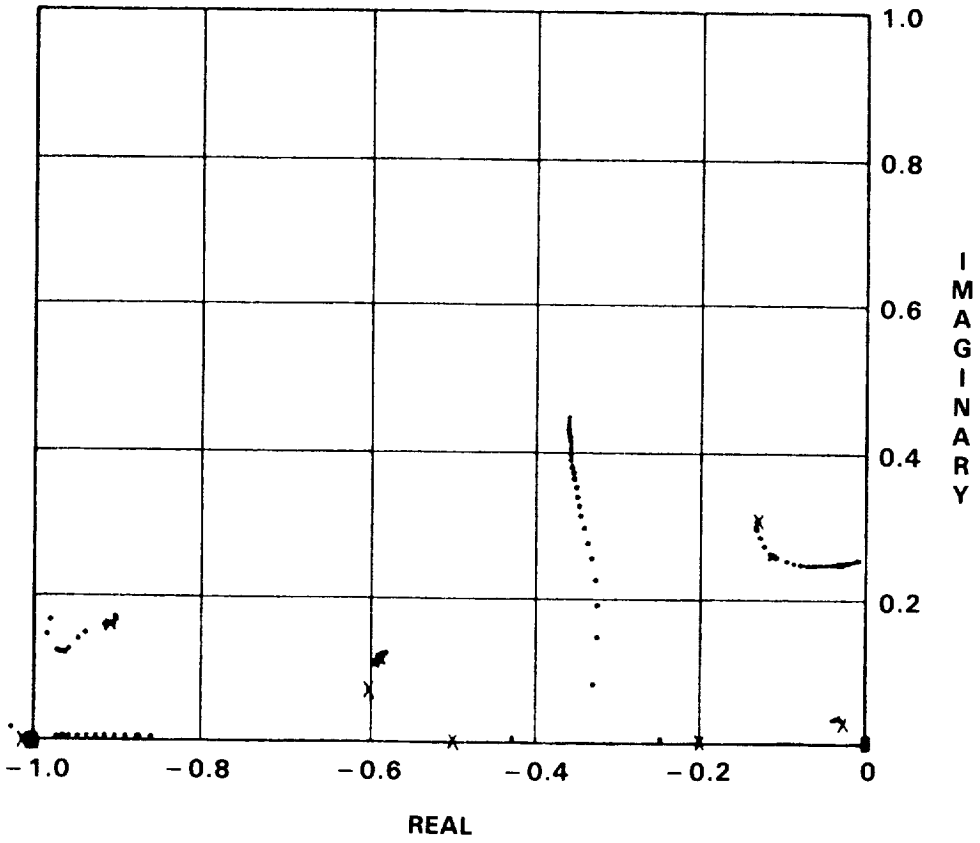

Figure 61. - Root locus plot, effect of DLC loop closure.

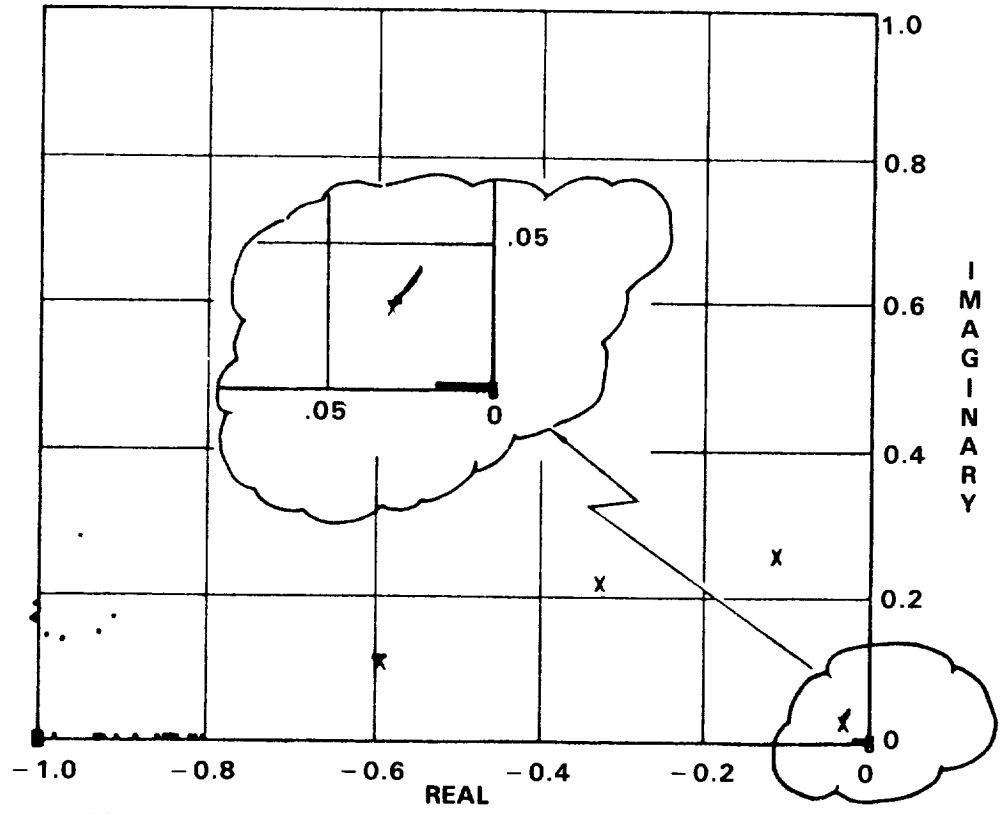

Figure 62. - Root locus plot, effect of distance error loop closure.

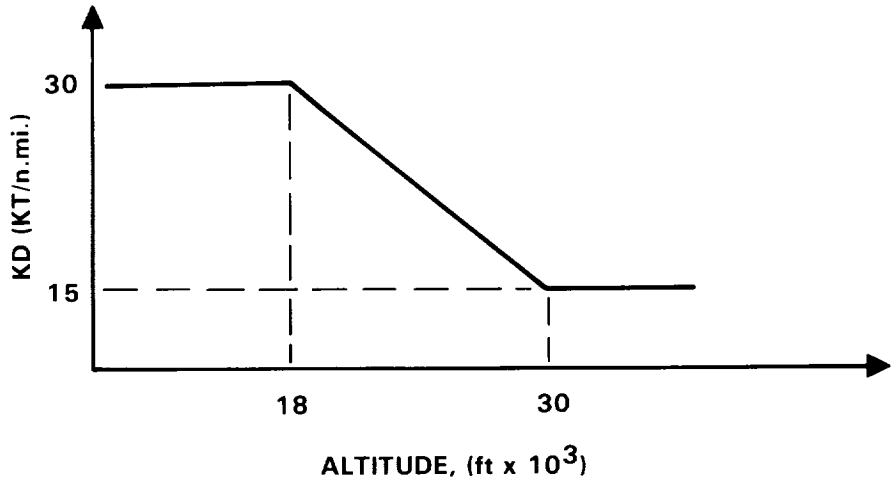

Figure 63. - Range error feedback gain schedule.

synthesis was instead carried out using a simulation program operating in the time domain. A three degree-of-freedom airframe model developed on the IBM interactive Continuous System Modeling Program (CSMP) which contains necessary system nonlinearities such as digital signal processing delays, servo hysteresis, and saturation effects was used. Several control gains, altitude error dead-zones and EPR saturation limits were evaluated using various wind conditions as system disturbances. The system damping, engine activities, and aircraft altitude response were evaluated and judged to be satisfactory. The final engine thrust feedback loop is shown in figure 64. Also shown on the figure is the DLC loop which was developed as described in the previous section. Examples of the simulation results using 50 knot headwind and tailwind steps are shown in figures 65 and 66.

2.6.1.4 Level-off during descent: Occasionally, airplanes are required to level off in their descent, for example when the high altitude air traffic controller hands the airplane off to the low altitude controller. When instructed to resume descent, the 4-D system must be able to reengage automatically and guide the airplane down through the metering fix at the preestablished time. The level-off mode concept is shown in figure 67. The required range at a given time is continually calculated from the precomputed 4-D descent trajectory. Range error is controlled by continually adjusting airspeed using the same control laws developed for the descent (figure 68). Airspeed hold is accomplished using the existing FMS cruise control laws through the autothrottle. Autopilot altitude capture and altitude hold are

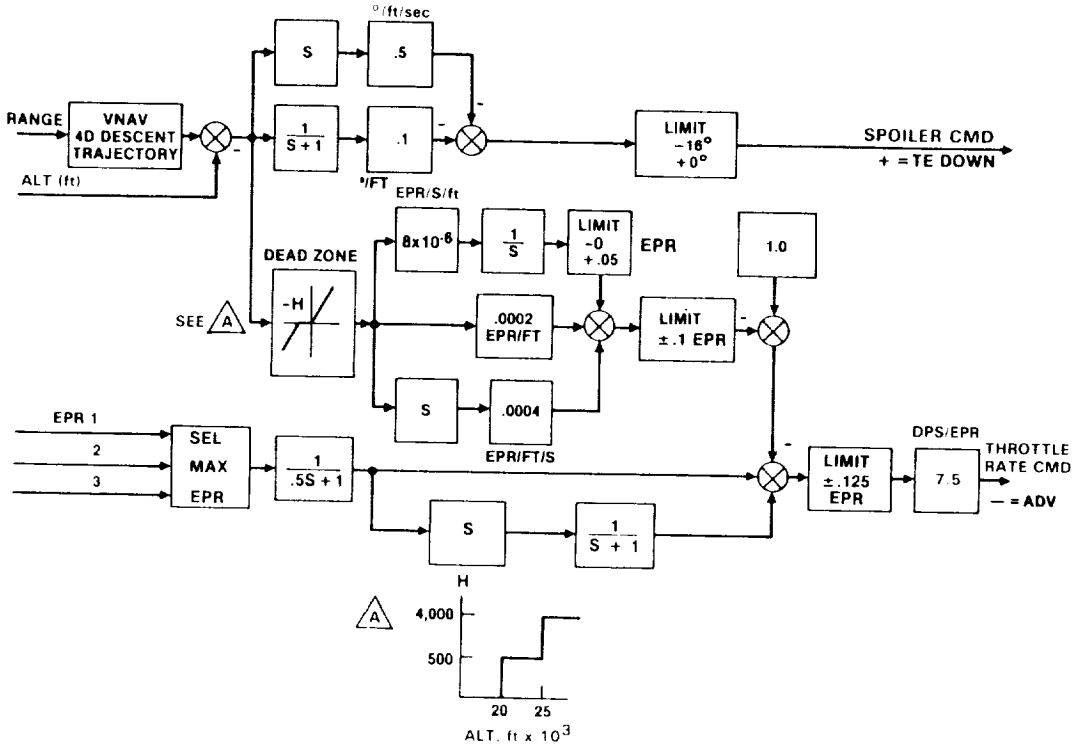

Figure 64. - Altitude error feedback.

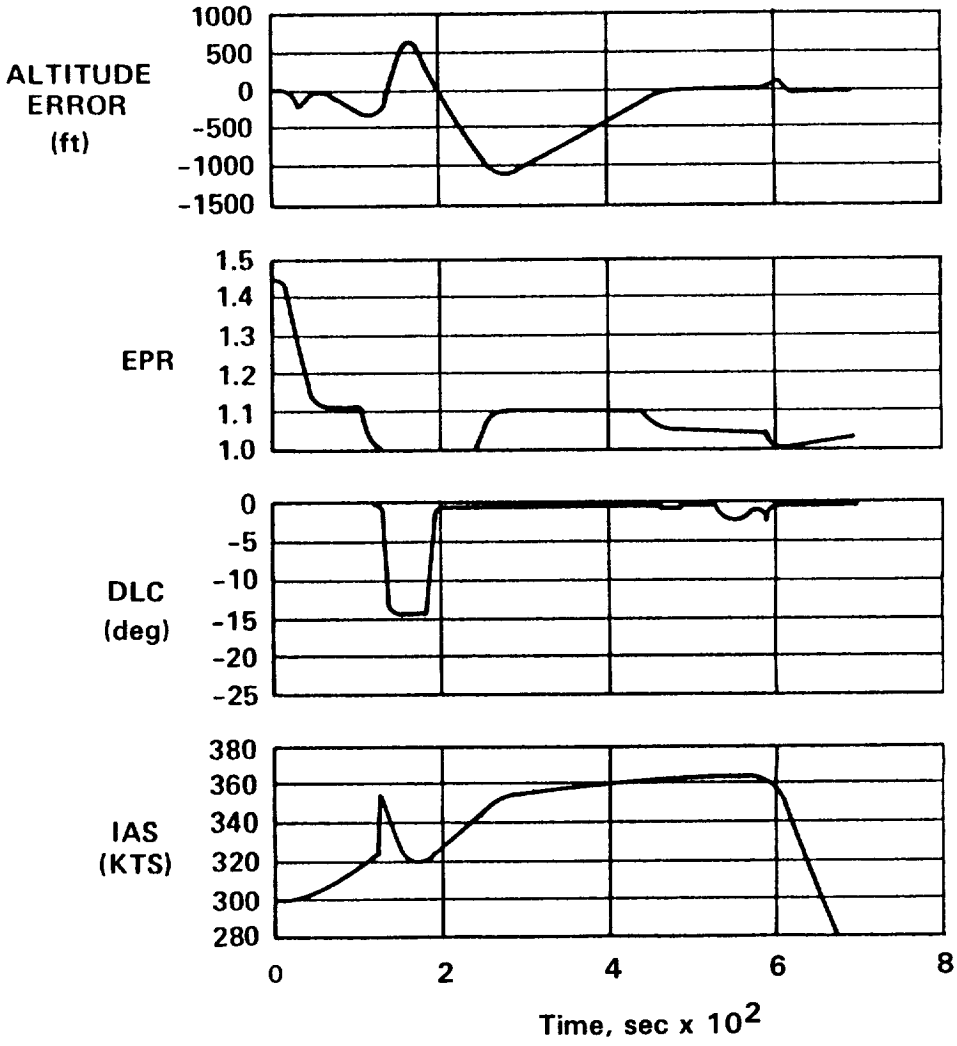

Figure 65. - 4-D descent simulation, 50 knots headwind step response.

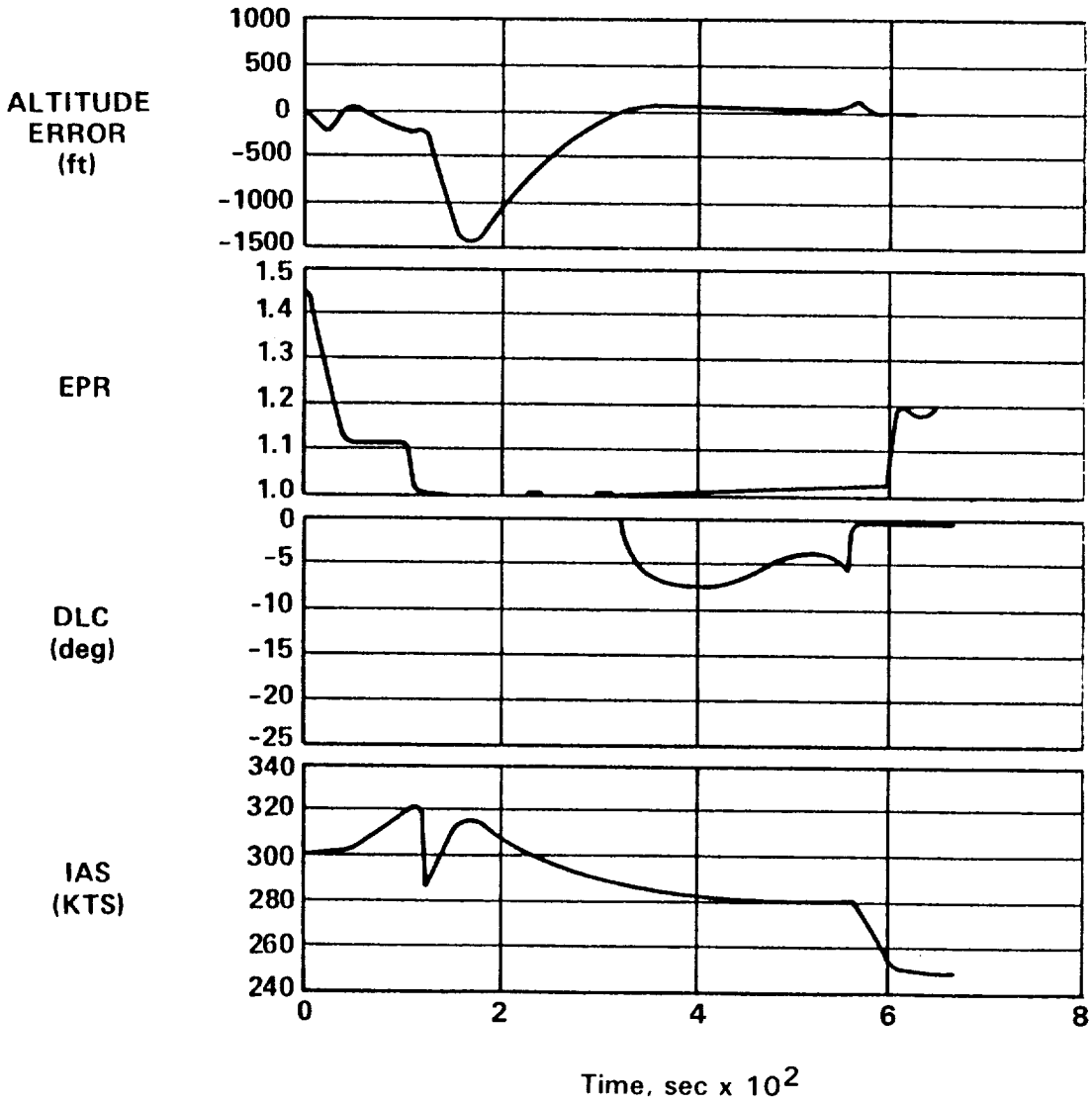

Figure 66. - 4-D descent simulation, 50 knots tailwind step response.

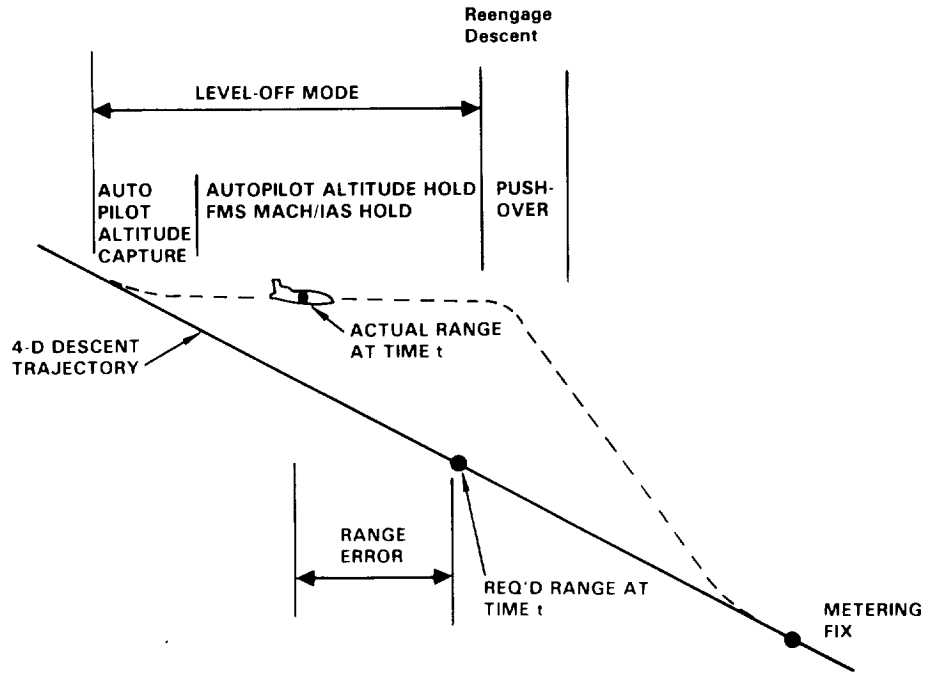

Figure 67. - Concept of leveling-off during descent.

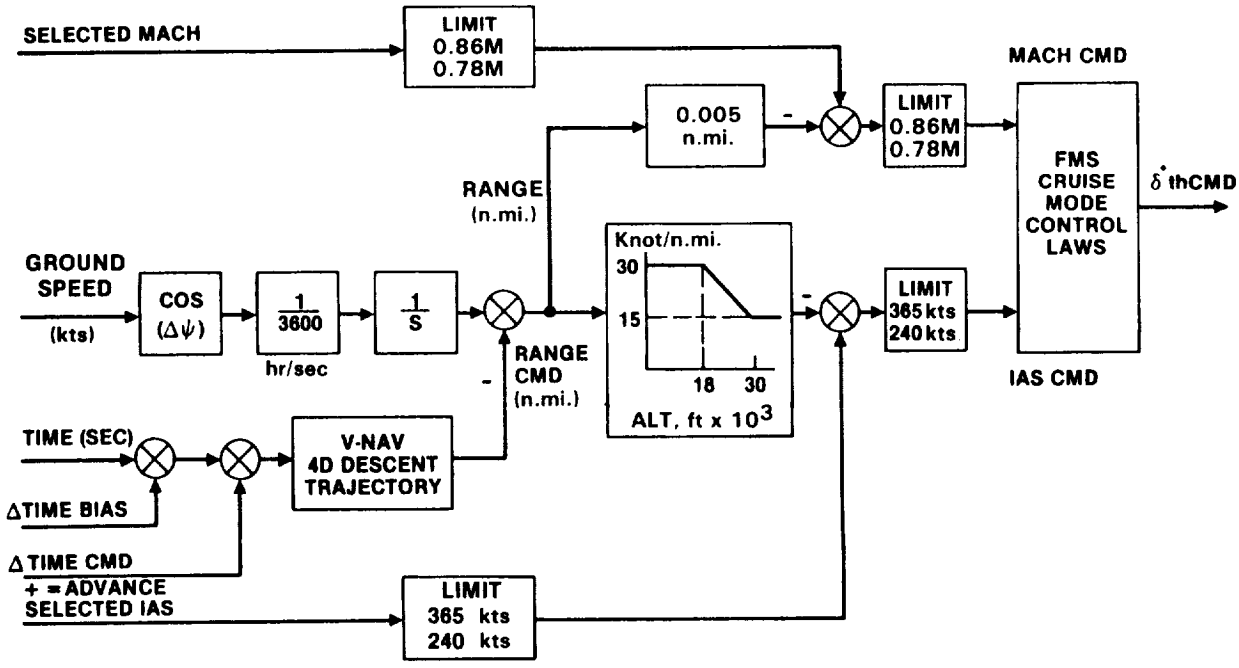

Figure 68. - Leveling-off control law.

used to capture and hold the ATC specified level-off altitude. The push-over mode is engaged when ATC instruction is received to resume the descent. If the level-off distance or time is within the flexibility envelope of the L-1011 (Section 2.3.3), the automatic 4-D descent control law will be able to null the altitude error developed during level-off and deliver the airplane to the metering fix window at its specified time.

Figures 69 and 70 show the simulation results of the level-off mode. In figures 69 and 70 the level-off occurs at 26,000 feet for a duration of 1 minute. In figures 71 and 72, the level-off occurs at 30,000 feet with two minutes duration, the maximum level-off flexibility for this condition. Both simulation cases returned to the metering fix at 11,000 feet with minimal time errors.

2.6.1.5 Vectoring during descent: During descent aircraft are occasionally vectored off the original course by the controller to avoid or to overtake other traffic. When cleared to return to the original course, the 4-D system must be able to guide the airplane to make good the original, or newly assigned, metering fix arrival time.

To execute the vectoring instruction, existing FMS navigation procedures are used to insert a waypoint in the direction of the ATC-specified heading to fly the new course (see procedures in Section 3). When instruction is received to return to the original track, a go-direct mode is executed to compute an optimal trajectory to return to the next original waypoint. To make good the assigned metering fix time, range error with respect to the original flight plan is computed by projecting the aircraft range onto the original track as illustrated in figure 73. This can be done by simply calculating the cosine of the angle difference between the original and the vectored track and multiplying by range covered since vectoring. The 4-D descent control laws can then be applied to effect speed changes, to null the range error, and make good the metering fix time objective.

2.6.1.6 Deceleration to E*D IAS: The 3-D FMS software calculates distances for flight idle, level flight decelerations at 10,000 feet and at E*D altitude. The computation assumes that the aircraft airspeed is always equal to the selected descent airspeed when deceleration altitude is first reached. Adequate level distances are then provided for the deceleration which will result in minimal E*D airspeed errors.

This is a fair assumption for the 3-D FMS because descent airspeed is always maintained. However, when airspeed adjustment must be made by the 4-D FMS for arrival time control, airspeed at level deceleration altitude capture can be conceivably much higher than the selected descent IAS. In this case, the originally calculated distance will be too short for the deceleration, resulting in large airspeed error when E*D is reached. Since E*D airspeed is normally restricted by ATC, a method to reduce E*D airspeed error must be provided.

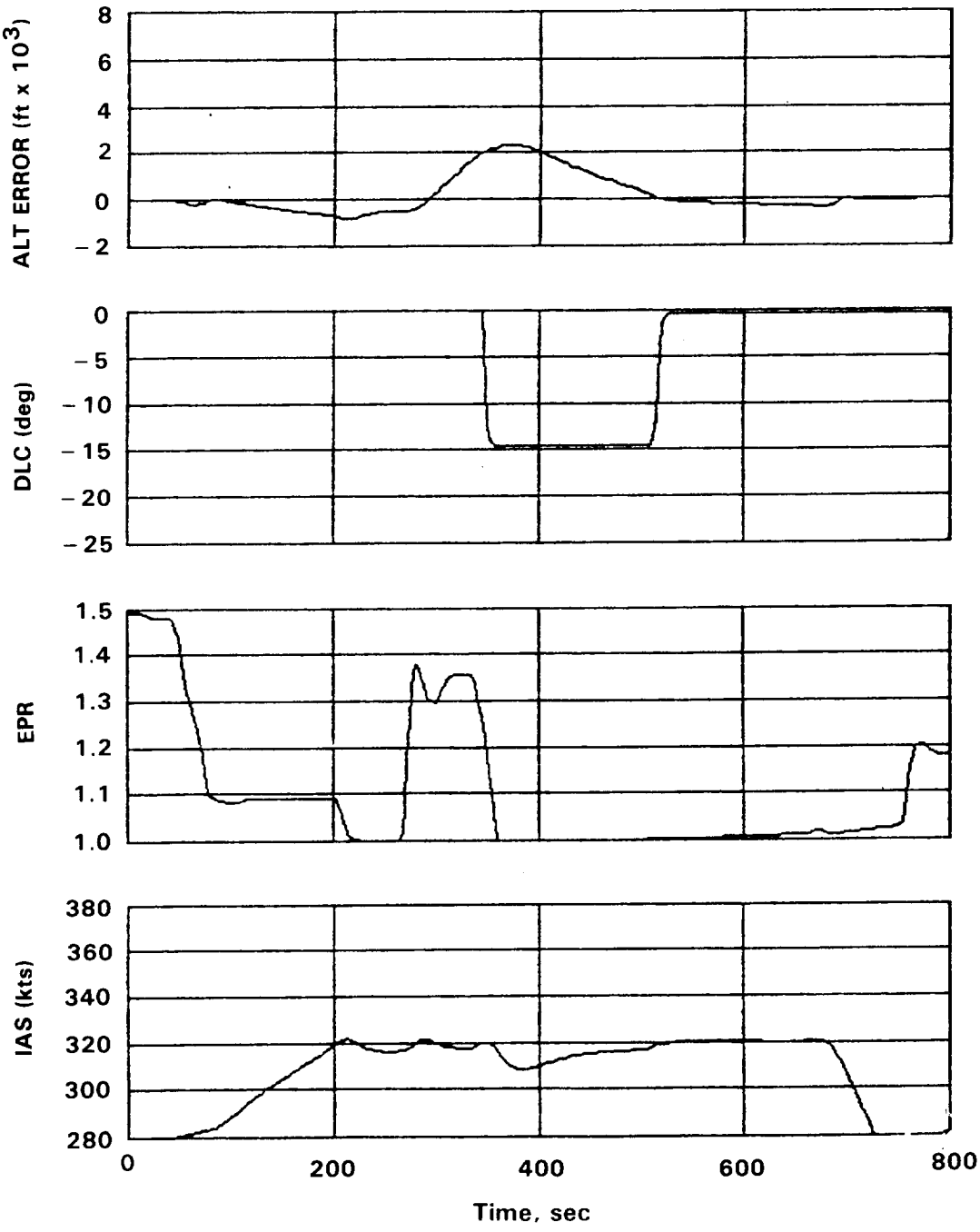

Figure 69. - Simulation time histories, one minute level-off at 26,000 feet.

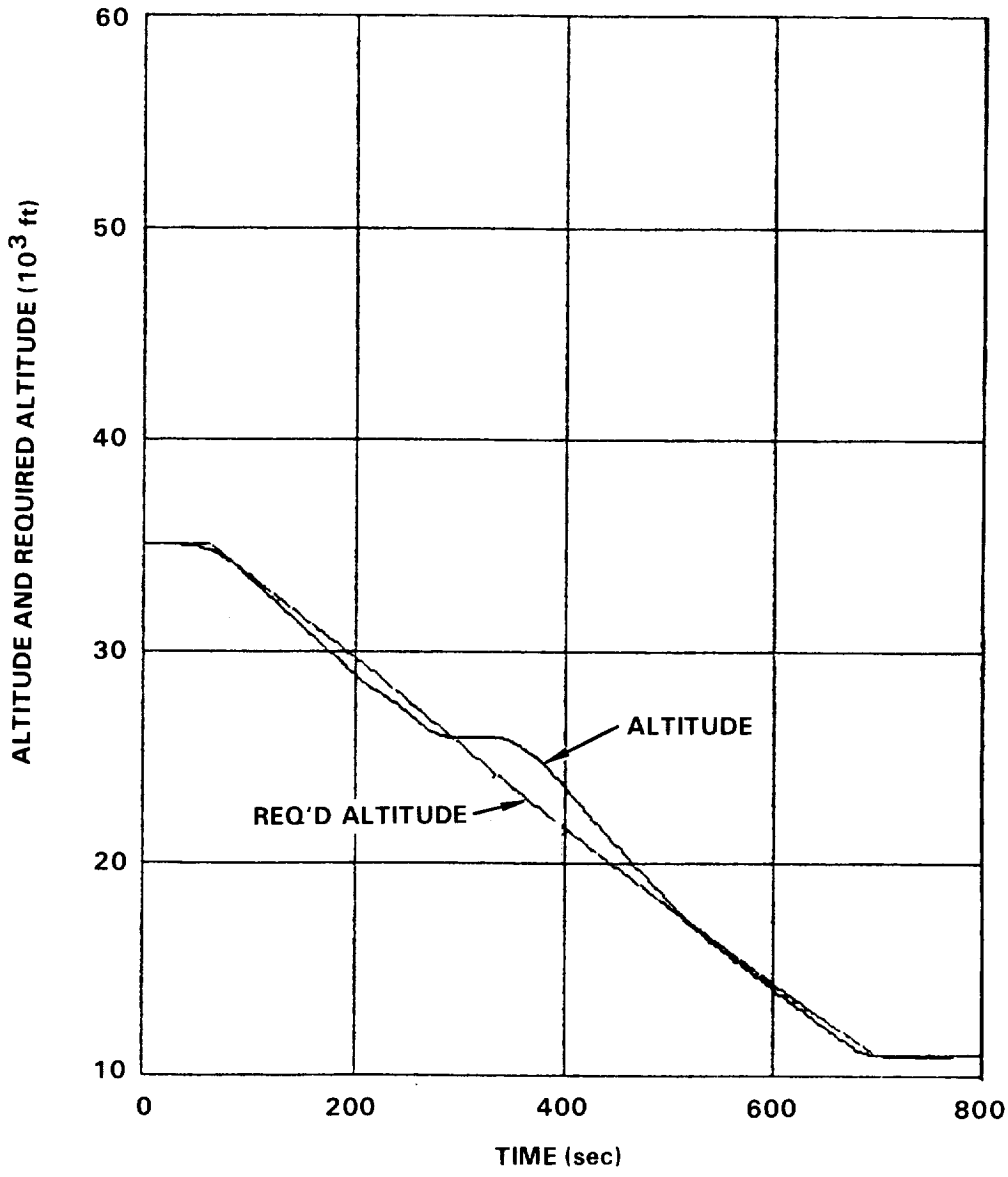

Figure 70. - Simulation time histories, one minute level-off at 26,000 feet.

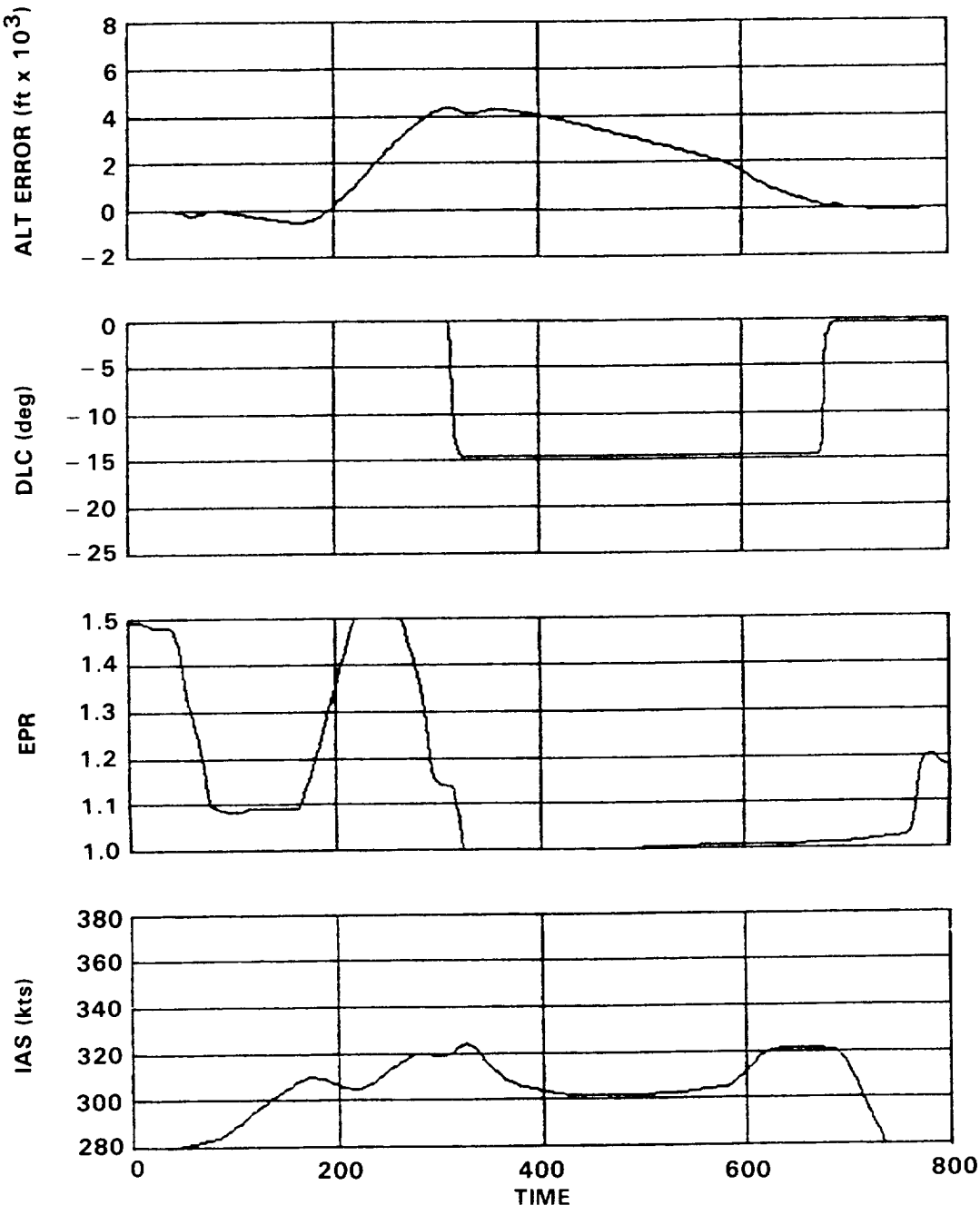

Figure 71. - Simulation time histories, two minute level-off at 30,000 feet.

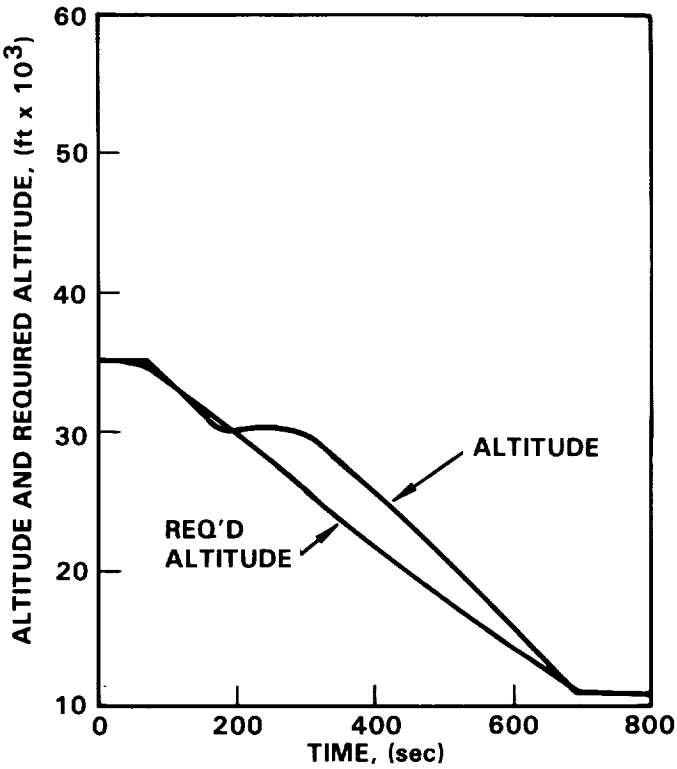

Figure 72. - Simulation time histories, two minute level-off at 30,000 feet.

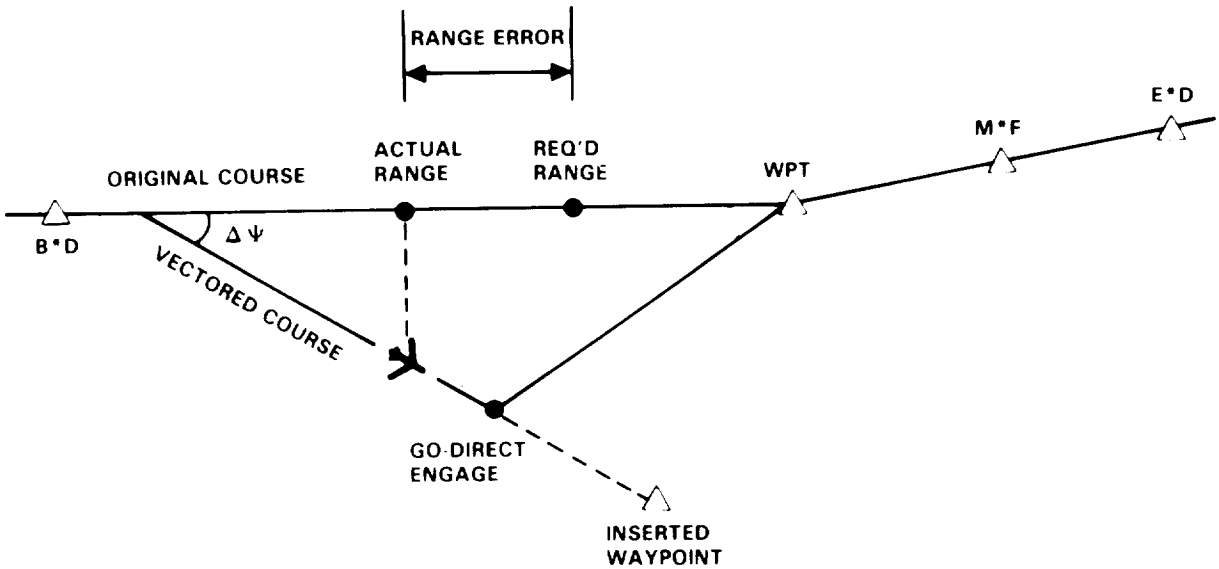

Figure 73. - Concept of vectoring during descent.

The method proposed in this study is shown in figure 74. Based on the actual airspeed of the aircraft, an incremental altitude (Δalt) is calculated such that by initiating a deceleration at this point, the aircraft's speed will be equal to the preselected descent airspeed the when level deceleration altitude is reached. The originally computed level deceleration distances will then be adequate and therefore will minimize E*D airspeed error.

The Δalt's were calculated based on the L-1011's performance for the deceleration rate of 0.5 knot per second as shown in figures 75 through 78. Various aircraft weights and five standard descent airspeeds were used. The calculations were based on the altitude of 10,000 feet since E*D is normally around this altitude. Negligible E*D airspeed error can result if E*D altitude is located slightly above 10,000 feet.

To compute the altitude to initiate the deceleration during flight, the following equations are used:

$$\text{Decel Alt} = \begin{cases} \text{E*D ALT} + \Delta\text{ALT}, & \text{when E*D} > 10{,}000 \text{ ft} \\ 10{,}000 + \Delta\text{ALT}, & \text{when E*D} \leq 10{,}000 \text{ ft} \end{cases} \qquad (58)$$

where:

$$\Delta\text{ALT} = (K1 + K2\ \text{IASD} + K3\ \text{IASD}^2) + (K4 + K5\ \text{IASD} + K6\ \text{IASD}^2)\ \text{IAS}$$

IASD = selected descent IAS schedule

IAS = actual IAS

Constants K1 through K6 are given in table IV for various aircraft gross weights.

2.6.1.7 Simulation results: The final range error feedback control laws for the Mach region and the IAS region are shown in figures 79 and 80 respectively. Feedback gains were obtained via the linear system analyses as decribed in Section 2.6.1.2. The following parameters were added during analyses in the time domain simulations: a time command for changing the M*F assignment during descent, a Δtime bias for nulling B*D arrival time error, an airspeed command rate limiter for eliminating excessive aircraft sink rate, and a pitch command fader for smoothing pitch transients during mode engagement.

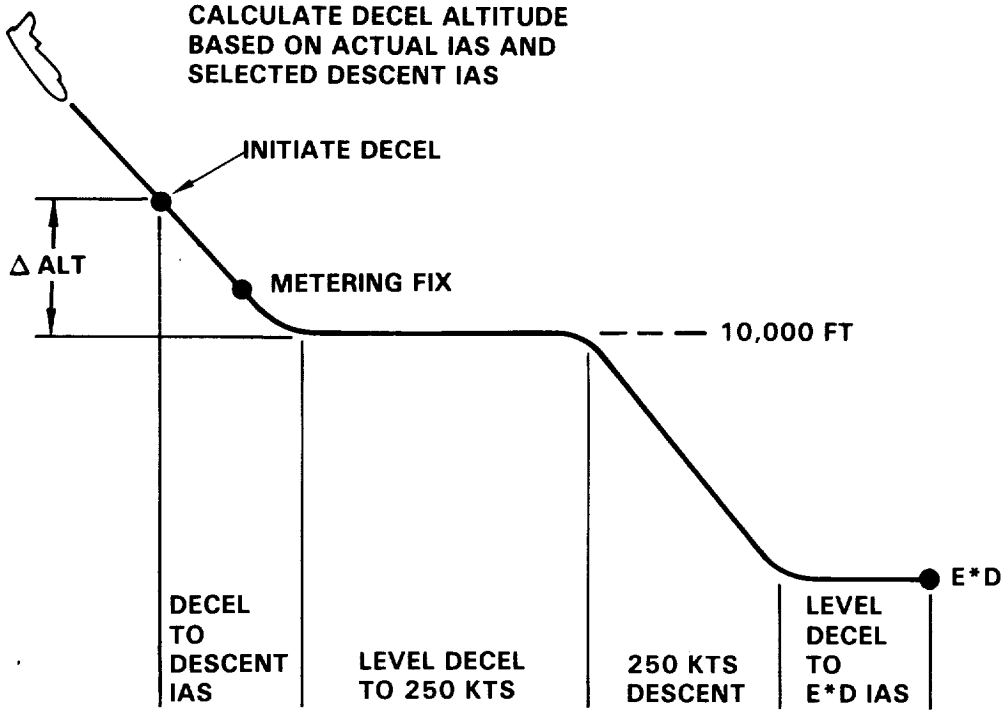

(a) E*D BELOW 10,000 FEET

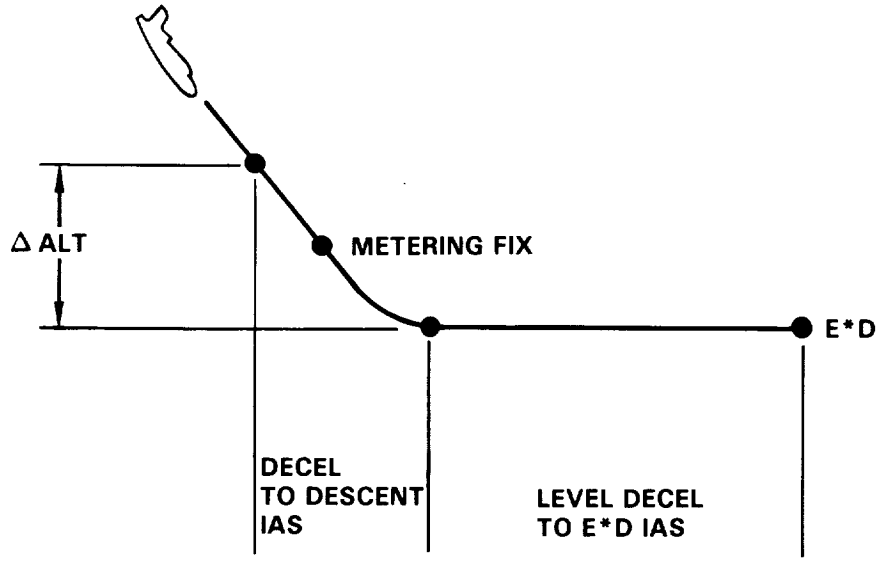

(b) E*D ABOVE OR EQUAL TO 10,000 FEET

Figure 74. - Deceleration to E*D.

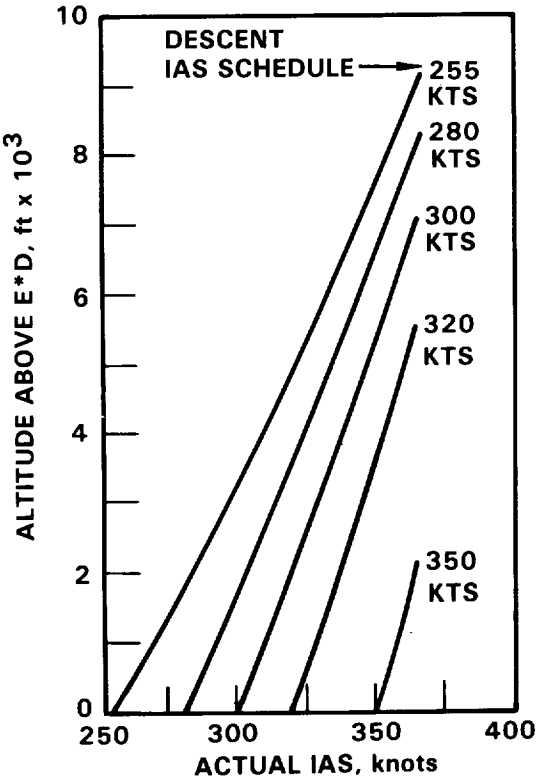

Figure 75. - Deceleration incremental altitudes, 250,000 pounds weight.

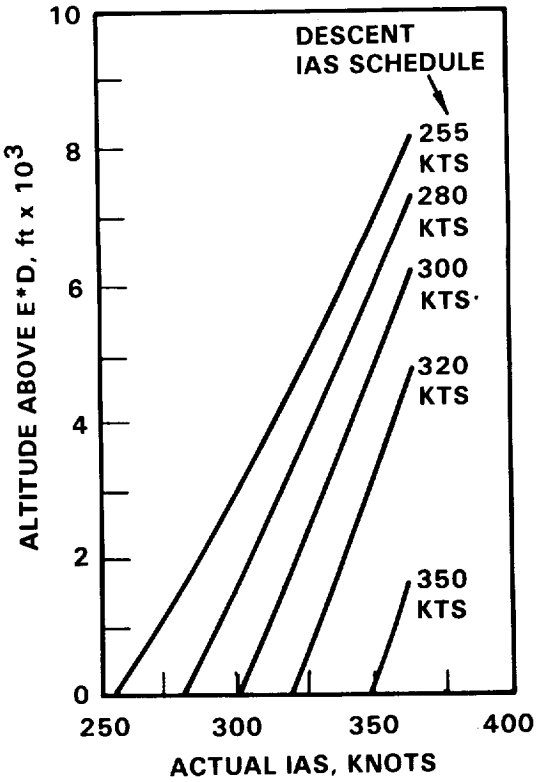

Figure 76. - Deceleration incremental altitudes, 300,000 pounds weight.

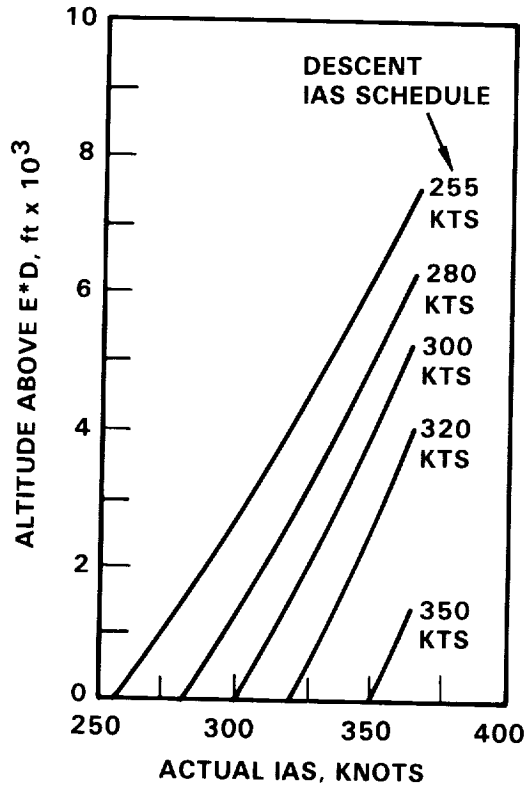

Figure 77. - Deceleration incremental altitudes, 350,000 pounds weight.

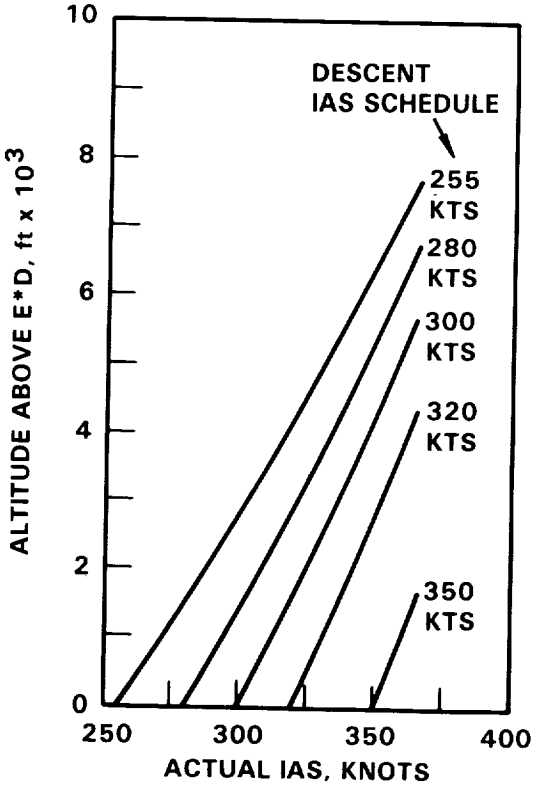

Figure 78. - Deceleration incremental altitudes, 400,000 pounds weight.

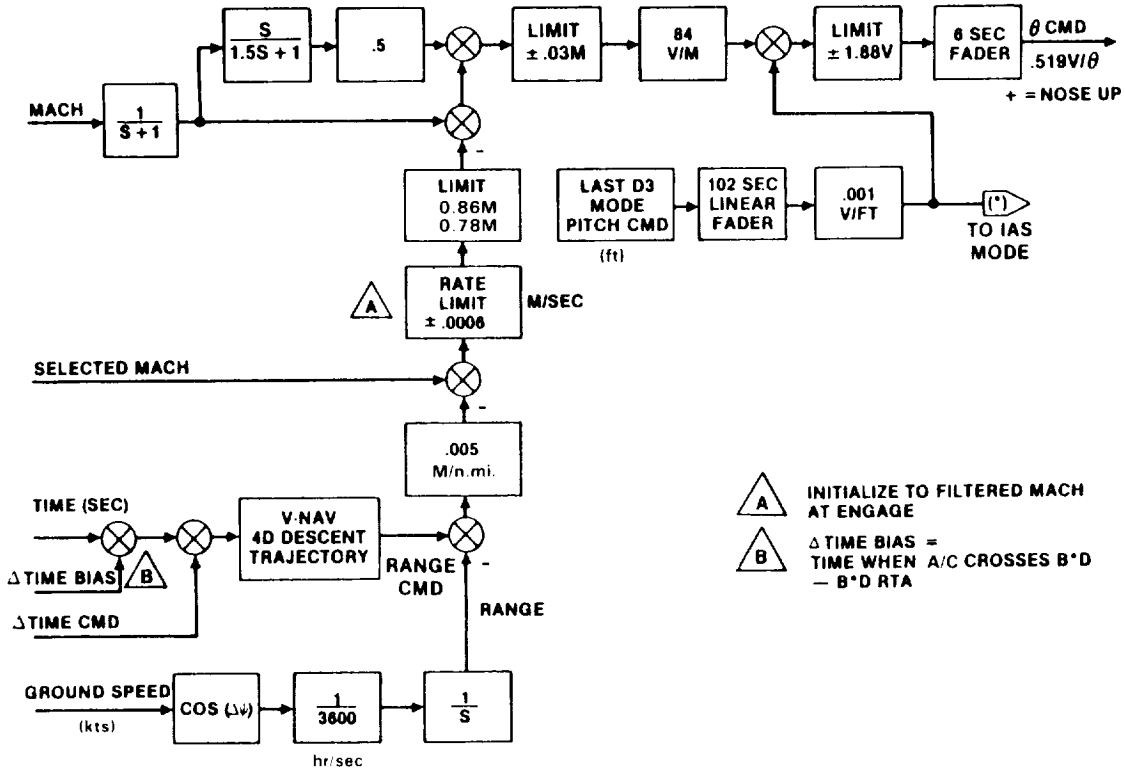

Figure 79. - Range error feedback, Mach region.

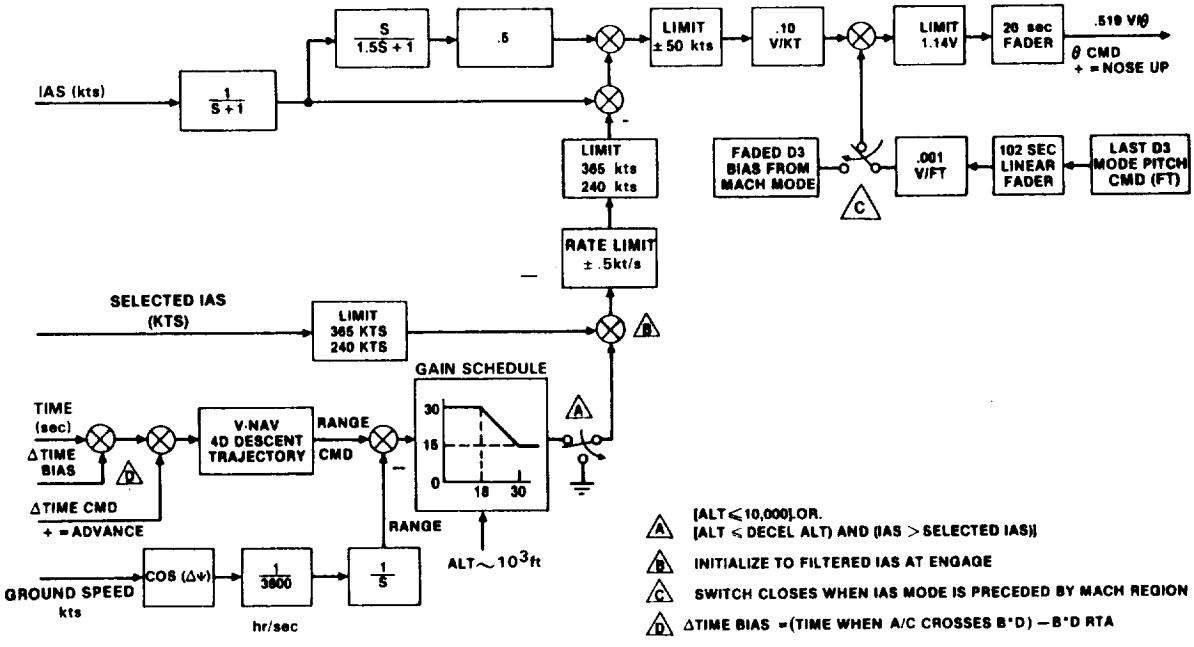

Figure 80. - Range error feedback, CAS region.

TABLE IV. - DECEL ΔALT COEFFICIENTS

W X 10^3 lbs	k1	k2	k3	k4	k5	k6
250	$-1.35 \times 10^{+4}$	164.8	-.7655	-41.51	.3834	4.007×10^{-4}
300	$-1.379 \times 10^{+4}$	145.2	-.6507	-16.93	.2525	4.163×10^{-4}
350	$-1.68 \times 10^{+4}$	147.1	-.5946	12.80	.0820	5.517×10^{-4}
400	$2.916 \times 10^{+4}$	-200.0	.0713	-98.82	.9315	-1.105×10^{-3}

The effect of using the segmented wind model was evaluated by simulation using the typical wind condition shown in figure 81. Figure 82 shows the 4-D descent performance obtained using a linear wind model and segmented wind model. When the linear wind model was used, a maximum speed of 365 knots IAS was required to correct the time errors resulting from unmodeled winds; also, a time error of -14.6 seconds was recorded at the metering fix altitude of 15,000 feet. For the segmented wind model, the speed remains very close to the nominal descent speed of 320 knots IAS, leaving a wide margin of speed change capability (time flexibility) for handling future ATC-imposed changes to the metering-fix arrival time assignment. An arrival error of 0.2 seconds was recorded at the metering fix, a significant improvement over using the linear wind model. The effectiveness of the control law was evaluated by comparison to a descent without the 4-D control law. The errors in metering time/altitude, and E*D airspeed are tabulated in table V. Time history plots are presented in Appendix A.

2.6.2 Cruise control law development.- The objective in the cruise region is to arrive at the beginning of descent (B*D) at its precomputed arrival time. This is accomplished by computing and flying a required airspeed when ground trajectory, flight time requirement and wind conditions are known.

An airspeed command generator, shown in figure 83, was developed based on the results of the cruise guidance algorithm of Section 2.5.2. An iterative computational process (equation 50) is used to compute a TAS command every 6.5 seconds using the following inputs:

- ground track trajectory - circular-arc and straight-line segments from current aircraft position to B*D
- remaining flight time requirement to B*D, i.e.,

$$T_c = \text{B*D RTA} - \text{GMT}$$

- predicted wind at each waypoint.

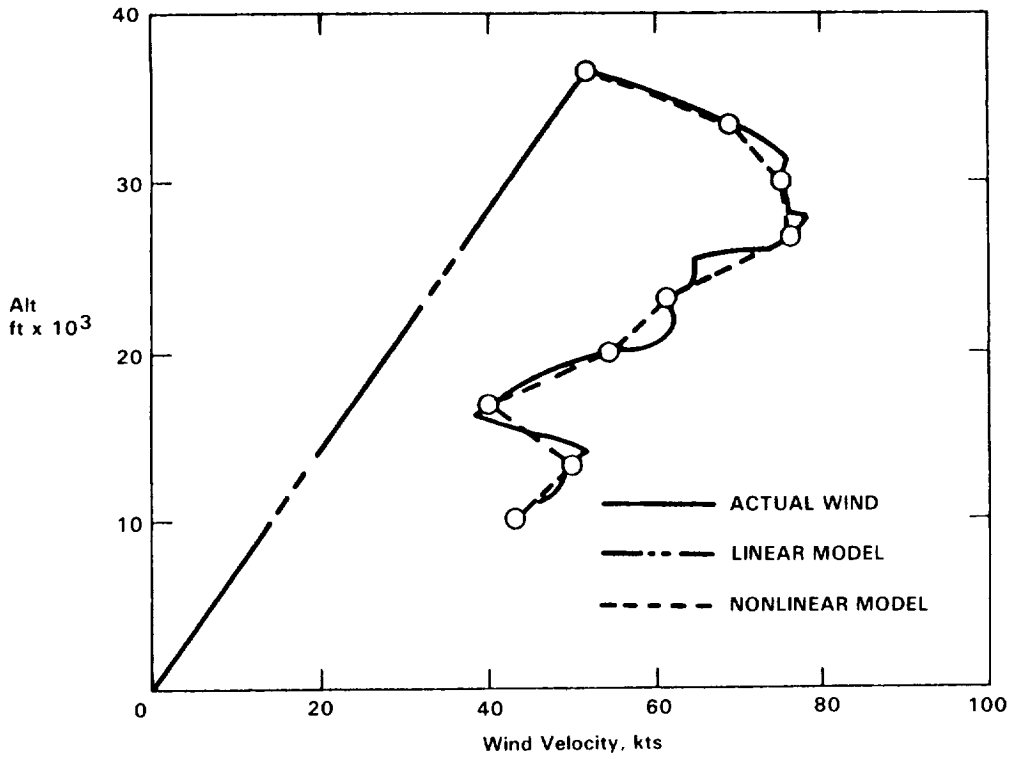

Figure 81. - Simulation wind model.

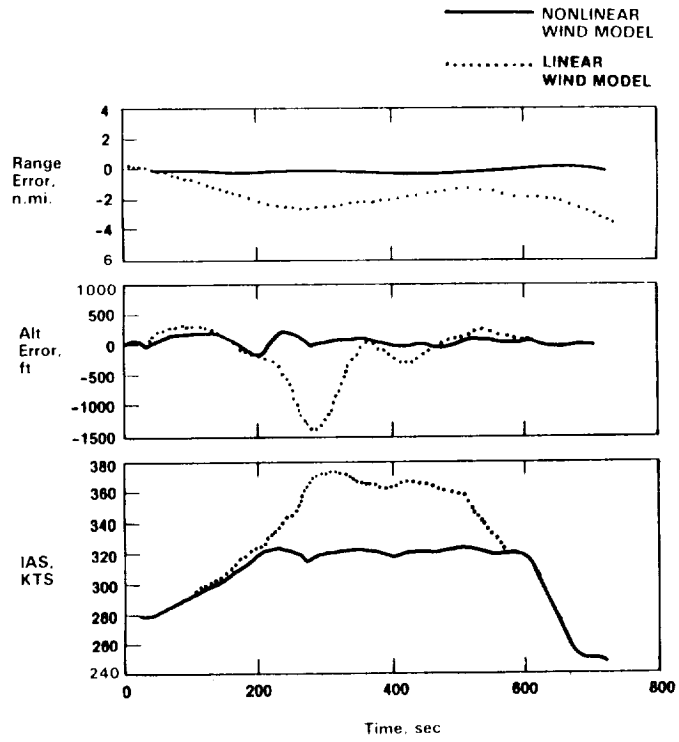

Figure 82. - Effects of wind modeling on descent performance.

TABLE V. - 4-D DESCENT SIMULATION RESULTS

	CONTROL OFF			CONTROL ON		
Wind Model	M*F Time Error, sec	M*F Alt Error, ft	E*D CAS Error, kts	M*F Time Error, sec	M*F Alt Error, ft	E*D CAS Error, kts
Linear	-47.6	-192	+5.2	-14.6	-37	-0.7
Segmented	+ 1.2	+226	-1.9	+ 0.2	+53	-1.8

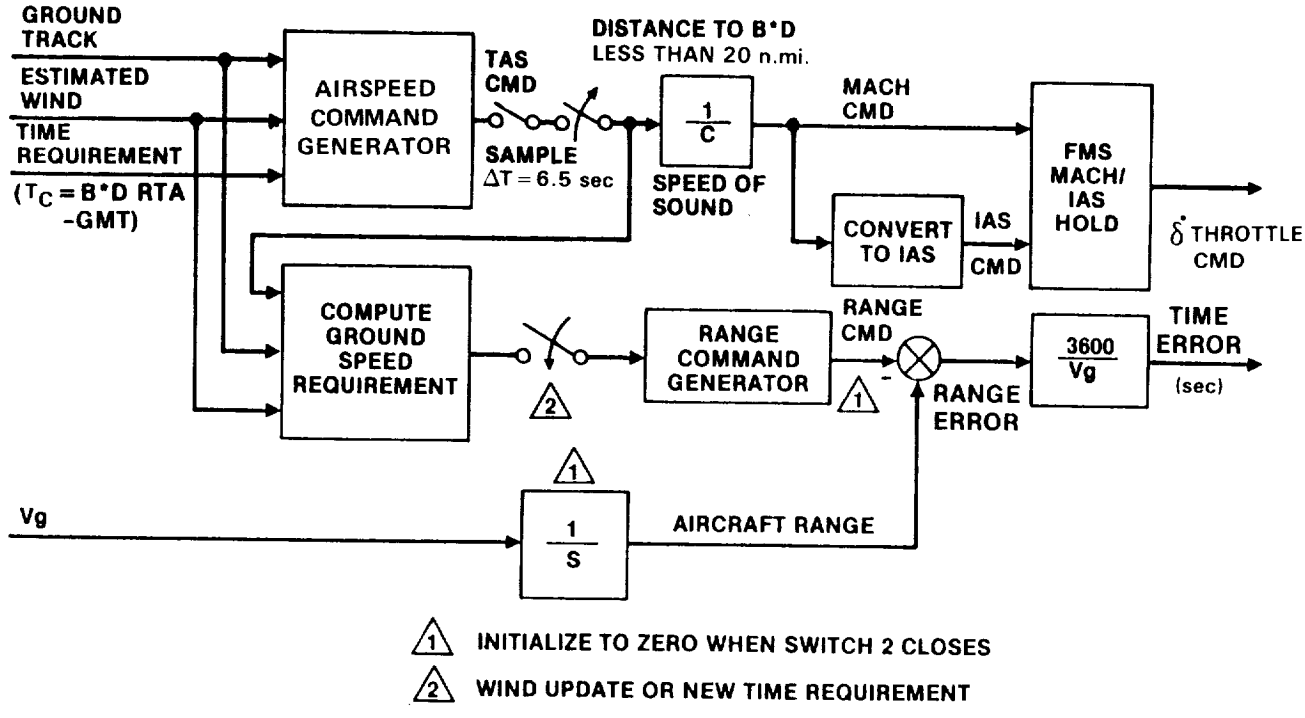

Figure 83. - 4-D cruise control law.

Ground track trajectory modeling and cruise wind prediction techniques are given in Sections 2.5.2 and 2.4.2 respectively. The resulting TAS commands are converted to Mach or IAS commands which are coupled to the FMS cruise control laws and the L-1011's autothrottle system for automatically flying the aircraft.

Range errors during 4-D cruise are calculated by comparing the aircraft's progress along the flight plan with a range command computed by the range command generator algorithm of Section 2.5.4. Time error is calculated by the equation:

$$\Delta\text{time} = 3600 \left(\frac{\text{aircraft range} - \text{range command}}{\text{aircraft ground speed}} \right) \qquad (59)$$

Time error is for information to the crew only; it does not apply to any control law.

To evaluate the performance of the cruise control law, the Dallas/Fort Worth Acton STAR was used with estimated waypoint winds as shown in table VI. An average of 20 knots unmodeled tailwind error was introduced. The resulting Mach commands computed by the airspeed generator are shown in the time histories of figure 84. Figure 85 shows the aircraft's range error with and without the 4-D cruise control law. Without the 4-D cruise control law, a 77.5 seconds early time error resulted; a 3.5 seconds early time error was recorded when the 4-D cruise control law was engaged.

TABLE VI. - 4-D CRUISE TEST TRAJECTORY

Waypoint	Distance to next waypoint, n.mi.	Track Heading (deg)	Estimated Wind (Kt)	Actual Wind (Kt)
Aircraft	176	70	40	40
Tuscola	38	73	65	45
B*D	-	-	60	54

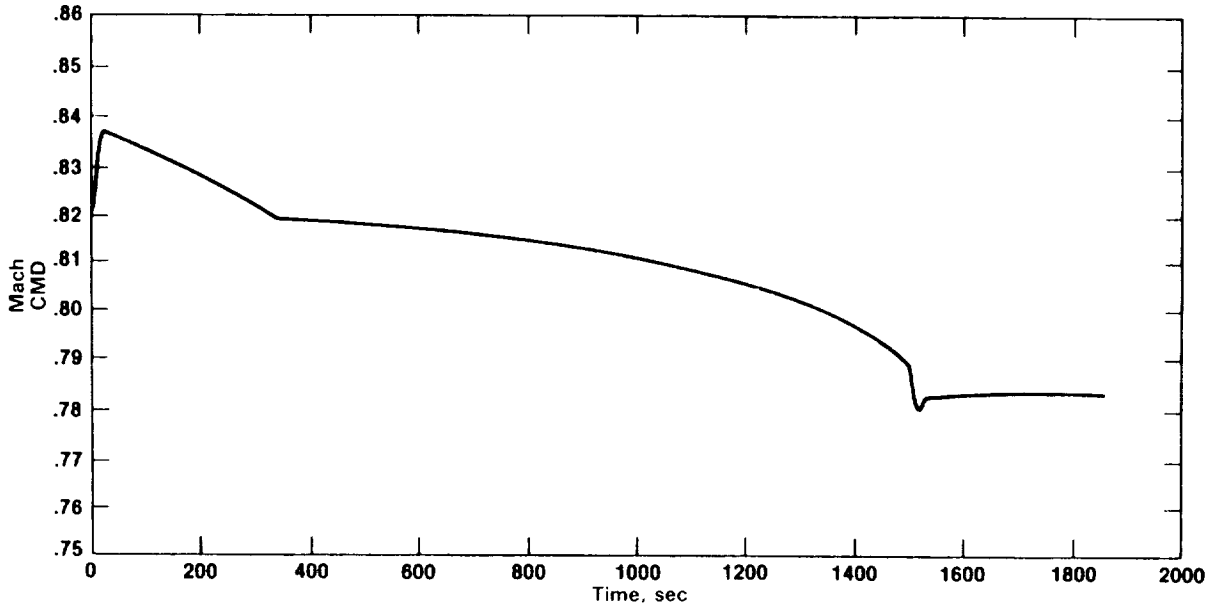

Figure 84. - 4-D cruise simulation, Mach command time history.

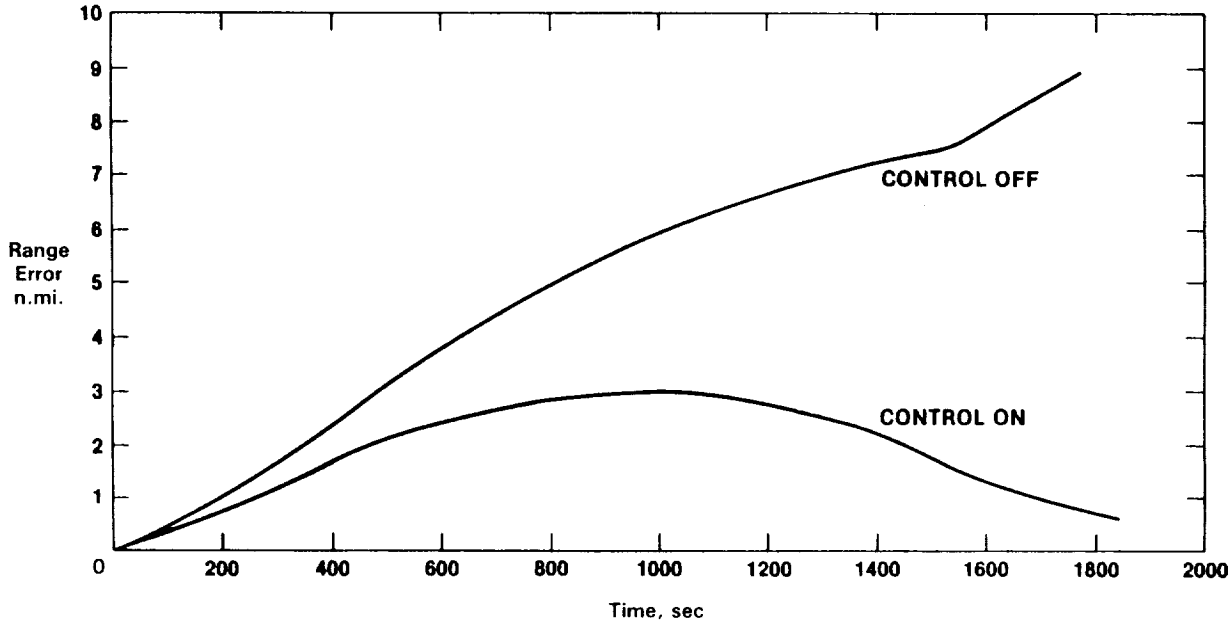

Figure 85. - 4-D cruise simulation, range error time history.

3. OPERATIONAL PROCEDURES

3.1 FMS Control and Display Unit Operation

The Control and Display Unit (CDU) enables the flight crew to instruct and provide data to the FMC, and to call up data for display on a gas discharge tube. See figure 86. Up to 7 lines of data may be displayed, with a maximum of 15 characters in each line. Line No. 1 is used to display the title of the data being displayed. Line 7 (the scratchpad) is normally blank, and is used to display data entered via the alphanumeric keyboard.

The data displayed on the screen is referred to as a "page" of data. Different pages are called up by pressing the CDU front panel pushbuttons. Many data pages permit changing or inserting data via the keyboard. To change or insert data, the index key adjacent to the line on the display to be changed is pressed to bring the line down to the scratchpad line. For example, if line 3 contained a waypoint, and it was desired to change it, pressing the second index key would cause the legend "IDENT?" to appear on the scratchpad. After the new waypoint was inserted via the keyboard, the legend "EXECUTE?" would appear on the scratchpad. If the bottom index key is now pressed, the new waypoint will be stored in the computer.

The index keys are also used on some data pages to call up more detailed data, or to select data pages to be displayed. For example, if the data page

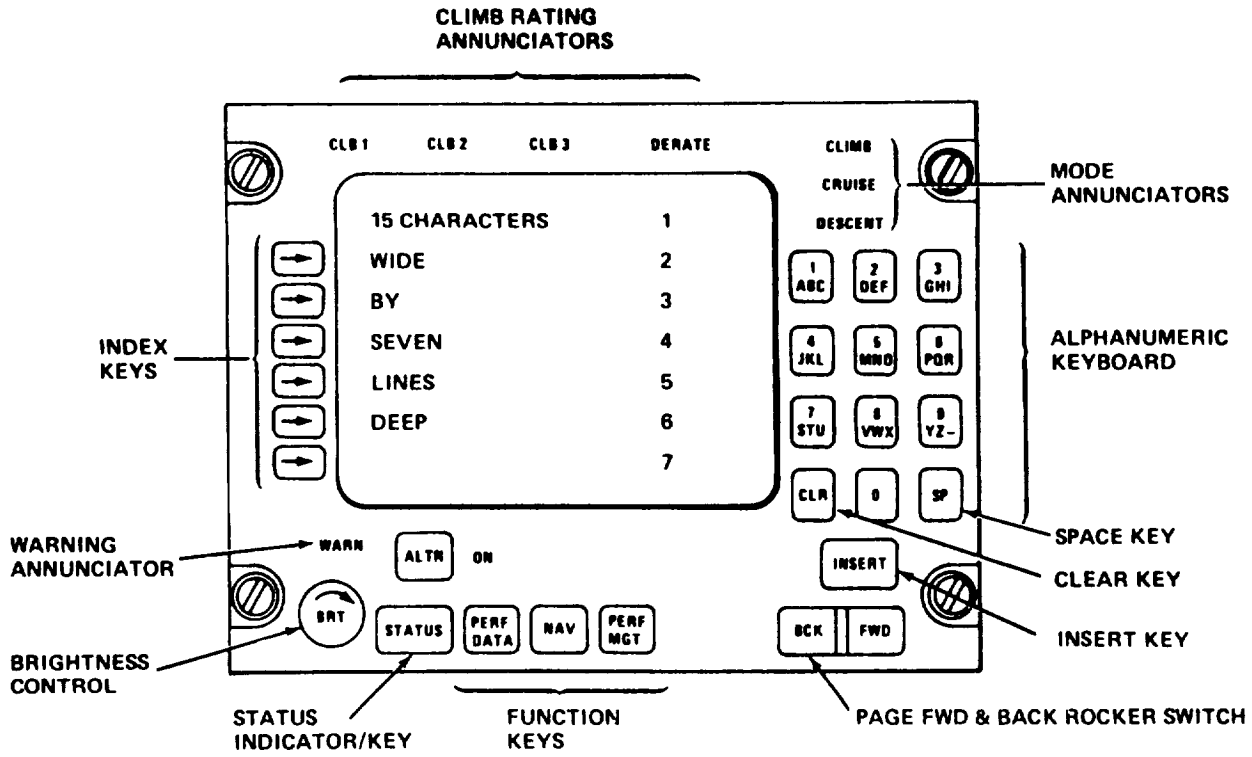

Figure 86. - FMS control and display unit.

shows a listing of the VHF stations stored in the computer, pressing the index key adjacent to any station in the listing calls up a data page listing the class, latitude, longitude, frequency, antenna altitude, and magnetic variation of the selected station. If the data displayed on a line is not permitted to be changed by the flight crew, pressing the index key adjacent to that line has no effect.

Data to be entered into the system memory are inserted using the alphanumeric keyboard. As the data are keyed in, they appear on the scratchpad. When entering alphanumeric data, each depression of a key enters the next character on the key; for example, pressing the upper left key once enters a "1" on the scratchpad; pressing it twice enters an "A", three times enters a "B", four times a "C". Continued pressing of a key continues to circulate through the four characters associated with the key. The SP (Space) key is used when entering two successive characters which appear on the same key. For example, to enter "ADF", the operator will press the top left key twice, press the top center key twice, press SP, press the top center key four times. When entering purely numerical data, pressing the SP key is unnecessary, even when two consecutive digits to be entered are identical. If an incorrect character is entered on the scratchpad, pressing CLR removes the last character entered and shifts the remaining characters in the scratchpad right one position. When the data have been entered on the scratchpad and checked visually by the operator, pressing the INSERT key inserts the scratchpad data into the proper line.

When data to be displayed cannot be contained on one page, the data are formatted into "booklets" of two or more pages. The BCK/FWD rocker switch permits viewing other pages of the booklet. To view the next page in the booklet, the FWD half is pressed. To view the previous page, the BCK half is pressed. The legend "END" appears at the bottom of the last page. If the switch is pressed and held, the display cycles through the several pages of a booklet. The NAV key calls up a menu page which permits selection of navigation functions by pressing the index key adjacent to the desired function. The PERF DATA key calls up a menu page which then permits selection by indexing of emergency operating modes (engine out), system test (on ground), and performance related data displays (rated EPR's, SAT, TAS, etc). The PERF MGT key calls up a performance management page. The page displayed depends on the system performance management mode. The STATUS indicator/key either flashes or lights steadily to alert the flight crew to an abnormal condition. Pressing STATUS calls up a booklet which shows the BITE system status. The BITE system self checks the FMS and tests the validities of data inputs to the FMS.

The mode annunciators light continuously to show the system performance management mode as summarized in Table VII.

TABLE VII. - MODE SUMMARY

System Mode	Arm Status	Annunciator Lighted
Semiautomatic	Thrust Mgt not engaged or climb & descent not armed. Thrust Mgt engaged & Climb armed. Thrust Mgt engaged & Descent armed.	None CLIMB DESCENT
Climb	N/A	CLIMB
Cruise	Climb armed Climb not armed Climb not armed and less than 2 minutes to B*D	CLIMB CRUISE CRUISE with DESCENT flashing
Hold (cruise mode more than 750 feet from cruise altitude)	Climb armed Descent armed	CLIMB DESCENT
Descent to new flight level	N/A	DESCENT
Descent to E*D	N/A	DESCENT

The CLB1, CLB2, or CLB3 indicator lights to indicate the engine climb rating being used. DERATE lights if a manual derate has been entered. The WARN annunciator lights (and STATUS flashes) if the FMC fails one of its self-test procedures. When WARN lights, if the FMC failure permits, a message is displayed on the CDU screen indicating the test failed. The BRT control adjusts the brightness level of the CDU display. The ALTN key permits viewing page selected by other CDU in systems utilizing dual independent page viewing.

3.2 4-D CDU Procedures

The following sections describe the FMS CDU pages which allow the flight crew to interact with the 4-D Flight Management System. These CDU procedures reflect the outcome of several workshops held with Dallas/Fort Worth ARTCC and TRACON personnel, discussions with Lockheed L-1011 engineering test pilots, and represent minimum changes to the existing production FMS operational procedures. Shaded areas on the accompanying figures are used to show existing display formats; unshaded areas/pages represent new features required for 4-D.

3.2.1 Enter GMT (see figure 87). - The production FMS displays Greenwich Mean Time with the least significant digit equal to one minute, although the updating of real time within the flight management computer is maintained very accurately. The illustrated change to this CDU page simply displays GMT with the least significant digit equal to one second.

3.2.2 M*F ETA. - Figure 88 shows that no changes are necessary to the CDU procedures to be able to display the estimated time of arrival at the metering fix (designated M*F). Although much has been added to the FMS software to allow calculation of M*F ETA, to the flight crew it is simply another waypoint (like GHI) which is located in the descent between B*D and E*D. The ETA is shown with least significant digit equal to one minute to be consistent with today's ATC practices.

3.2.3 Enter M*F RTA.- A new CDU page as shown in figures 87 and 88 was created to allow the flight crew to interact with the 4-D FMS and the ATC controller when the metering fix arrival time assignment is given.

Figure 89 informs the crew that M*F is presently estimated at GMT 19:33; i.e.,

M*F E 19:33

under the present CRZ Mach number of 0.820 and with a planned descent speed schedule of 0.820 M/320 IAS. Information is also given that if necessary the existing time flexibility could accommodate an M*F arrival time assignment of 19:29 to 19:37 GMT; i.e.,

CHG: 29/37

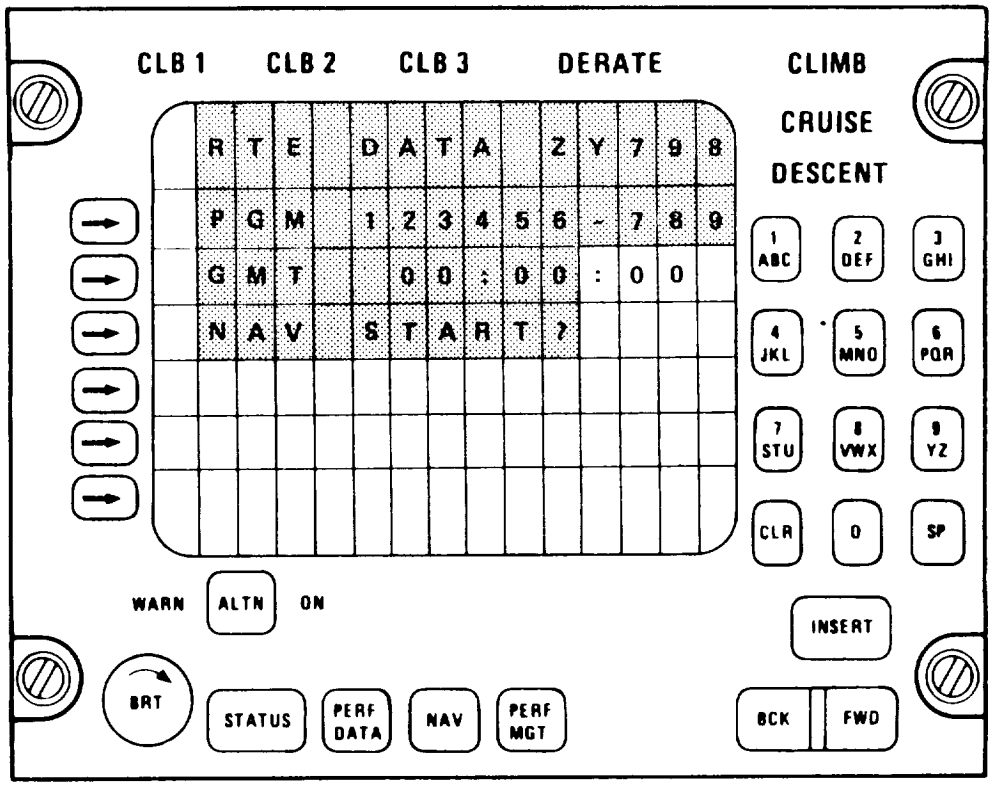

Figure 87. - Enter GMT.

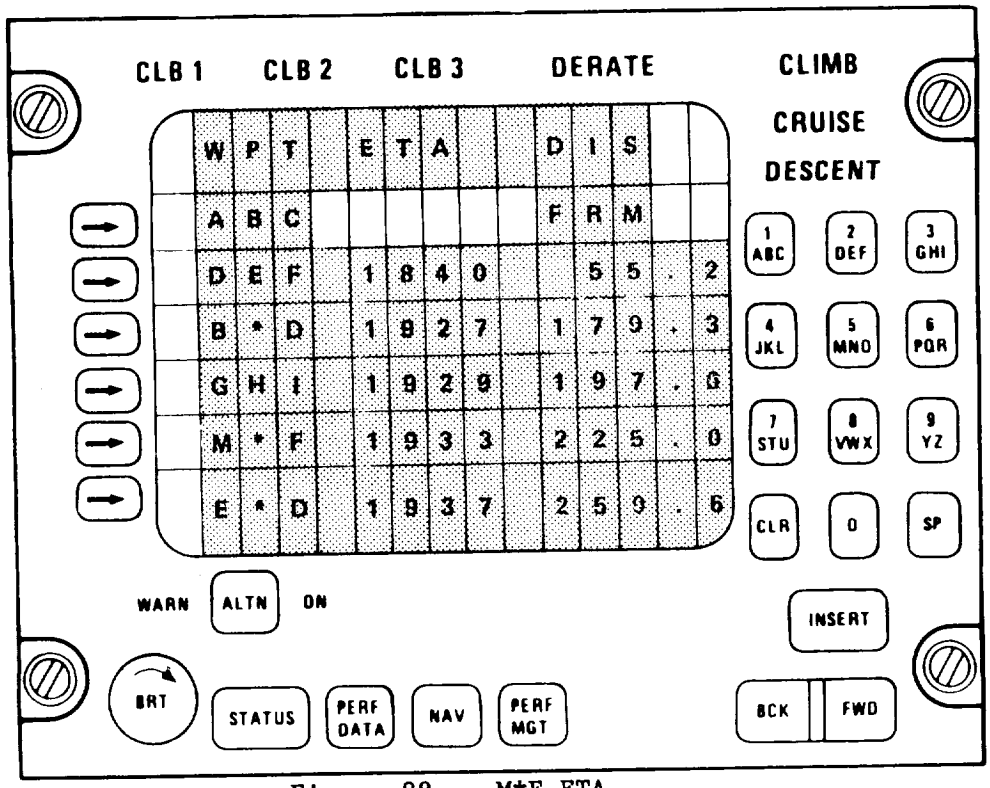

Figure 88. - M*F ETA.

Armed with this information, the crew advises ATC of the M*F ETA and awaits either acceptance (which should usually be the case) or the receipt of a new arrival time assignment. If the ETA is accepted, no further action is necessary; the system will use the ETA as the required time of arrival (RTA).

If, however, ATC specifies a different RTA, the crew will know immediately if it falls within the capabilities of the system (in this case 19:29 to 19:37) and can advise ATC if the new objective cannot be met by speed changes alone. If the RTA is possible, pressing the index button adjacent to the M*F ETA line activates the scratchpad line (see figure 89) so that the M*F RTA can be entered into the system . Note that the entire RTA can be entered, e.g., 19:35, or that the crew has the option of specifying later (L) or sooner (S) and the number of minutes. In the illustration L2 was entered resulting in the RTA of 19:35 i.e.,

R19:35 L2

The R means RTA and L2 reminds the crew that a two minute delay has been entered into the system.

After the M*F RTA has been entered, note that the FMS computer has changed the planned descent speed schedule of 0.820/320 to 0.800/300 to accommodate the delay. This information is immediately available to the crew to relay to ATC in the acknowledgement radio transmission.

3.2.4 Vectoring.- Sometimes it becomes necessary for ATC to vector an aircraft off course to avoid conflict with other traffic or severe weather. This can occur in cruise prior to the beginning of descent as in figure 90, or after descent initiation, prior to M*F as in figure 91. For either case, the CDU page shown in figure 92 serves as an illustrative example.

The current M*F required time of arrival (RTA) is shown as 19:35 and is 225.0 n.mi. away; i.e.,

M*F 19:35 225.0

assuming that all waypoints shown in the waypoint list are flown in succession.

Because of traffic, ATC calls and requires an immediate vectoring off course; to expedite compliance with this requirement, the pilot disengages FMS and manually turns the aircraft to the new heading.

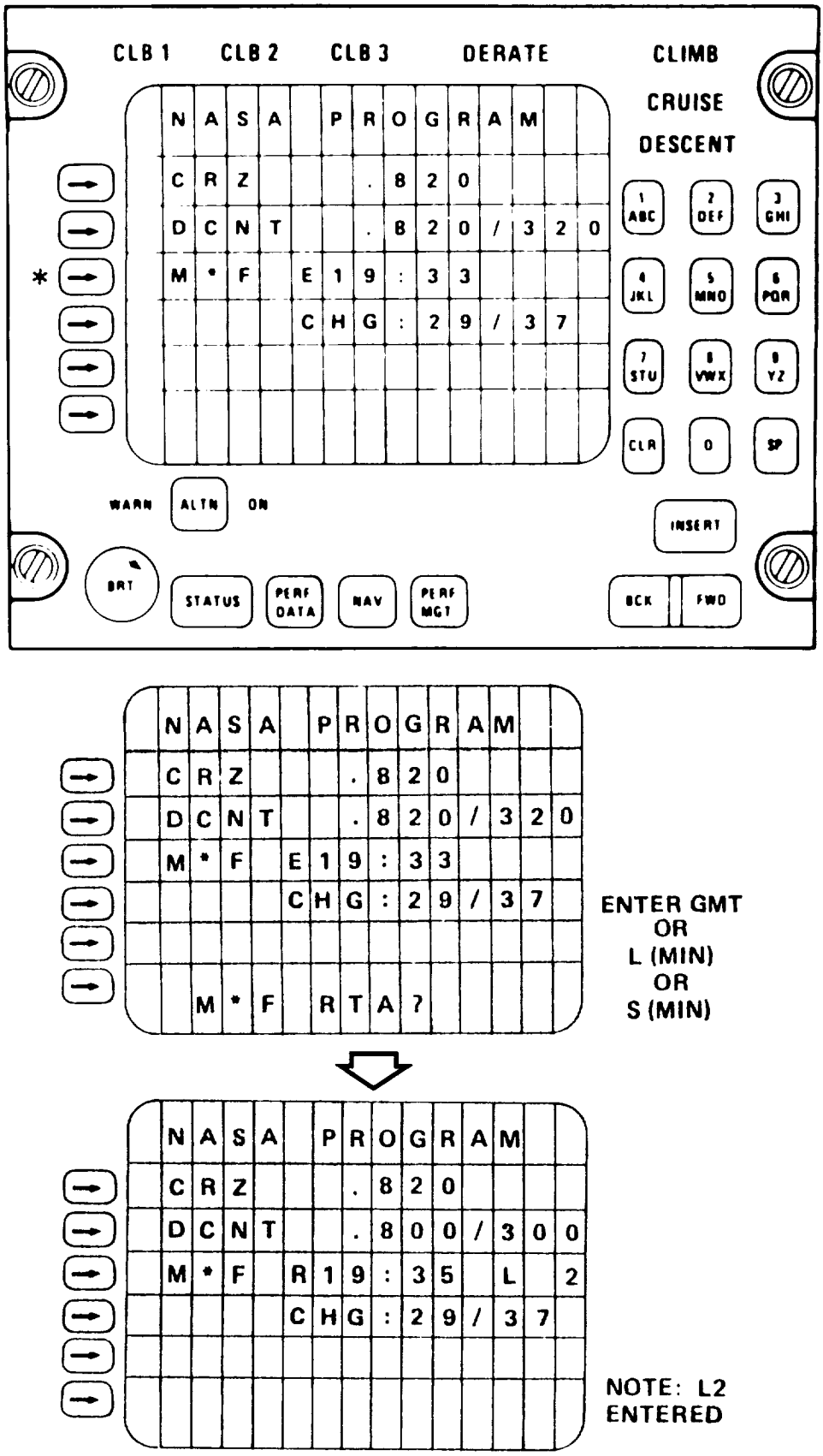

Figure 89. - Enter M*F RTA

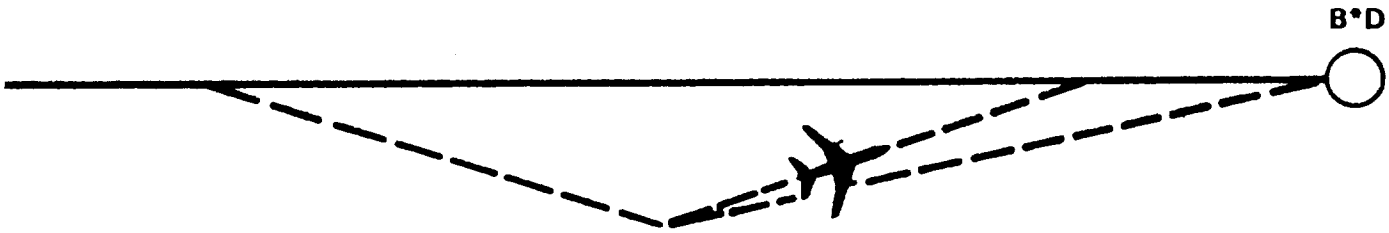

Figure 90. - Cruise vectoring.

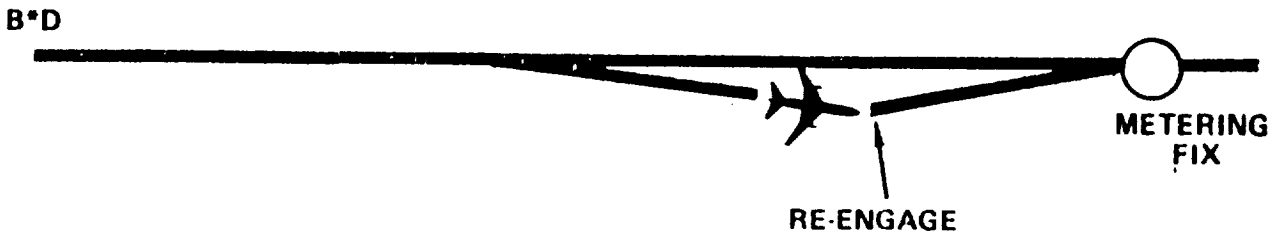

Figure 91. - Descent vectoring.

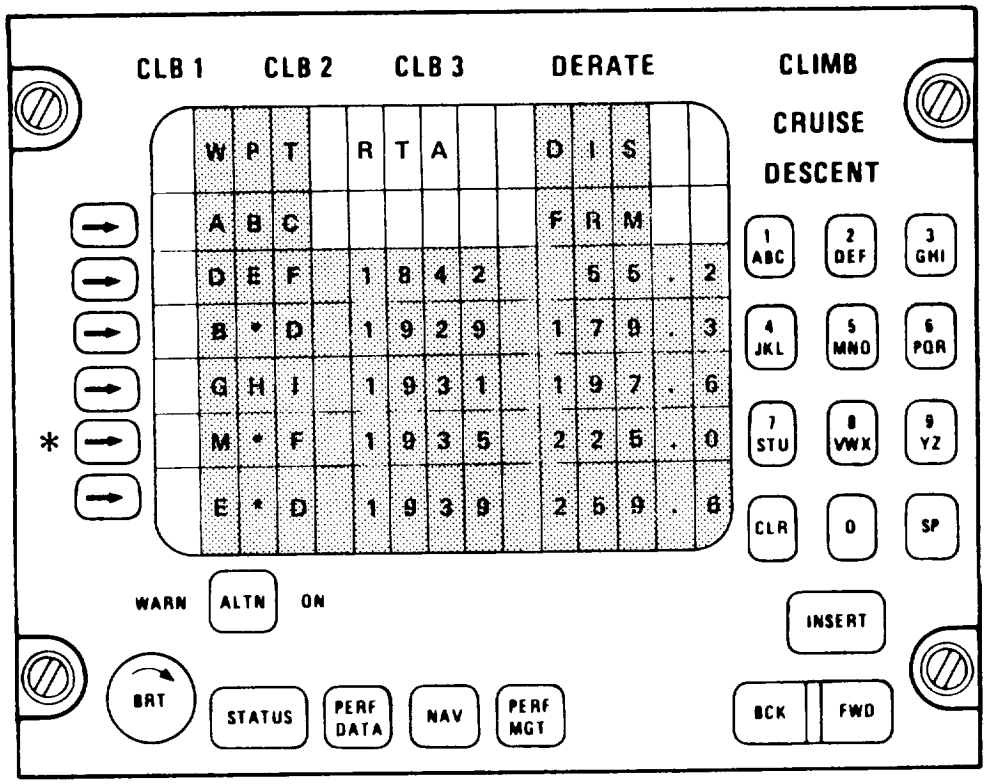

Figure 92. - Vectoring.

ATC then instructs the pilot to maintain this heading until, at pilot's discretion, the aircraft can be turned direct to M*F at a time to meet the RTA. Depressing the index button adjacent to the M*F data line calls the waypoint detail page for M*F as shown in figure 93. By watching the ETA DIRECT to M*F statement at the bottom of the page, the pilot can initiate an FMS GO DIRECT procedure when the ETA reads 19:35, the original RTA.

3.2.5 Level-off in Descent.- At times, flight crews are instructed to level off during descent into the terminal airspace, for example when the high altitude controller hands the aircraft off to the low altitude controller. When instructed to resume the descent, the 4-D aircraft must be capable of re-engaging the descent profile and arriving within the metering fix window at the assigned time. This is illustrated in figure 94.

No new CDU procedures are required to effect the 4-D level-off (see figure 95). The existing interim hold page appears if a hold is initiated in descent. The 4-D software keeps track of the M*F RTA requirement such that when the descent is re-engaged, the aircraft again captures the descent profile and makes good the RTA.

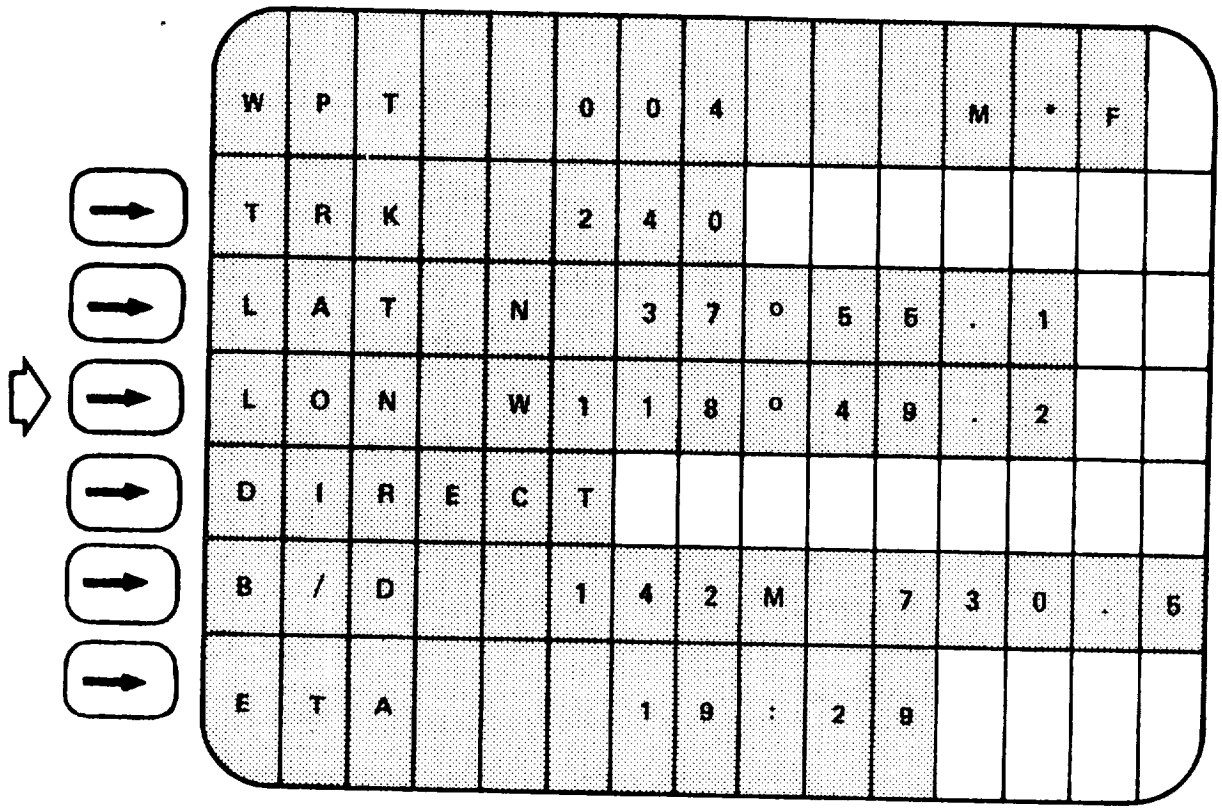

Figure 93. - Waypoint detail page.

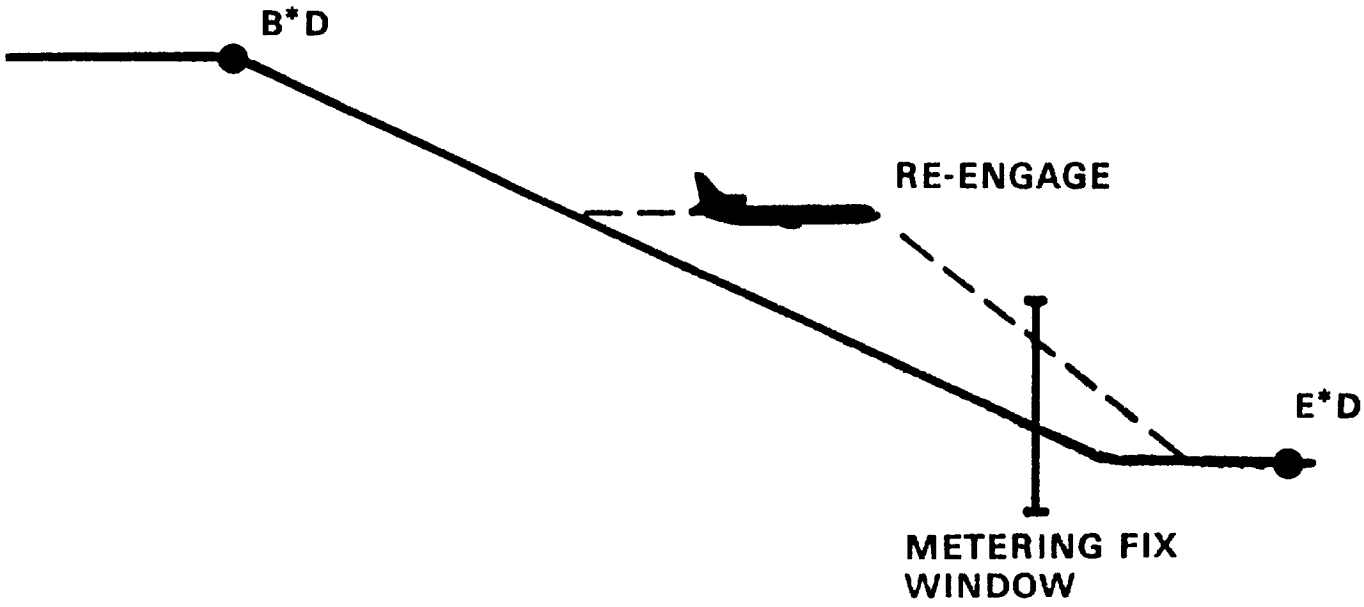

Figure 94. - Level-off in descent

3.2.6 Descent Profiles.- A new booklet of CDU pages was programmed primarily to facilitate flight test engineering activities. Although not intended for airlines operational use, they are included here for completeness.

By depressing the index button adjacent to ALTITUDE, TIME, or WIND (figure 96) pages of descent data relating range/altitude, range/time, and wind and altitude can be called up for display. The altitude and time profile pages are passive; that is, they reflect the results of system entries made via other CDU procedures. The wind profile page, however, is active, in that wind direction and speed can be entered for any 500 foot increment of altitude in the descent. The provision is also made for entering "valid time" for the forecast or pilot-reported wind data entered. This allows the statistical blending of these data with current observations as discussed in earlier sections of this report. Wind direction can be entered by either magnetic or true heading convention to facilitate entering information reported by preceding aircraft; the FMS automatically performs the magnetic/true heading conversion based on its knowledge of changes in magnetic variation along the intended flight plan.

This wind entry procedure is provided to bridge the gap between present manual methods of entering wind data and the time when this information will be data-linked to the aircraft automatically.

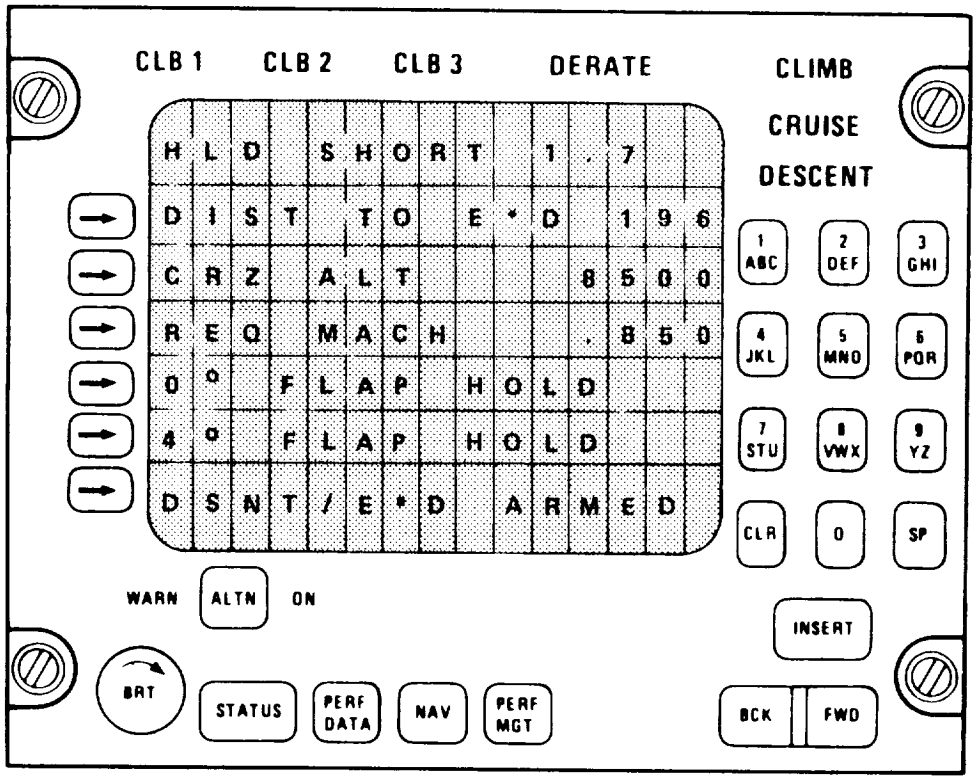

Figure 95. - Level-off in descent.

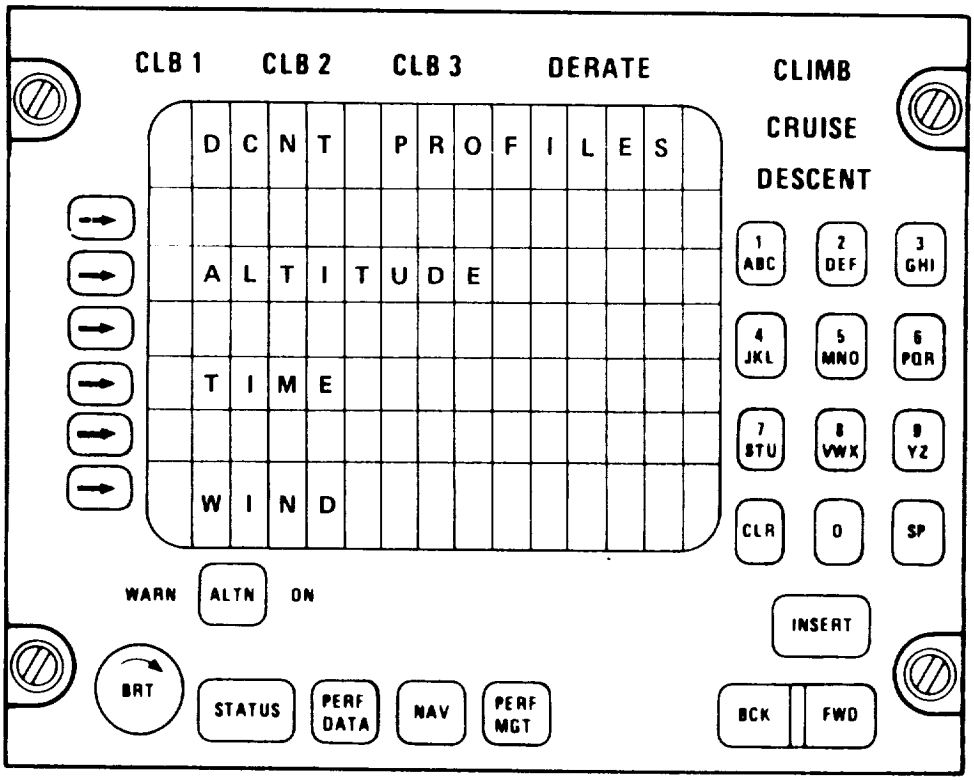

Figure 96. - Descent profile data.

4. FMS SOFTWARE

4.1 Background

Lockheed developed and certified the first flight management system (FMS) in 1977; the FMS has been flying in commercial airline revenue service in the L-1011 since that time. In order to protect its proprietary interests, Lockheed chose to develop all 4D-related software for the NASA ATOPS Program using internal funds. Because of this, detailed FMS computer coding data are not furnished with this report. The sections that follow will, however, describe in general the internally-funded software development that accompanied the NASA-funded 4-D design and analysis tasks.

4.2 Computer Organization

The 4-D FMS computer program consists of some 50,000 instructions and used the L-1011 FMS program as a basis. The program was modularized, then modified to accept the 4-D algorithms and operational procedures. The target machine is the L-1011-500 Flight Management System computer (an ARMA 1813 Micro D), designed in general accordance with ARINC Specification 582, but with additional memory and I/O capability to support the research activities associated with the NASA ATOPS program. Figure 97 illustrates the elements of the Advanced FMS used for the NASA/Lockheed ATOPS program - the Flight Management Computer (FMC) and the Control and Display Unit (CDU). The FMC is the central controller and data processor of the FMS system. The CDU enables the flight crew to enter data and instructions into and receive data from the FMC. The CDUs are located in the L-1011 center console, just forward of the throttles as shown in figure 98.

4.3 Interactive Assembler Development

In addition to the generation of the actual 4-D FMS software, other Lockheed-funded activities supporting the NASA ATOPS Program accomplished the following specific achievements:

- An advanced assembler which can assemble programs for virtually any airborne computer was developed and tested.
- An interactive compiler/loader was provided.
- A machine-language load module generator was developed.

The L-1011 Flight Management System source modules have been installed under the IBM TSO system, with full screen interactive edit via IBM 3278 terminals. Figure 99 shows a typical terminal installation in an engineering office. The assembler output is immediately available via the 3278 terminals, requiring no waiting for print outputs. After all modules are compiled a link editior is used to tie them together into one continuous program. Figure 100

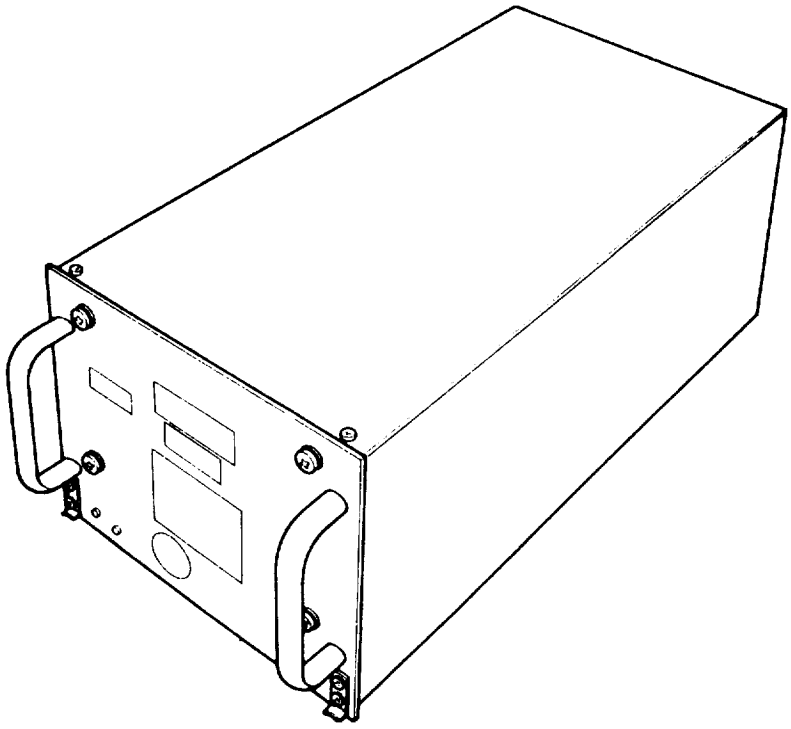

FLIGHT MANAGEMENT COMPUTER

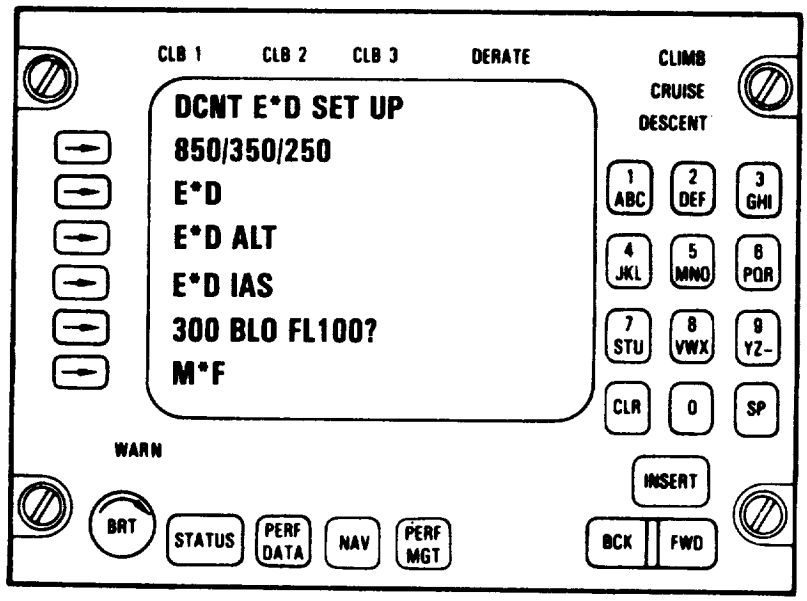

CONTROL AND DISPLAY UNIT

Figure 97. - Advanced flight management system.

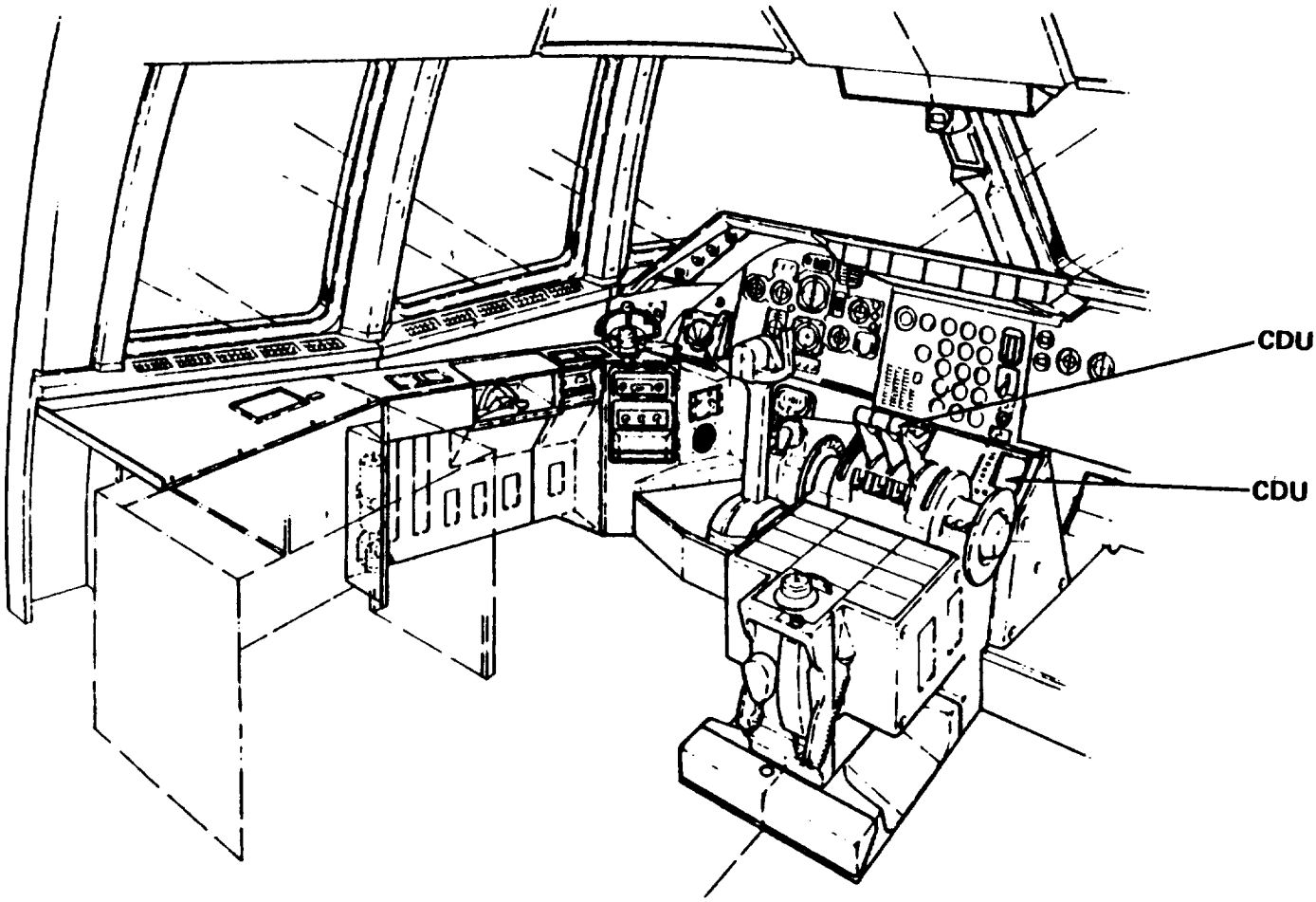

Figure 98. - FMS flight station equipment location.

Figure 99. - TSO terminal, advanced software development office.

Figure 100. - Central computer complex.

is a view of Lockheed-California Company's central computer complex which hosts the software development tools described above.

4.4 Software Laboratory

A software development laboratory was established at the Lockheed Flight Test Center at Palmdale, California and is fully operational. FMS software that has been prepared and assembled in the engineering offices (see Section 4.3) is transmitted via high-speed link from Lockheed's central computer complex in Burbank, California, directly into the airborne FMS computer located in the Palmdale lab, a distance of over 50 miles. Figure 101 is a photograph of the software laboratory in its early development. At this point, the software can be operationally tested on the target computer at device and system level, and full scale integration tests conducted at aircraft level using the L-1011 Hot Mock-up facility prior to actual flight tests.

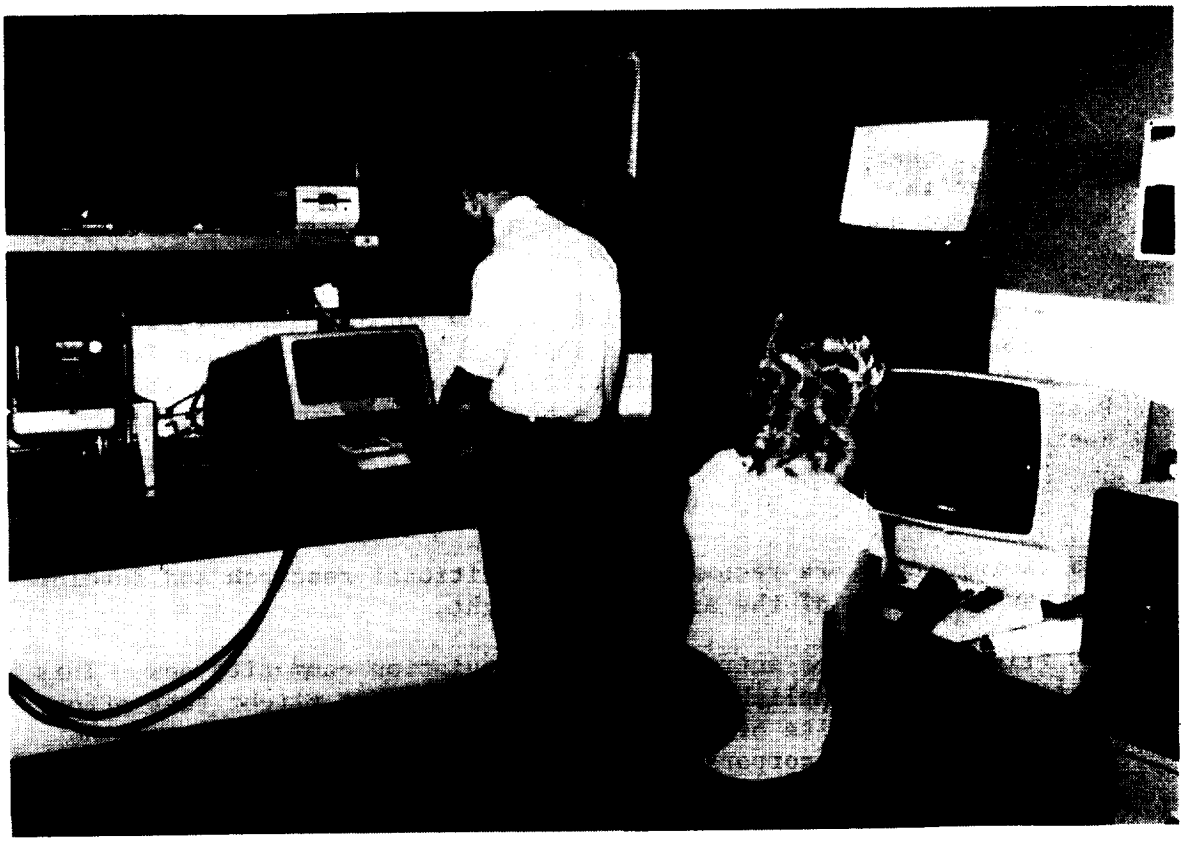

Figure 101. - Advanced software development laboratory.

5. CONCLUSIONS AND RECOMMENDATIONS

5.1 Conclusions

The following are conclusions reached as a result of the activities performed under the ATOPS program.

- A 4-D flight management system can be designed which is capable of fitting in with today's ATC environment

- The 4-D equipped aircraft can serve a useful purpose today by conserving fuel. It also offers the potential for enhancing safety and reducing workload for the flight crew and the ATC controller.

- Today's state-of-the-art allows the 4-D equipped aircraft to accept an arrival time requirement before take-off, fly the entire flight in a fuel optimum manner, accept changes to the flight path or the time assignment from ATC and arrive at the metering fix boundary of terminal airspace on schedule.

- Time and path flexibility are necessary system features for successful 4-D operation. Time flexibility is required to compensate for unmodeled wind and performance errors, and along with path flexibility, to accommodate changes imposed by ATC.

- Better wind information (e.g., data-linked to the aircraft) increases the amount of flexibility budget that can be made available for handling changes to the arrival time. However, it appears that enough flexibility exists with today's technology to allow successful 4-D operations for all but the most severe weather conditions.

5.2 Recommendations

The following items are recommended for additional research and development to further the state of the art of 4-D flight.

- 4-D flight should be introduced to the aviation community now. This could best be accomplished by supporting a modest flight test effort to verify the results of lab simulation, and then inviting airline participation by incorporating the 4-D algorithms into existing FMS equipment.

- Research should be conducted by industry working with the Air Traffic Service to compare the ARTCC descent models with actual aircraft performance data, for each of today's most prevalent aircraft types. This should be done for all STARs at each of the major airport

terminal areas in the United States. Results obtained from this effort could then be used to optimize flight and reduce air traffic congestion.

- Effort should begin on developing a ground-to-air and air-to-air data link capability using available technology, such as the ARINC Communication Addressing and Reporting System (ACARS) to furnish the 4-D equipped aircraft with near real-time wind data from preceeding flights.

- An ongoing dialogue should be maintained with ATC, the airlines, and the system developers such as Lockheed and NASA, to assure that the progress made satisfies real needs and fits into the ATC system.

APPENDIX A

CLOSED LOOP DESCENT SIMULATION PLOTS

This appendix contains computer-generated graphs (figures 102-112) illustrating the results of a closed-loop 4-D descent simulation. The effects upon altitude, descent range, and speed are presented as well as control surface activity, attitude, and thrust and drag requirements. The descent speed schedule used to obtain this data was Mach = 0.82/IAS = 320 kts. The descent trajectory was computed using the nonlinear wind model of figure 81; the performance simulation was conducted using the actual winds of figure 81.

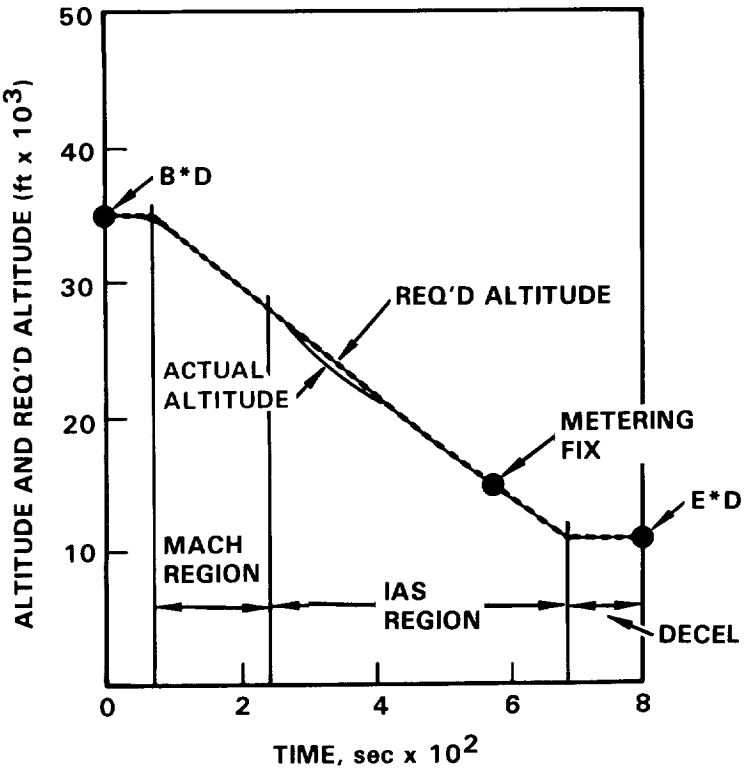

Figure 102. - Descent profile, W = 360000 lb.

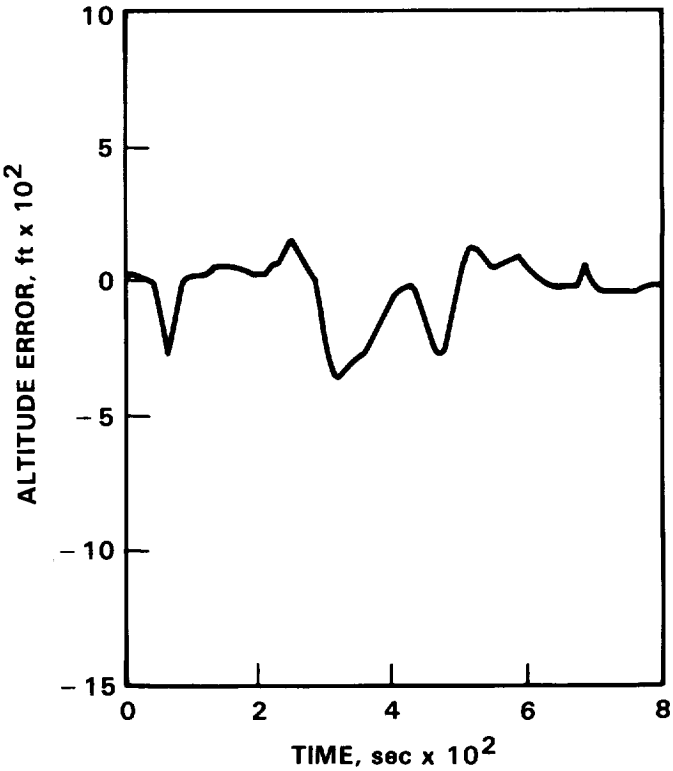

Figure 103. - Altitude error.

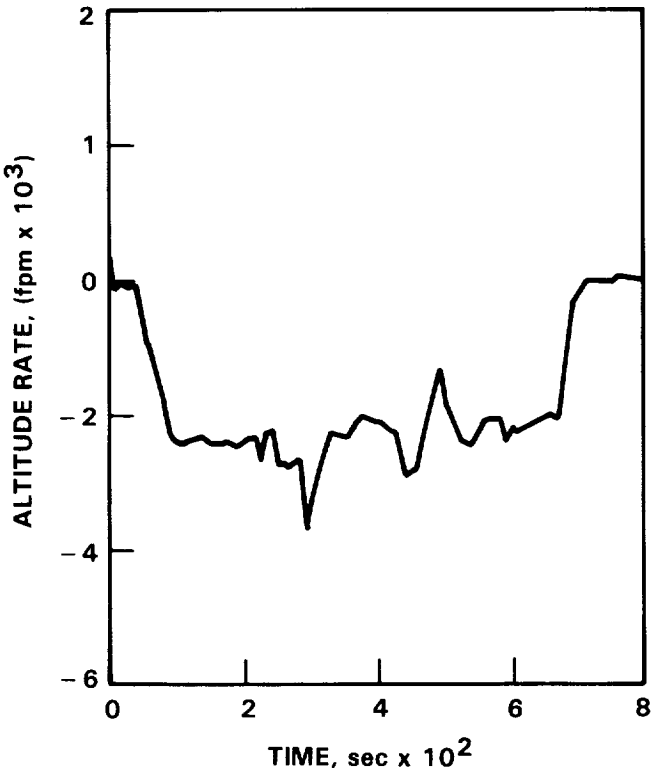

Figure 104. - Altitude rate.

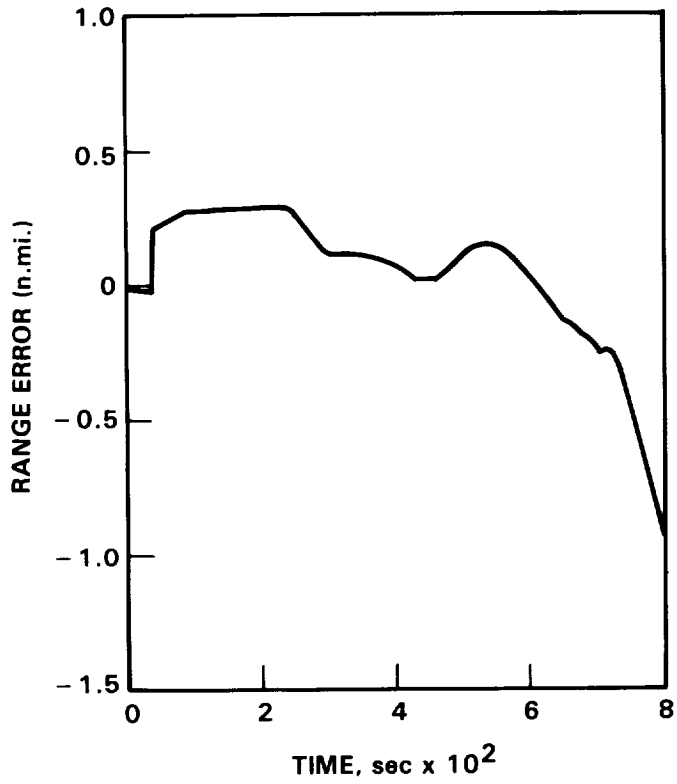

Figure 105. - Range error.

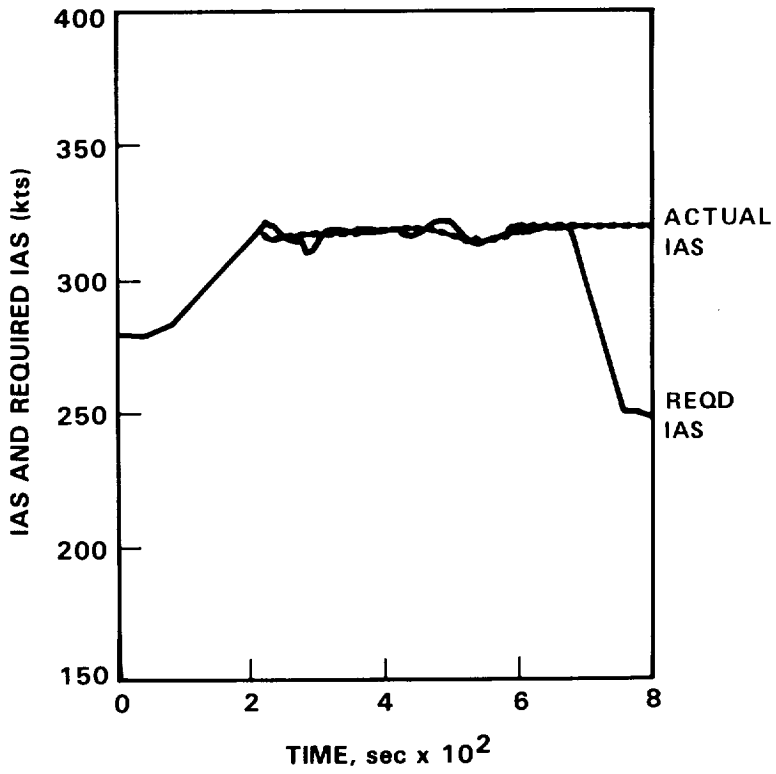

Figure 106. - IAS and required IAS.

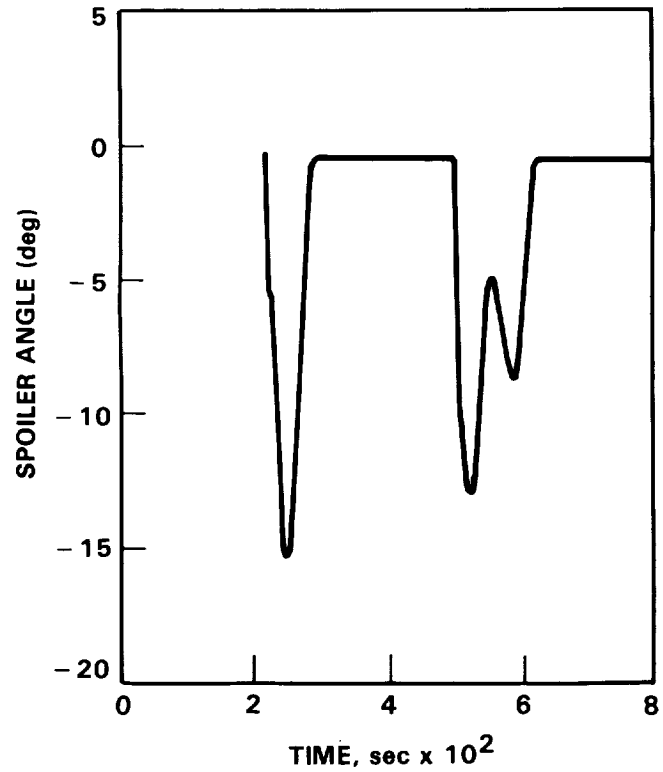

Figure 107. - Spoiler angle.

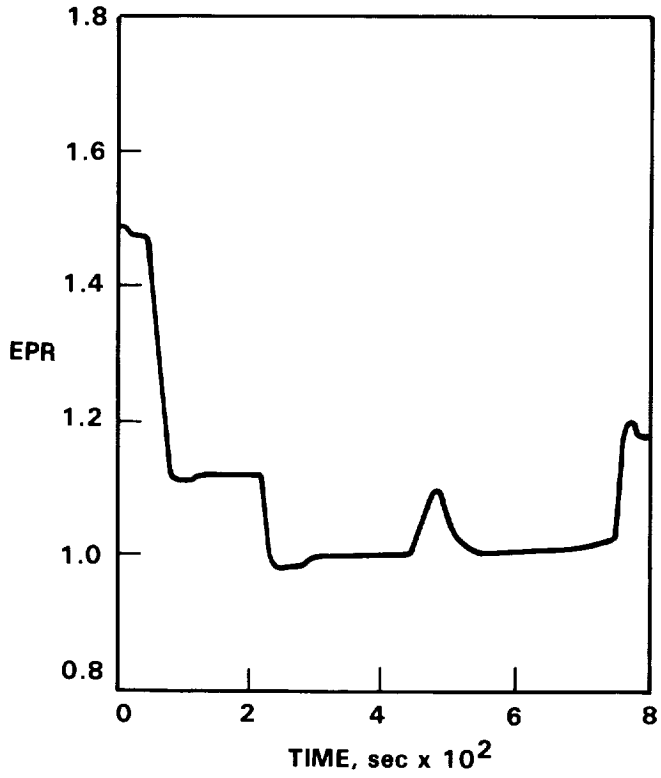

Figure 108. - Engine pressure ratio.

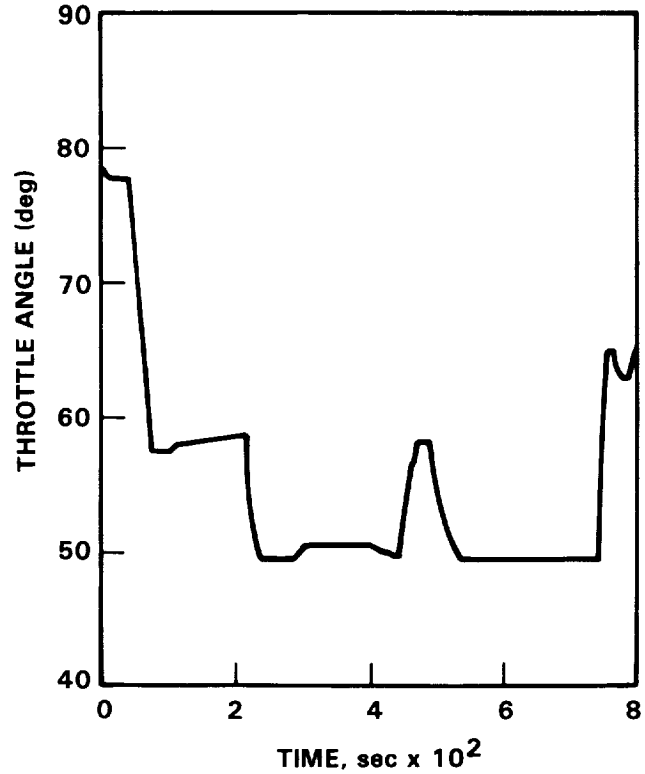

Figure 109. - Throttle angle.

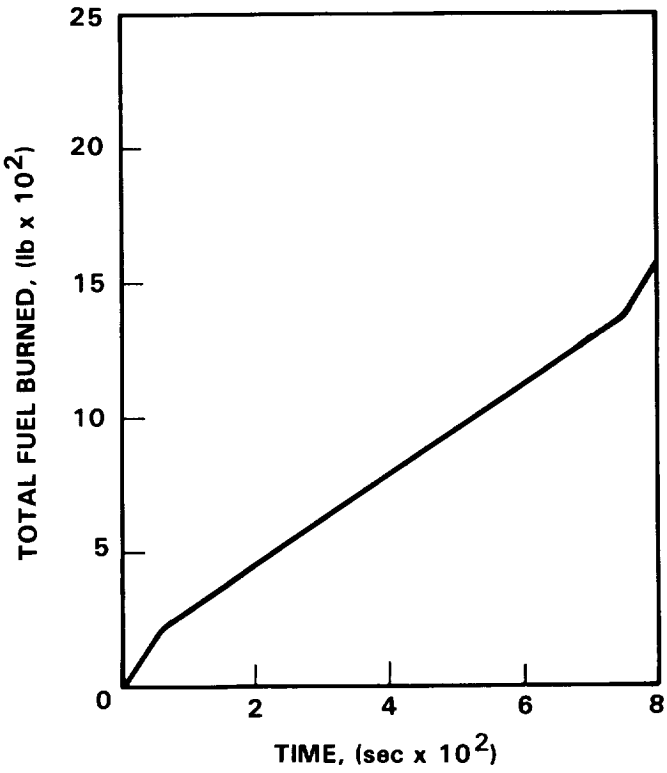

Figure 110. - Total fuel burned.

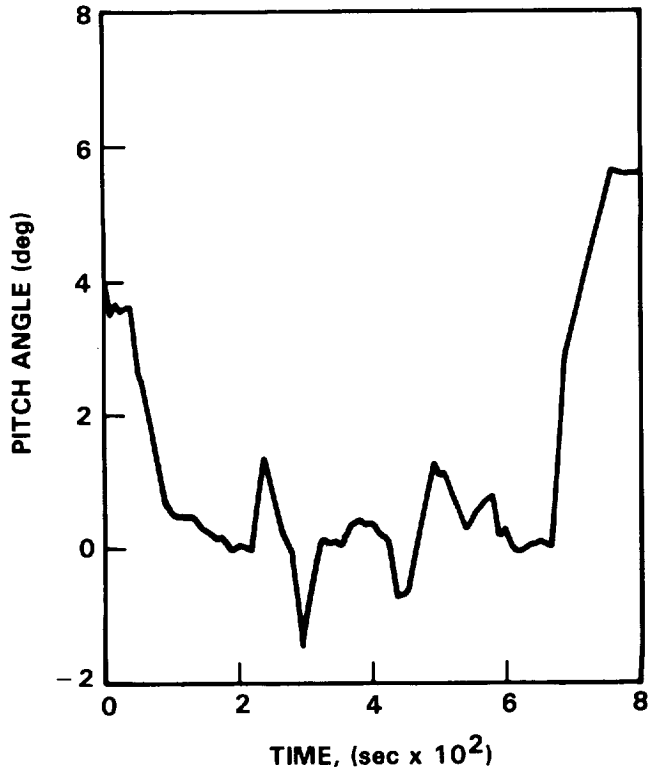

Figure 111. - Pitch angle.

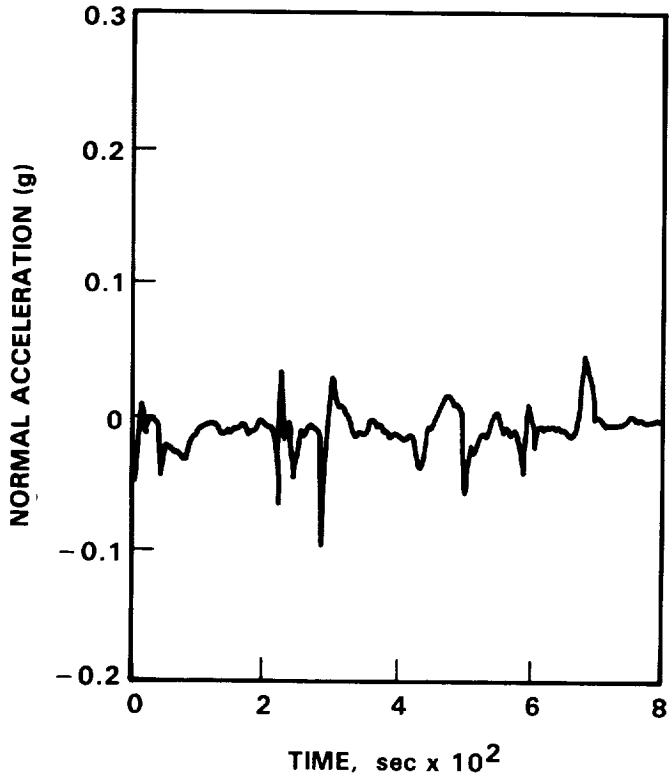

Figure 112. - Normal acceleration.

REFERENCES

(1) Sindermann, B.M.; and Newman, T.J.: Application of Automatic Guidance and Control for Optimum Cost/Fuel Savings for the Lockheed L-1011 Aircraft. Presented at 18th IEEE Conference on Decision and Control, Fort Lauderdale, Florida, December 12-14, 1979.

(2) Erwin, Ralph: Strategic Time-based ATC. Aeronautics and Astronautics, vol. 16, 1978, pp. 56-61.

(3) Erwin, Ralph; et al.: Strategic Control Algorithm Development. DOT No. DOT-TSC-OST-74-3 vol. i-iv, 1974.

(4) Federal Aviation Administration: Local Flow Traffic Management, Advisory Circular 90-73, 1977.

(5) U.S. Department of Transportation, Federal Aviation Administration: National Airspace System Plan - Facilities, Equipment and Associated Development. 1981.

(6) Knox, C.E; and Cannon, D.G.: Development and Test Results of a Flight Management Algorithm for Fuel-Conservative Descents in a Time-Based Metered Traffic Environment. NASA TP 1717, 1980.

(7) Heimbold, R.L.; Lee, H.P.; and Leffler, M.F.: Development of Advanced Avionics Systems Applicable to Terminal-Configured Vehicles. NASA CR-3280, 1980.

(8) Charles, B.N.: Lag Correlations of Upper Winds. Journal of Meteorology, vol. 16, 1959, pp. 83-86.

(9) Gott, E.: Linear Regression of Interlevel Wind Velocities. IEEE Transaction on Geoscience Electronics, vol. GE-7, no. 1, 1969.

(10) Daniels, G.E.; and Smith, O.E.: Scales and Component Wind Correlations Between Altitude Levels for Cape Kennedy, Florida, and Santa Monica, California. NASA TN D-3815, 1968.

(11) Vaughan, W.W.: Interlevel and Intralevel Correlations of Wind Components for Six Geographical Locations. NASA TN D-561, 1960.

(12) Valley, S.L.; ed.: Handbook of Geophysics and Space Environments. Air Force Cambridge Research Laboratories, McGraw-Hill, 1965, pp. 4.1-4.54.

(13) Foudriat, E.C.: A General Algorithm for Relating Ground Trajectory Distance, Elapsed Flight Time, and Aircraft Airspeed and Its Application to 4-D Guidance. NASA TN D-7876, 1975.

1. Report No.	2. Government Accession No.	3. Recipient's Catalog No.
NASA CR-3700		

4. Title and Subtitle	5. Report Date
DEVELOPMENT OF THE L-1011 FOUR-DIMENSIONAL FLIGHT MANAGEMENT SYSTEM	February 1984
	6. Performing Organization Code

7. Author(s)	8. Performing Organization Report No.
H. P. Lee and M. F. Leffler	LR 30279
	10. Work Unit No.

9. Performing Organization Name and Address	11. Contract or Grant No.
Lockheed-California Company P.O. Box 551 Burbank, California 91520	NAS1-16199
	13. Type of Report and Period Covered Contractor Report Sept 1980 - July 1982

12. Sponsoring Agency Name and Address	14. Sponsoring Agency Code
National Aeronautics and Space Administration Washington, D.C. 20546	

15. Supplementary Notes

Langley Technical Monitor: Leonard V. Clark
Final Report

16. Abstract This report describes the development of 4-D guidance and control algorithms for the Lockheed L-1011 Flight Management System. 4-D Flight Management is a concept by which an aircraft's flight is optimized along the 3-D path within the constraints of today's ATC environment, while its arrival time is controlled to fit into the air traffic flow without incurring or causing delays. The methods developed herein have been designed to be compatible with the time-based en route metering techniques that have been recently developed by the Dallas/Fort Worth and Denver Air Route Traffic Control Centers. The ensuing development of the 4-D guidance algorithms, the necessary control laws and the operational procedures are discussed. Results of computer simulation evaluation of the guidance algorithms and control laws are presented, along with a description of the software development procedures utilized.

17. Key Words (Suggested by Author(s))	18. Distribution Statement
4-D Air Traffic Control Flight Management System Fuel Efficiency Automatic Flight	Unclassified - Unlimited Subject Category 04

19. Security Classif. (of this report)	20. Security Classif. (of this page)	21. No. of Pages	22. Price*
Unclassified	Unclassified	150	A07

* For sale by the National Technical Information Service, Springfield, Virginia 22161

NASA-Langley, 1984